The specificity and regulation of human histone deacetylase 8

by

Carol Ann Pitcairn

A dissertation submitted in partial fulfillment
of the requirements for the degree of
Doctor of Philosophy
(Chemical Biology)
in the University of Michigan
2015

Doctoral Committee:

Professor Carol A. Fierke, Chair
Associate Professor Patrick O'Brien
Professor Stephen W. Ragsdale
Associate Professor Raymond C. Trievel

Dedication

I dedicate this dissertation to God and to my beloved family.

God has given me extraordinary family and friends. I will be forever thankful for the wonderful individuals whose lives have intersected or run parallel with mine for a time. It has been an adventure with marvelous companions on the journey!

My parents instilled in me a drive for education, although I don't think anyone expected me to take my education to the extreme of a doctoral degree. I also learned from my family that when you do something, you give it all you've got. Thus, I have completed 22 years of school. Like my mom always says, "I'm accomplishing my goals." Support and encouragement from my parents have brought me to this place, and I am incredibly thankful. I cannot express my love for my family in words on a page.

.

Acknowledgements

I thank Dr. Carol A. Fierke for being an excellent mentor and role model. I am overjoyed to have achieved this milestone and Carol was integral to my success. I aspire to be as good a mentor as she is. I am thankful to be a part of the lab group she has assembled, and for her guidance throughout the Ph.D. process.

I want to thank my undergraduate research advisor, Dr. Nina V. Stourman for her guidance and support, as well as the faculty in the Chemistry Department at Youngstown State University. I also want to thank my mentors and former lab-mates for their advice, assistance, and support: Dr. Yaru Zhang, Dr. Corissa Lamphear, Dr. Caleb G. Joseph, and Dr. Noah A. Wolfson.

Although our protein turns purple (when it bothers to be expressed) and our assays are complicated, the HDAC subgroup is the subgroup that has the most fun. Members of this cluster, from 2011 to present, include Dr. Caleb G. Joseph, Dr. Noah A. Wolfson, Dr. Byungchul Kim, Dr. Ningkun Wang, Dr. Lubomír Dostál, Eric D. Sullivan, Jeffrey E. López, Katherine R. Leng, and George R. Murphy III. I thank them for helpful discussions, collaborations, group protein purifications, and laughter.

From the bottom of my heart I thank Katherine R. Leng, Jeffrey E. López, Nancy Wu, Yu Chen, and Dr. Jenna Hendershot for friendship and our snack times, iced tea runs, exercise, matching days, story time, and the occasional, well-timed, much-needed hug.

I thank my family in Christ at Crossroads Community Baptist Church for lovingly providing a kind ear to listen, words and smiles of encouragement, food, and fun.

Finally, I want to give my deepest thanks to my parents and my family. My family is the epitome of unconditional love. I thank them for: emotional support, long phone calls, lots of food, joyful visits when I was too busy to travel, and for understanding when I skipped family events. Thank you for teaching me to love Jesus and people. Thank you for nurturing my self-confidence and motivation. Thank you for being proud of me.

Table of Contents

List of Tables

List of Figures

List of Acronyms

ARID1A: AT Rich Interactive Domain 1A

ATP: adenosine triphosphate

BDNF: brain-derived neurotrophic factor

CdLS: Cornelia de Lange syndrome

CK2: casein kinase 2

COBALT: constraint-based alignment tool for multiple protein sequences

CoREST: repressor element-1 silencing transcription factor (REST) corepressor 1

CPNE3: copine-3

CREB: cAMP responsive element-binding protein

DEAE: diethylaminoethyl

DNAJB8: DnaJ homolog subfamily B member 8

DTT: dithiothreitol

*Ec*MetAP: *E. coli* methionine aminopeptidase

EDTA: ethylenediaminetetraacetic acid

EGFP: enhanced green fluorescent protein

ERRα: Estrogen-Related Receptor α

GABC: general acid-base catalysis

HDAC: histone deacetylase

HEPES: 4-(2-hydroxyethyl)-1-piperazineethanesulfonic acid

Hsp: heat shock protein

ICP-MS: inductively coupled plasma mass spectrometry

IIp45: invasion inhibitory protein 45

IL-10: interleukin 10

KAT (also HAT): lysine acetyltransferase

LpxC: UDP-3-O-((R)-3-hydroxymyristoyl)-N-acetylglucosamine deacetylase

MALDI-TOF: Matrix-assisted laser desorption/ionization with time-of-flight mass spectrometer

MEF: myocyte enhancer factor

MOPS: (N-morpholino)propanesulfonic acid

NAD^+: nicotinamide adenine dinucleotide

N-CoR: nuclear receptor corepressor

NSLS: National Synchrotron Light Source

NUP98: nucleoporin 98 kDa

NuRD: nucleosome remodeling deacetylase

PDB: Protein Data Bank

PEG: polyethylene glycol

PKA: protein kinase A

PKC: protein kinase C

PKG: protein kinase G

PP1: protein phosphatase 1

PTM: post-translational modification

SAHA: suberanilohydroxamic acid

SAINT: significance analysis of interactome

SAMDI: Self-Assembled Monolayers for MALDI-TOF Mass Spectrometry

SEC16A: protein transport protein Sec16A

SILAC: Stable Isotope Labeling by Amino acids in Cell culture

SMC1A: structural maintenance of chromosomes 1A

SMC3: structural maintenance of chromosomes 3

SMRT: silencing mediator of retinoic acid and thyroid hormone receptors

STAG2: stromal antigen 2

SUMO: small ubiquitin-like modifier

TCEP: tris(2-carboxyethyl)phosphine

TEV: tobacco etch virus

TLS: Translation Libration Screw

TSA: trichostatin A

VMD: Visual Molecular Dynamics

Abstract

Post-translational modifications (PTMs) of proteins increase the complexity of the proteome, alter protein function, and play important roles in cellular function. Lysine acetylation, catalyzed by lysine acetyltransferases, is an important post-translational modification of proteins, including histones, transcription factors, and cytoplasmic proteins. The modification is reversible; hydrolysis is catalyzed by histone deacetylases (HDACs). Lysine deacetylation is important for regulating cellular processes, and aberrant deacetylation is implicated in diseases including cancer. HDAC8 is a metal-dependent HDAC that is activated by Zn(II) and Fe(II) under *in vitro* conditions, and altering the metal ion identity affects activity. This enzyme is a therapeutic target for cancers, parasitic infection, and a developmental disorder; however, therapeutic research is impeded by the lack of knowledge regarding HDAC substrate recognition and regulation and by the challenge of identifying HDAC substrates and binding partners. My research has focused on the substrate specificity, metal dependence, and regulation by phosphorylation of HDAC8. I have shown that the sequence specificity of HDAC8 toward peptide substrates is dependent on the identity of the catalytic metal ion. Additionally, I have investigated regulation of HDAC8 by phosphorylation on residue Ser39, using the S39E mutant as a mimetic, demonstrating that this modification significantly alters metal binding properties of HDAC8, decreases HDAC8-catalyzed deacetylation of peptides, and alters substrate binding. I have shown that HDAC8 exhibits changes in substrate specificity for singly acetylated octamers and nucleosome *in vitro*, compared to peptide substrates representing the same sites. Elucidating the mechanisms that regulate HDAC8 substrate specificity is important for determining the role of this enzyme in normal and pathophysiological processes in the cell.

Chapter 1

HDAC8 substrates: Histones and beyond[1,2]

Overview

Post-translational modifications (PTMs) on proteins increase the complexity of the proteome, alter protein function, and play important roles in cellular processes. There are over 300 post-translational modifications (1). Protein acetylation is one such modification which has seen significant growth in research interest over the past twenty years and the annual publication rate continues to increase (2). Protein acetylation occurs in two forms: N-terminal N^{α}-acetylation and N^{ε}-acetylation of the amino acid lysine. Lysine acetylation is enzymatically reversible. Lysine acetyltransferases (KATs; also known as histone acetyltransferases (HATs)) catalyze addition of the acetyl moiety to the amine side chain on a lysine residue to form N^{ε}-acetyl-lysine, and as of July 2015 there are more than 3,800 sites of lysine N^{ε}-acetylation reported in the mammalian proteome (1). Deacetylation, hydrolysis of this modification to yield lysine and acetate, is catalyzed by acetyl-lysine deacetylase enzymes called histone deacetylases (HDACs). Protein acetylation, and therefore deacetylation, is important for regulating cellular processes such as transcription, signaling, and cytoskeletal dynamics (3, 4). HDACs are targets for cancer therapeutics, but a key limitation of developing these drugs is that the functions of the 18 HDAC isozymes are poorly understood. Here I discuss the current understanding of substrate specificity as it pertains to the best-studied metal-dependent human histone deacetylase, HDAC8. In the following chapters I will present my research designed to address the gaps in our knowledge of HDAC8 function and regulation, including substrate

[1] Reproduced in part, with permission from John Wiley and Sons, from Wolfson, N. A.; Pitcairn, C. A.; Fierke, C. A., HDAC8 substrates: Histones and beyond. *Biopolymers.* 2013;99(2):112-26.

[2] Original text written by Noah A. Wolfson and Carol Ann Pitcairn and updated by Carol Ann Pitcairn to reflect relevant recent advances published in the literature.

recognition determinants, metal-dependent substrate specificity, and post-translational modification.

Introduction of HDACs

Protein lysine acetylation is a reversible posttranslational modification observed in organisms from bacteria to humans (reviewed in 5). The modification affects protein properties including protein-protein and protein-DNA interactions, protein stability, and enzymatic activity (reviewed in 3, 6). Initially, acetylation was studied as an epigenetic marker on histones. Histone acetylation can regulate the accessibility of DNA to the transcription machinery, thereby changing the protein expression profiles of cells (reviewed in 7). Due to the role of acetylation in transcription and its effects on the proteome, it is not surprising that many diseases have been associated with the aberrant acetylation of histones (reviewed in 8). In the last twelve years, the focus of the protein acetylation field has evolved from a histone-centric model to a proteome-centric model, even coining the term “lysine acetylome” (9). This change in mindset has resulted from the identification of acetylated lysine residues that affect the function of numerous non-histone proteins (e.g. 9, 10). Currently, over 3,800 acetylation sites have been experimentally identified on mammalian proteins (1) and acetylated proteins are important in many cellular processes, including gluconeogenesis and DNA damage repair (9, 10). Regulation of the acetylation state of proteins via KATs and HDACs is important since the abnormal acetylation state of both histone and non-histone proteins can contribute to the development of many disease states (reviewed in 11, 12, 13), and so it follows that there are multiple acetyltransferase and deacetylase enzymes.

Lysine deacetylase isozymes can be broken into four classes based on their phylogenetic similarity (14). Class I (HDAC1, 2, 3, and 8), class II (HDAC4, 5, 6, 7, 9, and 10), and class IV (HDAC11) enzymes catalyze deacetylation using a metal dependent mechanism (14, 15), while class III (Sirt1-7) enzymes use an NAD^+ cofactor to perform deacetylation (16, 17). This dissertation pertains to metal-dependent HDACs. Crystal structures have demonstrated that the HDAC deacetylase domain has an arginase-deacetylase fold, which consists of a multi-strand β-sheet surrounded by α-helices, and

in HDACs the active site contains a single divalent metal ion site with His and Asp ligands (5, 18, 19). HDAC6 is unique in that it contains two deacetylase domains and a zinc-finger domain (reviewed in 20).

The metal-dependent HDACs are metallohydrolases, and a metal-water is the nucleophile in the reaction, which is activated by a general acid-base catalysis mechanism (GABC) (reviewed in 19), as described later. Not much is known regarding the substrate specificity of the HDAC isozymes, however the loop L2 residue D101 is conserved and suggested to confer substrate selectivity, based on structures of HDAC8-substrate complexes (reviewed in 19). Interestingly, several HDACs have putative non-deacetylase functions. HDAC3 may be a molecular chaperone for orphan nuclear receptor TR2 (reviewed in 21). HDACs 4, 5, and 7 promote protein sumoylation; HDAC4 and HDAC5 are suggested to have small ubiquitin-like modifier (SUMO) E3 ligase activity, and HDAC7 may act as a SUMO E3 ligase as well (22-24).

Class I HDAC isozymes 1, 2, and 3 are found in protein complexes and play important roles in the regulation of transcription. HDAC1 and HDAC2 are components of the Sin3 complex, the repressor element-1 silencing transcription factor (REST) corepressor 1 (CoREST) complex, and the nucleosome remodeling deacetylase (NuRD) complex, which are involved in transcription regulation (reviewed in 5). HDAC3 forms a complex with the nuclear receptor corepressor (N-CoR) and silencing mediator of retinoic acid and thyroid hormone receptors (SMRT) (reviewed in 5). HDAC3 also shuttles between the nucleus and cytoplasm, is important for mitosis and transcriptional regulation, and has both nuclear and cytoplasmic substrates (reviewed in 21). HDAC8, which will be discussed in detail below, differs from the other class I enzymes in its lack of identified protein complexes. HDAC8 is the shortest human HDAC (377 amino acids), while the other HDACs have long N-terminal or C-terminal tails (reviewed in 5). Class I HDACs undergo post-translational modifications including phosphorylation and acetylation, and these modifications regulate catalytic activity and protein-protein interactions (reviewed in 25, 26).

Class II HDACs are regulated by post-translational modifications and protein-protein interactions, and several of these isozymes shuttle between the nucleus and

cytoplasm. HDAC6 activity is decreased by phosphorylation (reviewed in 21) and interaction with invasion inhibitory protein 45 (IIp45) results in a decreased HDAC6 half-life as well as HDAC6 inhibition (27). HDAC7 plays a role in osteoblast maturation via protein-protein interaction with the transcriptional regulator Runx2 (28). HDAC4, HDAC5, and HDAC7 shuttle between the nucleus and cytoplasm, which is regulated in several ways including a phosphorylation-dependent interaction with 14-3-3 proteins (HDACs 4, 5, and 7) (29-32) and cysteine oxidation (HDACs 4 and 5) (33-35). Interactions with various proteins retain HDAC4 in either the cytoplasm or nucleus, including 14-3-3 proteins, MEF2C, DNAJB5, and thioredoxin 1 (Trx1), and HDAC4 has both nuclear and cytoplasmic substrates, such as the transcription factor p53 and cytoplasmic chaperone DNAJB8 (reviewed in 21). HDAC10 is considered a cytoplasmic deacetylase, however putative substrates include Hsp70 as well as nuclear, non-histone, proteins (reviewed in 21). HDAC6 is localized to the cytoplasm, where its substrates include tubulin and Hsp90 (reviewed in 5, 20, 21), however there is also evidence of a role for HDAC6 in transcription and nuclear localization (reviewed in 20).

HDACs are involved in many biological processes and are implicated in disease states including cancers, neurodegenerative disorders, and heart disease (5). Due to the abundance and importance of HDAC substrates, one of the foremost questions in the field is the determination of the substrate specificity of HDACs. This area of research seeks to identify which of the 18 deacetylases catalyzes deacetylation of each of the >3,800 mammalian acetylation sites. This question is complex, because cellular conditions and regulatory mechanisms may alter both the catalytic activity and the substrate specificity of HDACs. Understanding the substrate selectivity and regulation of HDACs will illuminate the disease mechanisms in which they partake and will inform development of therapeutics for the treatment of acetylation-related diseases.

Three pan-HDAC inhibitors (suberoylanilide hydroxamic acid (SAHA), Romidepsin, and most recently Belinostat) have been approved by the FDA to treat T-cell Lymphomas (Figure 1-1), and another inhibitor, panobinostat, is approved to treat multiple myeloma (reviewed in 36, 37-41). Natural products have produced many HDAC inhibitors (HDACi), including sodium butyrate, trichostatin A (TSA), and romidepsin (42). However, most HDAC inhibitors are unselective, class selective, or effective toward a few

HDACs, so continued study to increase inhibitor selectivity is important from a therapeutic standpoint. Human and parasitic organism HDACs remain the targets of drug design for conditions including cancer and parasitic diseases (reviewed in 36, 43). HDACi design also continues to provide insight into the structure-function properties of these enzymes, such as the flexibility of HDAC8's substrate and inhibitor binding interface demonstrated by inhibitor-bound HDAC8 crystal structures (44). There is a limit to the information gleaned from inhibitor design studies, and rational drug design necessitates knowledge of metal-dependent HDAC isozyme specificity, so substrate recognition and HDAC regulation continue to be important areas of research.

Mechanistically and structurally, HDAC8 is the best studied of the HDAC homologues. Furthermore, HDAC8 is proposed to recognize a number of non-histone substrates (e.g. 45, 46, 47) and is therefore a good model for developing techniques to elucidate HDAC substrate specificity. The HDAC8 isozyme is also implicated in disease states, as described later. In this review we discuss the current view of HDAC8 regulation, and compare HDAC8 to other promiscuous enzymes to identify factors that determine substrate specificity.

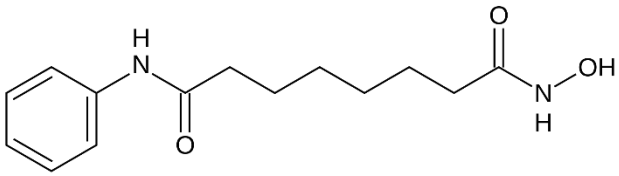

Suberoylanilide hydroxamic acid (SAHA)

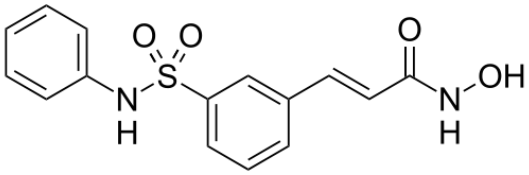

Belinostat

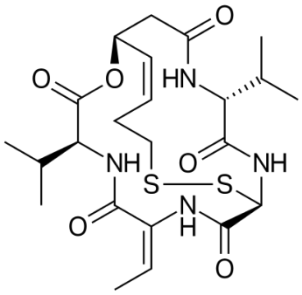

Romidepsin (FK228)

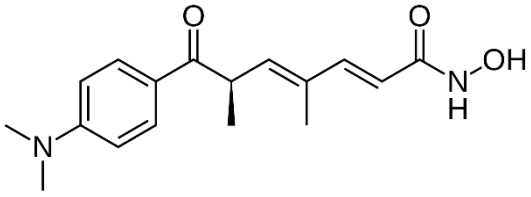

Trichostatin A (TSA)

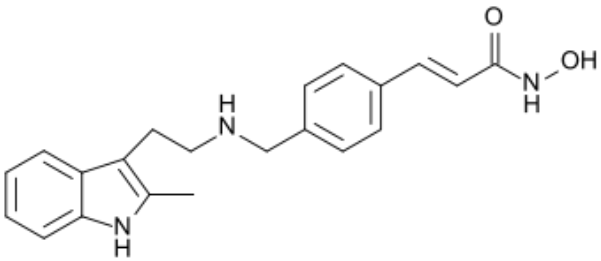

Panobinostat

Figure 1-1: Select HDAC inhibitors

SAHA, belinostat, and romidepsin, are FDA-approved as treatments of T-cell lymphomas. Panobinostat is FDA-approved to treat multiple myeloma. TSA is a hydroxamic acid inhibitor used for *in vitro* and *in vivo* studies (36).

Biological importance of HDAC8

HDAC8 is important to the pathology of several disease states, including cancers and developmental disorders. HDAC8 mRNA levels are upregulated in several urothelial (bladder) cancer cell lines and cancerous tissue samples (48). HDAC8 is targeted in developing treatments for childhood neuroblastoma, as higher HDAC8 mRNA levels have been correlated with characteristics of poor disease outcome (49) and HDAC8-specific inhibition yields effective antitumor activity in cells and mouse models (50). Clinically observed HDAC8 mutations are involved in some cases of the developmental disorder Cornelia de Lange syndrome (discussed later), in which patients exhibit facial, skeletal, and intellectual abnormalities (47, 51). Additionally, the HDAC8 homolog found in the tropical flatworm *Schistosoma mansoni* (smHDAC8) is an antiparasitic target for therapeutics and inhibitors specific for smHDAC8 over hHDAC8 are in development (52).

HDAC8 knockouts after birth are non-lethal (53), consistent with the ability of humans to tolerate pan-HDAC inhibitors as an anti-cancer treatment (54). However, protein expression profiles can vary significantly during development and several HDAC knockouts are lethal during mammalian embryonic development (11). For example, cells lacking HDAC3 die before embryonic day 9.5; deletion of HDAC3 leads to hyperactivity of the nuclear receptor PPARα and problems with embryonic gastrulation (55). Similarly, HDAC8 expression is crucial to development, as mice lacking this enzyme die soon after birth (53). Death is due to brain hemorrhaging caused by developmental defects in the mouse skull resulting from problems with neural crest patterning. These skull defects are similar to those that occur upon overexpression of the transcription factors Otx2 and Lhx1, suggesting that HDAC8 either directly regulates these proteins or affects regulators of these proteins (53). The mechanism of HDAC8 regulation of Otx2 and Lhx1 has yet to be determined. Furthermore, since HDAC8 knockouts are not lethal after birth (53), it is unclear whether HDAC8 no longer regulates these proteins, this regulation still occurs but is not vital for viability, or another HDAC compensates for the lack of HDAC8. Interestingly, recent reports catalog the features of human patients expressing loss-of-function HDAC8 mutants. The phenotypes were wide-ranging and included brachycephaly, anteverted nostrils, widely spaced teeth, small hands and feet, gastrointestinal anomalies, and intellectual disability (51). Some of the observed features

overlap with those typical of Cornelia de Lange syndrome (CdLS). The non-CdLS phenotypes unique to HDAC8 dysfunction included features linked to skull development, which is consistent with the mouse knockout findings (51, 53).

Known HDAC8 substrates

Upon the discovery of HDAC8 in 2000, it was demonstrated to catalyze deacetylation of a number of acetylated histone variants *in vitro* (56-58). These histone substrates included full-length H2A/H2B, H3, and H4 histones, acetylated at non-specific lysines (56, 57). Concurrent studies showed that peptide sequences representing the H4 histone tail with an acetylated lysine at position K16ac were also substrates *in vitro* (57, 58). Several studies have used the H4 histone tail sequence as a peptide template to investigate the preferred substrate amino acid sequences of HDAC8 (discussed below) (59-62). Despite the widespread use of histones as generic HDAC8 substrates, the actual role and specificity of HDAC8 in catalyzing deacetylation of histones *in vivo* remains unclear.

Shortly after HDAC8 was identified, the first acetylated non-histone proteins were reported (63, 64), which prompted the search for other possible HDAC substrates. The search for new HDAC8 substrates was further broadened to include non-nuclear substrates upon the discovery that this enzyme is present in the cytoplasm of smooth muscle cells (65, 66). The k_{cat}/K_M for HDAC8-catalyzed deacetylation of a coumarin-conjugated peptide corresponding to the C-terminal region of the p53 transcription factor (Figure 1-2) is 2.7-fold greater than for a coumarin-conjugated H4K16ac histone peptide, with k_{cat}/K_M values of 7,500 $M^{-1}s^{-1}$ (67) and 2,800 $M^{-1}s^{-1}$ (68), respectively. Since the k_{cat}/K_M parameter reflects the relative catalytic efficiency of an enzyme with different substrates (reviewed in 69 pp. 111, 116-117), these values suggest that HDAC8 has a modest preference for catalyzing deacetylation of p53 over the H4 histone. It is important to note that these k_{cat}/K_M values for HDAC8 were measured using the commercially available Fluor-de-Lys assay (Enzo Life Sciences). This assay uses peptide substrates containing a methylcoumarin fluorophore conjugated to the C-terminal side of the acetyl-lysine residue. After deacetylation, digestion by trypsin cleaves the coumarin fluorophore, causing an increase in fluorescence at 460 nm; deacetylation is measured from an

increase in the fluorescence signal (70) (Figure 1-2B). While this assay has been a valuable tool for studying histone deacetylases, the methylcoumarin fluorophore increases the activity of HDAC8 (71) and HDAC8-catalyzed deacetylation of unlabeled acetylated p53 and H4 histone peptides is slower than this assay reports (71, 72). Furthermore, coumarin-conjugated peptides are unlikely to reflect HDAC substrate specificity in the context of full-length proteins.

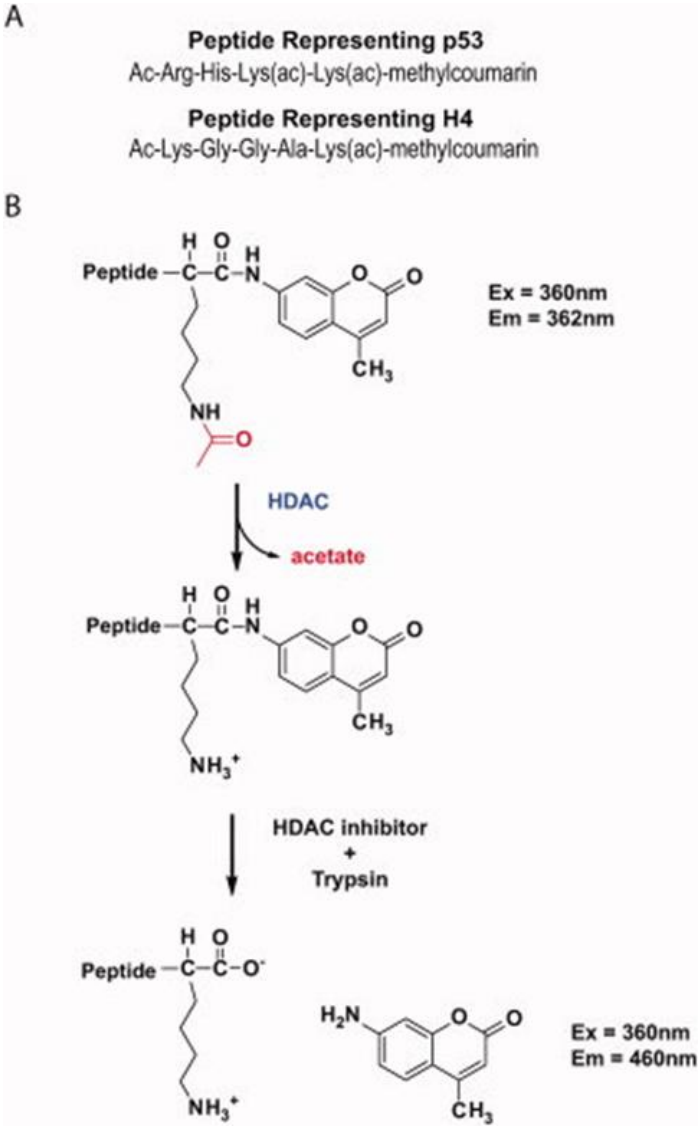

Figure 1-2: The Fluor-de-Lys® assay (Enzo Life Sciences)

A. The sequence of two HDAC8 peptide substrates used in the Fluor-de-Lys assay. B. Schematic of the Fluor-de-Lys assay and the wavelengths at which the fluorophores are measured. Reproduced from (73) with permission from John Wiley and Sons.

The steady state kinetic parameters for catalysis of the deacetylation of peptides can provide insight into both kinetic mechanism and substrate recognition. HDAC8-catalyzed deacetylation of the p53 and H4 coumarin peptides has a low value of k_{cat}/K_M (10^3 – 10^4 $M^{-1}s^{-1}$) in comparison to enzymes that function near diffusion-controlled limits (10^6 – 10^8 $M^{-1}s^{-1}$) and a high value for K_M (320 µM, H4 peptide) (68) compared to other HDAC isozymes (~30 µM) (74). These data suggest a simple Michaelis-Menten kinetic model whereby substrate binding and dissociation is rapid, and is followed by rate-limiting deacetylation. This conclusion is bolstered by the observed enhancement of the k_{cat} value for deacetylation of peptides labeled with a more reactive trifluoroacetyl group (75, 76). Therefore, substrate specificity is determined by both the affinity of HDAC8 for a peptide substrate and the activity of HDAC8 in the enzyme-substrate complex. Assuming that the kinetic constants for deacetylation of these peptides mimic the full-length proteins, the low k_{cat}/K_M and high K_M values for HDAC8-catalyzed deacetylation of H4 and p53 peptides compared to the activity of other HDAC isozymes (67, 74) (68) suggest that HDAC8 may not catalyze deacetylation of these sites *in vivo*. However, it is possible that natural, full-length, substrates may be better optimized for efficient deacetylation to allow for regulation of these post-translational modifications. In addition to these proposed substrates, *in vitro* kinetic studies combined with cellular assays have yielded several promising candidates for *in vivo* HDAC8 substrates.

There are a number of factors that must be taken into account when parsing whether substrates are acted upon by a given enzyme *in vivo*. HDAC selectivity is minimally described by the relative values of k_{cat}/K_M for deacetylation, the relative concentrations of the HDAC isozymes, and the concentrations of competing substrates. Relative k_{cat}/K_M values indicate the substrate preference of an enzyme when discriminating among multiple substrates (reviewed in 69 pp. 110-111). The majority of enzymes have k_{cat}/K_M values of 10^5-10^6 $M^{-1}s^{-1}$ (77). These values are generally slower than the diffusion controlled rate constants for substrate binding, which can be as high as 10^7-10^8 $M^{-1}s^{-1}$ (reviewed in 69 pp. 158-166). Consistent with this, the k_{cat}/K_M values for the HDAC8 homolog HDAC1 and the homologous enzyme, arginase I, are on the order of 10^5 $M^{-1}s^{-1}$ (74, 78), suggesting that similar values should be achievable for efficient HDAC8 substrates. A caveat to drawing conclusions from *in vitro* kinetic parameters is

that some enzymes require an activator, such as a binding partner or covalent modification, for optimal activity. Since many HDAC isozymes associate with large protein complexes *in vivo*, it is possible that other proteins in the complex could activate the catalytic activity or enhance the substrate affinity to increase the value of k_{cat}/K_M in the cell. Additionally, HDAC8 may activated by a small molecule *in vivo,* perhaps via allosteric regulation. *N*-Acylthiourea binds in two locations and has been shown to activate HDAC8, *in vitro* and in cells, by interacting with the active site and an allosteric site (79).

Candidate non-histone HDAC8 substrates

The identification of HDAC8 substrates is an ongoing topic of investigation. Methods such as co-immunoprecipitation, *in vitro* kinetic measurements, cellular HDAC8 knockdowns, and proteomic mass spectrometry are employed; and proposed substrates include structural maintenance of chromosomes 3 (SMC3), Estrogen-Related Receptor α (ERRα), the inv(16) fusion protein, cAMP responsive element-binding protein (CREB), AT Rich Interactive Domain 1A (ARID1A), transcription factor p53, and heat shock protein Hsp20 (47, 73, 80-83).

A recently identified HDAC8 substrate is SMC3, a protein subunit of the cohesin complex. Human SMC3 is acetylated at K105 and K106 during S phase, and this is important for the cohesion of sister chromatids during the cell cycle (80, 84-86). SMC3 was recently reported to be an HDAC8 substrate *in vivo*, based on cellular studies, and lack of HDAC8-catalyzed deacetylation of SMC3 is implicated in CdLS (47, 80). The proposed cellular model requires HDAC8-catalyzed deacetylation of SMC3 for the disassembly and regeneration of cohesin following anaphase and the separation of the chromosomes (Figure 1-3) (47, 87). Deacetylation of SMC3 releases components such as RAD21 protein fragments and allows the reassembly of the cohesin complex (47). HDAC8 is also immunopurified with cohesin components SMC3, SMC1A, and STAG2 (81). In cases where HDAC8 abnormalities contribute to CdLS, it is likely via loss-of-function mutations or decreased stability of HDAC8, leading to decreased deacetylation of SMC3 and disruption of the cohesin complex cycle (47, 51). Knockdown and inhibition of HDAC8 in HeLa cells both yielded increased acetylated SMC3 levels, and fibroblasts

and lymphoblastoid cells expressing mutant forms of HDAC8 exhibit decreased levels of HDAC8 protein and increased levels of acetylated SMC3 (47). It should be noted that while the data implicate acetylated SMC3 as an HDAC8 substrate, HDAC8 mutations only account for a small percentage of CdLS occurrence (51). Phenotypes of patients with HDAC8 mutations reveal some (though not all) clinical characteristics consistent with CdLS as well as features unique to HDAC8 patients (non-canonical CdLS characteristics) (51). Despite the ambiguity of HDAC8's role in disease, SMC3 appears to be a probable HDAC8 target.

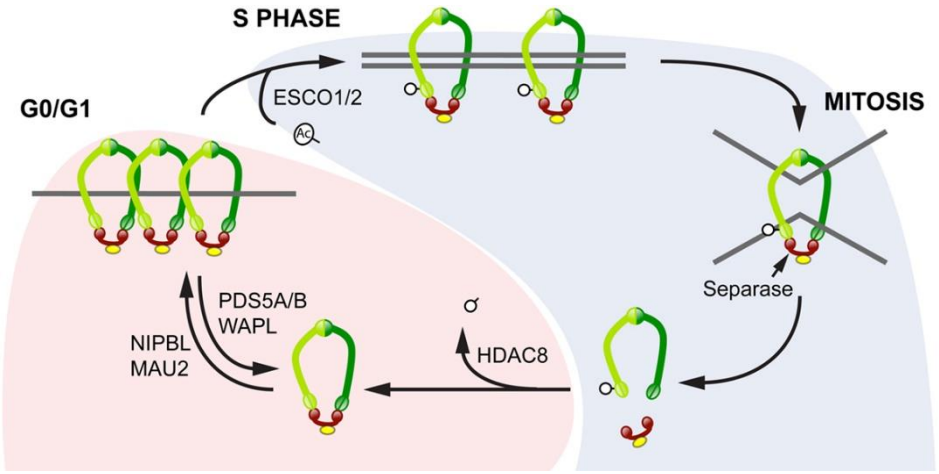

Figure 1-3: The proposed model of HDAC8 and SMC3 in cohesin dissassembly

This figure is adapted from (87). The cohesin complex consists of SMC3 (light green), SMC1 (dark green), RAD21 (red), and stromalin (SA) (yellow). Acetylation is depicted in white. During anaphase, the cohesin is cleaved and following telophase the complex is reassembled. The prerequisite for reassembly is deacetylation of SMC3 by HDAC8. Not shown: Deacetylation facilitates removal of RAD21 fragments bound to SMC3 after cleavage by separase (47).

A second proposed HDAC8 substrate is the ERRα. This orphan receptor is expressed in a number of organs, including the heart, kidney, and muscle, where it controls processes that are essential for maintaining energy homeostasis (reviewed in 88). ERRα can be acetylated at four positions (K129, K138, K160, and K162), where these posttranslational modifications inhibit DNA binding (46). A role for HDAC8 in catalyzing the deacetylation of ERRα was suggested by the demonstration that the acetylation state of ERRα was altered by simultaneous incubation with HDAC8, the histone acetyltransferase PCAF, and ^{14}C-acetyl-CoA (46). Furthermore, incubation of purified acetylated-ERRα with HDAC8 enhances the affinity of ERRα for DNA, which is consistent with HDAC8-catalyzed deacetylation of ERRα. One caveat to these experiments is that this assay included metal chelators and low salt, conditions where HDAC8 has limited catalytic activity (67, 89). An alternative explanation of these data is that HDAC8 binds to ERRα to increase the DNA affinity and/or decrease acetylation catalyzed by PCAF. However, addition of the non-homologous deacetylase Sirt1, to these

in vitro assays also decreases acetylation of ERRα, suggesting that both enzymes recognize ERRα as a deacetylase substrate. Finally, RNAi-dependent decreases in cellular HDAC8 or Sirt1 levels are accompanied by increases in ERRα acetylation *in vivo* (46). Taken together, these results suggest that HDAC8 catalyzes deacetylation of ERRα *in vivo*. Consistent with this, the acetylation site K129ac in ERRα has Arg in the -1 position (the amino acid on the N-terminal side of the acetyl-lysine), and RKac motifs have been demonstrated to be favorable for HDAC8 catalysis (60, 71). Additional analysis, such as directly measuring ERRα acetylation patterns by mass spectrometry in the presence and absence of HDAC inhibitors would further validate ERRα as an *in vivo* substrate of HDAC8.

The third proposed HDAC8 substrate is the aberrant inv(16) fusion protein found in a significant portion of patients with acute myeloid leukemia (90). This fusion protein combines the N-terminus of the transcription factor domain core binding factor β, with the C-terminus of the smooth muscle myosin heavy chain (91). In COS7 cells, co-immunoprecipitation experiments demonstrated that overexpressed HDAC8 associates with inv(16) (45). Furthermore, HDAC8 co-localizes and immunoprecipitates with smooth muscle myosin heavy chain (83) suggesting that HDAC8 may interact with this domain within the inv(16) fusion protein. Other HDAC isozymes do not immunoprecipitate with inv(16) under similar conditions, which suggests that HDAC8 may be the main HDAC that interacts with inv(16) *in vivo*. The addition of the HDAC inhibitor TSA inhibits the transcriptional repression activity of inv(16) (45), suggesting that HDAC8 activity is important for inv(16) regulation. An alternative explanation of these data is that inv(16) is a binding partner with HDAC8 rather than a substrate, as HDAC inhibitors have been shown to disrupt the association of HDACs with non-substrate binding partners (92). The acetylation site in the core binding factor β is RSKacFE (9). Peptide library studies have demonstrated that Phe in the +1 position is favorable for HDAC8 catalysis (60, 71) although Ser at the -1 position attenuates deacetylation (71). While the core binding factor β is acetylated *in vivo* (9), there is not yet direct evidence that inv(16) is acetylated (93). Taken together, these data indicate that inv(16) is either an HDAC8 substrate or forms a functionally important complex with HDAC8.

The transcription factor CREB is also a potential HDAC8 substrate. Acetylation at three CREB sites (Lys91, Lys96, and Lys136) helps to activate this protein (94). HDAC8 and CREB overexpressed in HEK293 cells co-immunoprecipitate, demonstrating that these two proteins associate. When HDAC8 is overexpressed in cells, phosphorylation of CREB decreases, which in turn inhibits CREB transcriptional activation (95). Likewise, treatment of cells with the pan-HDAC inhibitor TSA (96) or HDAC8-specific BMX (97) increased CREB phosphorylation levels, suggesting that HDAC8 activity is important for CREB phosphorylation. Specific inhibition of HDAC8 in neuroblastoma mouse models had anticancer effects which were postulated to occur through a CREB-mediated effect on transcription (50). However, pulldown experiments demonstrate that CREB can interact with a number of HDAC isozymes (95), complicating identification of CREB as an HDAC8 substrate *in vivo.* Due to the high amino acid identity between class I HDACs (>30%) (98), overexpression and pulldown experiments may not yield results that are representative of *in vivo* situations. Therefore, these experiments suggest, but do not confirm, a direct connection between HDAC8 deacetylase activity, the phosphorylation status of CREB, and the regulation of CREB activation. Alternatively, HDACs may function as protein scaffolds to mediate the inhibitory interaction between CREB and protein phosphatase 1 (PP1) (reviewed in 99) (95, 100, 101), leading to a decrease in CREB phosphorylation and activity.

Additional substrates have been suggested over the years, and more continue to be reported. The transcription factor p53 remains a classical candidate substrate. Knockdown of HDAC8 has been shown to increase the acetylation observed on Lys382 of p53 while the acetylation state of Lys373 did not change, suggesting that the former site may be an HDAC8 substrate (82). A more recently identified target is ARID1A. ARID1A was identified as an HDAC8 substrate by Stable Isotope Labeling of Amino Acids in Cell Culture (SILAC) followed by mass spectrometry to analyze changes in global protein acetylation upon inhibition of HDAC8 (80). HDAC8-catalyzed deacetylation of a representative ARID1A peptide lacking a methylcoumarin moiety exhibits a k_{cat}/K_M value of 740 ± 36 $M^{-1}s^{-1}$, which is similar to that of the p53-methylcoumarin peptide (800 ± 50 $M^{-1}s^{-1}$) (67, 72, 80). The fluorophore enhances HDAC8 activity toward the p53 peptide (71), so among unlabeled peptides HDAC8 is more active toward ARID1A.

Therefore, HDAC8 is more specific toward catalyzing deacetylation of the ARID1A peptide, which may indicate that this protein is an *in vivo* substrate. HDAC8 also co-immunoprecipitates with Hsp20 and HDAC8 inhibition is correlated to increased Hsp20 acetylation, suggestion another possible substrate (83).

The current cellular methods for identifying substrates of HDAC isozymes *in vivo* have limitations. Since HDAC selectivity depends on the relative concentrations of the HDAC isozymes and the concentrations of all of the acetylated lysine substrates, overexpression of HDAC and/or HDAC substrates can alter the normal pattern of deacetylase activity. Therefore, experiments using overexpressed proteins suggest that a particular interaction can occur *in vivo*, but does not prove that this contact occurs under physiological conditions. Additionally, the distinction between substrates and binding partners is ambiguous in pulldown experiments. For example, the Cristea group mapped an interactome network for the 11 metal-dependent HDACs using pulldowns and mass spectrometry (81). These data provide information regarding biological processes and proteins but do not identify substrates versus binding partners. It is possible that are some HDAC-substrate interactions are too transient and/or weak to withstand pulldown experiments and that these experiments identify non-substrate binding partners. The interactome study did, however, report association of HDAC8 with the cohesin complex proteins, which is consistent with SMC3 being a substrate (81). Alternate techniques, such as crosslinking, may be necessary to increase the detectable lifetime of an HDAC-substrate complex and increase the likelihood of identifying substrate-HDAC8 interactions. Importantly, the observation of enhanced protein acetylation after knockdown of an HDAC isozyme does not necessarily mean that the HDAC isozyme directly catalyzes deacetylation of that site. Therefore alternative methodologies such as crosslinking in the presence of HDAC8 inhibitors and *in vitro* deacetylation assays on target proteins need to be explored to enhance the future identification of HDAC8 substrates.

HDAC8 complex formation

The other class I HDACs, HDAC1, 2, and 3, are observed in complexes in the cell and their substrate specificity largely depends on the combination of proteins incorporated into their complexes (reviewed in 102). HDAC1 and 2 associate with Sin3 scaffolded complexes which serve a range of functions within the cell. The substrate specificity and function of these HDAC isozymes can change by altering the protein composition of the complex (reviewed in 103). Although HDAC8 is phylogenetically similar to the other class I HDACs, divergent evolution (14) may have altered how HDAC8 interacts with protein cofactors, possibly allowing this isozyme to function independent of other proteins. Recombinant HDAC8 catalyzes deacetylation and displays substrate specificity in the absence of additional protein cofactors (18, 56, 57, 59-61, 67, 71, 74, 76, 89, 104, 105), suggesting that HDAC8 can catalyze deacetylation *in vivo* in the absence of a protein complex. In the HDAC protein interactome, HDACs 1, 2, and 3 are grouped in large networks with significant overlap, partially due to shared functional complexes such as NuRD and CoREST (81). HDAC8, however, does not share in this linked network. This suggests HDAC8 has a unique cellular function. Nonetheless, HDAC8 does associate with other proteins (81), and these interactions likely affect the biological function and selectivity of this enzyme.

Identifying HDAC8 binding partners and distinguishing between binding partners and substrates are difficult tasks. Furthermore, binding partner data is somewhat inconsistent. 17 HDAC8 interaction partners were identified by pulldowns and subsequent SAINT mass spectrometry analysis (Significance Analysis of INTeractions), yet all but two of these have been absent in other pulldown studies (81). Differences in binding partner determinations may result from experimental differences such as cell line, HDAC8 overexpression (HDAC8-EGFP was used in (81)), or experimental and analytical methods. Some interactions may not withstand pulldown washing conditions, and mass spectrometry may not identify low abundance proteins or peptides that are not amenable to ionization. Additionally, different binding partners are likely to be observed at different points in the cell cycle, and under different cellular conditions (*e.g.* stress). Nevertheless, the interaction partners identified in the SAINT screen include cohesin components (SMC3, SMC1A, and STAG2), placing HDAC8 within the cell cycle process, protein and

ion transport proteins (SEC16A, CPNE3, and NUP98), as well as several proteins of other/unknown function (81). At least 14 of the proteins have acetylation sites, which means they could be substrates, such as SMC3 (discussed earlier).

Several binding partners have been identified by other means and illustrate the complicated nature of this search. Previous experiments have provided evidence that the HDAC1/HDAC2 complex associates with both the PP1 and CREB, leading to decreased CREB phosphorylation (101). Because an inactive HDAC1 mutant still affects CREB activity, the function of the HDAC1/HDAC2 complex was proposed to co-localize PP1 and CREB. However, it is possible that HDAC2 catalyzes deacetylation of CREB under these conditions (101). Similarly, both PP1 and CREB co-immunoprecipitate with HDAC8, and HDAC8 overexpression decreases CREB activity. These data are consistent with HDAC8 either acting as a scaffold to enhance the interaction between PP1 and CREB or catalyzing deacetylation of CREB.

HDAC8 also co-localizes with α-actin, as indicated by immunofluorescence staining (65, 83). This interaction was confirmed by pulldown experiments using human smooth muscle cells, demonstrating an endogenous association between α-actin and HDAC8 (66, 83). The function of this interaction was partially elucidated by demonstrating that siRNA knockdown of HDAC8 in human smooth muscle cells decreased the ability of cells to contract, when exposed to a collagen lattice. Furthermore, the siRNA-treated smooth muscle culture cells were smaller and unable to spread. These changes in cell morphology occurred without detectable changes to α-actin acetylation (66), suggesting that HDAC8 acts as part of a complex which modulates the cell cytoskeleton without α-actin deacetylation. Furthermore, pulldown experiments demonstrate that HDAC8 associates with the proteins Hsp20, myosin heavy chain, and cofilin (83) all of which can potentially affect actin dynamics (106, 107). It is currently unclear whether Hsp20 or cofilin are substrates for HDAC8. Because HDAC8 enhances cell contractility and associates with three proteins important for actin function, it is likely that HDAC8 is a component of a complex that modulates actin dynamics.

Additional potential HDAC8 interaction partners have been identified using a bacterial two-hybrid system (108). Two of the fifteen identified binding partners have been

examined in detail: the human Ever-Shorter Telomeres 1B (hEST1B) protein that activates telomerase activity and HOP1, an adaptor protein linking Hsp70 and Hsp90. The two-hybrid results were confirmed using co-immunoprecipitation of overexpressed hEST1B and HDAC8 in HeLa cells. HDAC8 knockdowns led to decreased telomerase activity through diminished levels of hEST1B. As HDAC8 activity does not affect the promoter region regulating hEST1B, the hEST1B level is likely not regulated by alteration in transcription. However, hEST1B levels are increased by addition of a proteasome-dependent pathway inhibitor or decreased by overexpression of ubiquitin and rescued by phosphorylated HDAC8. These results argue that phosphorylated HDAC8 protects hEST1B from polyubiquitination and subsequent degradation by the proteasome. The protective effects of phosphorylated HDAC8 on hEST1B levels are independent of deacetylase activity, remaining in the presence of the catalytically inactive His143Ala-HDAC8 mutant or after exposure of cells to TSA. Therefore, HDAC8 interacts with hEST1B but deacetylation is not required for the functional effect. To further explore the interaction between HDAC8 and HOP1 indicated by the two-hybrid experiment, the association of HDAC8 with known HOP1 binding partners was investigated. Pulldown experiments demonstrated that endogenous Hsp70 and Hsp90 co-immunoprecipitate with overexpressed HDAC8 (108). This result suggests that HDAC8, HOP1, Hsp70, and Hsp90 form a complex. One proposed mechanism for the effect of HDAC8 on telomerase activity suggests that the Hsp70-HDAC8 complex protects hEST1B from ubiquitination catalyzed by the E3 ubiquitin ligase CHIP (108). This in turn raises the levels of hEST1B and activates telomerase. Interestingly, interaction of HDAC8 with the Hsp proteins may help to elucidate the effect of HDAC8 on α-actin, since Hsp90 has been proposed to modulate α-actin dynamics (109, 110). Thus, it is possible that the HDAC8-HOP1-Hsp90 complex may regulate α-actin function.

Enzyme structure affects substrate specificity

The structure of HDAC8 yields clues about molecular recognition relevant to substrate selectivity. HDAC8 is the second smallest metal-dependent HDAC at ~42 kDa, containing little more than the catalytic domain (14, 56-58). This HDAC folds as a single

α/β domain with a core eight-stranded β-sheet surrounded by eleven α-helices (Figure 1-4A). The substrate binding surface, composed of nine loops and an 11Å tunnel leading to the active site, is proposed to have conformational flexibility based on the poor occupancy and varying positions of the loop residues in crystal structures (18, 44, 105, 111-116) (Figure 1-4B). Molecular dynamics simulations have demonstrated that residues 100 and 101 of loop L2 can flip in and out and that part of L2 can form an α-helix (116). These simulations and crystal structures of HDAC8 bound to largazole analogs demonstrate salt bridge interactions between the L1 and L2 loops (44, 116). HDAC8 flexibility is such that different loop L2 conformations are observed for two monomers in the same crystal structure (44). Furthermore, one crystal structure illuminates a bound TSA molecule interacting with residues in the hydrophobic core of HDAC8 (112) (Figure 1-5). While this may simply be an artifact, the alternative binding mode suggests that the surface of the protein can change conformation enough to allow hydrophobic molecules to intercalate between these loops and interact with the interior of the protein. The various loops in the HDAC8 structure are highlighted in Figure 1-4C.

Loops are a common structure in promiscuous enzymes (reviewed in 117) and examples of proteins, such as chymotrypsin (reviewed in 118) and carboxypeptidase A (reviewed in 119), that use loops to bind a range of substrates are abundant in nature. These loops create a number of different conformations that bind ligands through a combination of induced fit and select fit mechanisms (reviewed in 69 pp. 369-371, 120). The varied conformations and motifs provide a palette of binding sites to accommodate a multiplicity of substrates. Furthermore, long-range allosteric movements propagated through the loops may affect the active site and surrounding areas, potentially altering substrate preferences.

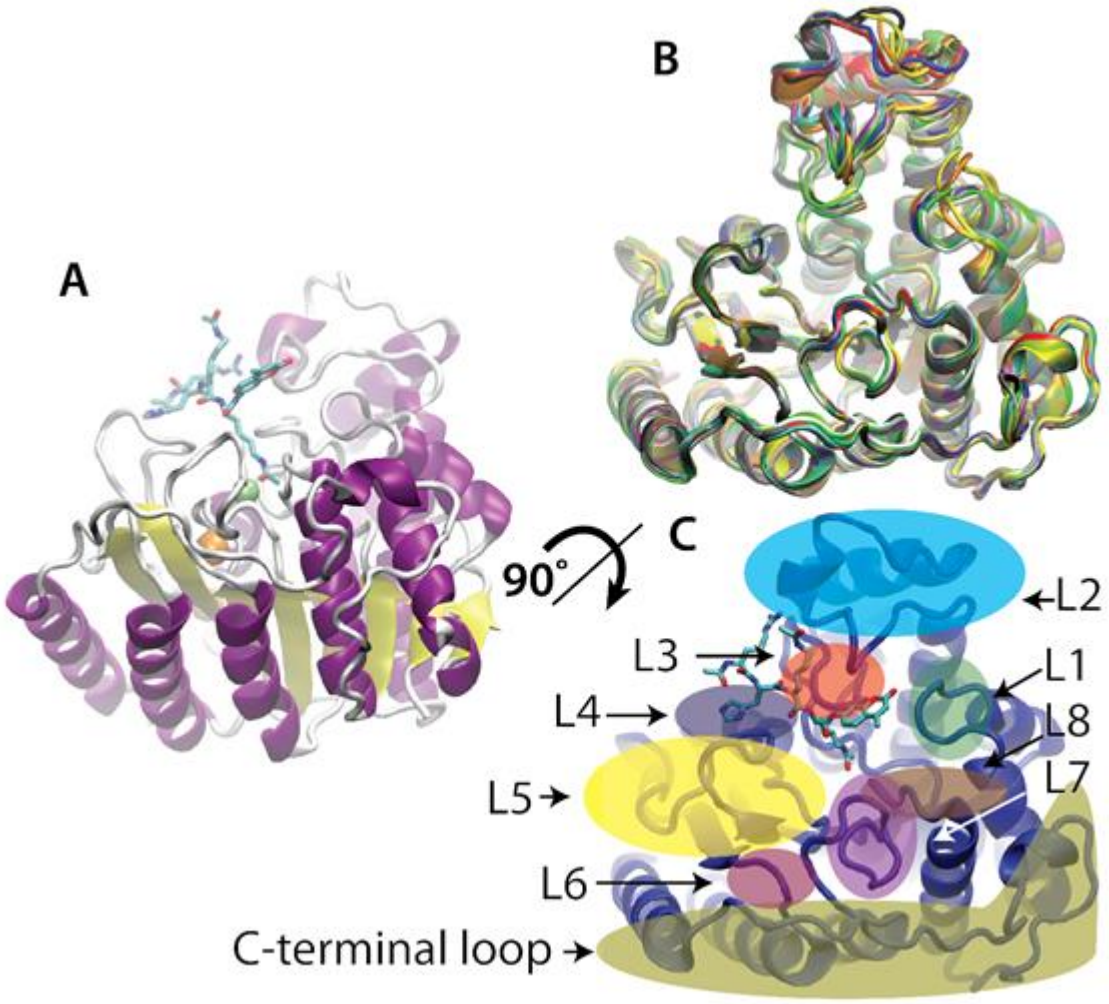

Figure 1-4: HDAC8 structures

HDAC8 structures. A. PDBID: 2V5W (111). Side view of HDAC8 with bound peptide substrate. Helices are purple, sheets are yellow, turns are white, the monovalent cations are orange, and the active site metal is colored green. The Fluor-de-Lys substrate representing the p53 sequence is colored cyan for carbon, red for oxygen, and blue for nitrogen. B. Front view of an overlay of 21 HDAC8 crystal structures in the PDB. PDBID: 2V5X, 2V5W, 1T69, 1T64, 1VKG, 1T67, 1W22, 3SFH, 3SFF, 3MZ3, 3EZT, 3FO6, 3MZ4, 3MZ6, 3MZ7, 3EW8, 3EZP, 3F07, 3F0R, 3EWF, and 3RQD (18, 105, 111-115). Structural variations are especially apparent in the L1, L2, and C-terminal loops. C. A map of the crystal structure of HDAC8 outlining the loop regions. Structure visualizations and overlay were generated with the Visual Molecular Dynamics (VMD) program and reproduced from (73) with permission from John Wiley and Sons.

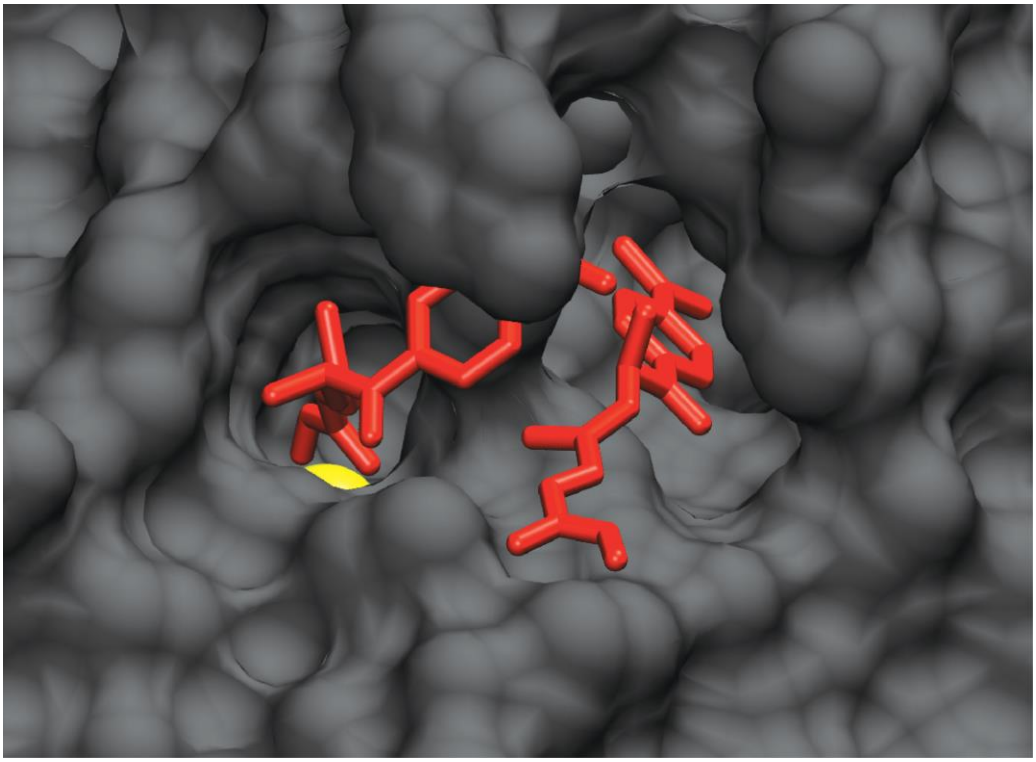

Figure 1-5: HDAC8 with two bound TSA molecules

PDBID: 1T64 (112). In this crystal structure, one molecule of TSA binds to the active site tunnel to coordinate the divalent metal ion (colored yellow) while a second TSA molecule binds nearby in between the L1, L2, and L3 loops. Image was created with the VMD program and is reproduced from (73) with permission from John Wiley and Sons.

In at least fourteen of the HDAC8 crystal structures, the enzyme crystallizes as a dimer along the substrate binding interface (18, 105, 111-114). As HDAC8 is a monomer in solution (115), the dimer interface may provide insight into long-range interactions between HDAC8 and its substrates (Figure 1-4A). To date, substrate specificity has mainly been evaluated using peptide substrates, therefore only short range interactions have emerged as HDAC8 substrate binding motifs (59-61, 71). Based on the crystal structure of bound peptides (105, 111) and biochemical measurements, these interactions include base stacking, hydrogen bonding, salt bridges, and electrostatic interactions. Base stacking between Tyr100 and the methylcoumarin of the Fluor-de-Lys peptides is observed in the crystal structure (105, 111). Similarly, base stacking between aromatic amino acids in the +1 position and Tyr100 may be important for substrate

recognition (60, 71). Additionally, hydrogen bonding between the back-bone amides of the substrate and the Asp101 side chain oxygens are important for molecular recognition (105). Salt bridges between positively charged arginines in the substrate and negatively charged carboxylate side chain oxygens, and general hydrophobic interactions can be seen in the peptide-enzyme interface (105, 111). Because of the limited number of interactions, the binding affinity may be dominated by a few strong contacts, as observed for the interaction between Tyr100 of HDAC8 and the methylcoumarin moiety of short Fluor-de-Lys peptides (71). This pi-pi interaction (~2 kcal/mol) (121, 122) is of comparable energy with other HDAC8-peptide contacts. In contrast, binding a protein substrate could involve many more contacts, including multiple hydrogen bonds (0.5-1.5 kcal/mol), hydrophobic (~1 kcal/mol), electrostatic (<1 kcal/mol) (reviewed in 69pp. 325-339), and solvent exposed salt bridge (~1-3 kcal/mol) (123) interactions. Therefore, the binding affinity could depend on a large number of interactions that together create a promiscuous substrate binding profile. Determinants of substrate specificity are still being evaluated for HDACs and further identification of binding motifs will be beneficial for understanding the biology of these enzymes.

The loops of the HDAC8 structure differentiate it from other HDACs. There are striking differences in loop size and structure between HDAC8 and the homologous polyamine deacetylase APAH (124),. These differences in the loops may be important for substrate binding, as APAH catalyzes deacetylation of small molecules including acetylated spermidine, putrescine, and spermine, while HDAC8 deacetylates macromolecules. In APAH, the L1 and L2 loops are much larger and contain many more hydrophobic residues than in the corresponding HDAC8 loops (Figure 1-6A,B), while the C-terminal loop and helix in HDAC8 are absent in APAH. Similarly, a comparison of the L1, L2, and C-terminal loops of different HDACs reveals interesting variations. The L1 and L2 loops of HDAC2 (125), 4 (126), 7 (127), and 8 (111) are more divergent in size, structure, and number of charged residues than other loops within these HDACs (Figure 1-6). For instance, the size and number of charges within the L1 and L2 loops change two-fold between HDAC8 and HDAC4. HDAC8 reportedly has a more substrate-accessible active site than un-complexed HDAC3, due in part to differences in the L1 and L6 loops (128). The substrate binding surface loops may confer isozyme-specific

substrate selectivity, as inhibitor selectivity for HDAC1 over HDAC8 has been observed and attributed to the decreased flexibility in HDAC1 loop L1 compared to L1 in HDAC8 (44, 129). Comparison of HDAC8 crystal structures illustrates that the L1 and L2 loops have the most structural variability of the loops in the proposed substrate binding surface, suggestive of a role in ligand binding. Additionally, the L2 loop interacts with inhibitors, suggesting that it may be important for molecular recognition of substrates (105). The L3 loop, which lies below the L2 loop and flanks the active site, also varies greatly in the number of charges in the loop among HDACs 2, 4, 7, and 8, consistent with a role in substrate or binding partner selectivity. The C- and N- terminal portions of the HDACs, which lie on the outer edge of the substrate binding surface, may also interact with ligands. In the HDAC crystal structures, the C-terminal loops vary in position, charge, and size and may be responsible for long distance interactions between HDACs and their substrates, or used for recognition of binding partners.

A

```
                                                                  L1 Loop
HDAC8   1    ----MEEPEEPAD-------------SGQSLV--------PVYIYSPEYVS------MCDSLAKIPKRASMVHSLIEAYA  49
HDAC2   12   ------------------------------------AKKKVCYYYDGDIGNYY----YGQGHPMKPHRIRMTHNLLLNYG  51
HDAC4   1    G-------------------------------AMTKPRFTTGLVYDTLMLKHQCTAGSSSSHPEHAGRIQSIWSRLQETG  49
HDAC7   480  GSRAQSSPAAPASLSAPEPASQARVLSSSETPARTLP-FTTGLIYDSVMLKHQCSCGDNSRHPEHAGRIQSIWSRLQERG  559
APAH    1    MRVIFSEDHKLRN-------------AKTELYGGELVPPFEAPFRAEWILAAV----KEAGFDDVVAPARHGLETVLKVH  63
                                                                  L2 Loop
HDAC8   50   LHKQMRIVK----PKVASMEEMATFHTDAYL-----QHLQKVSQEGD--DDHPDS-----IE-YGLGYDC-PATEGIFD-  110
HDAC2   52   LYRKMEIYR----PHKATAEEMTKYHSDEYI-----KFLRSIRPDNM--SEYSKQ-----MQRFNVGEDC-PVFDGLFE-  113
HDAC4   50   LRGKCECIR----GRKATLEELQTVHSEAHTLLYGTNPLNRQKLDSKKLLGSLAS-VFVRLPCGGVGVDSDTIWNEVHSA  124
HDAC7   560  LRSQCECLR----GRKASLEELQSVHSERHVLLYGTNPLSRLKLDNGKLAGLLAQRMFVMLPCGGVGVDTDTIWNELHSS  635
APAH    64   DAGYLNFLETAWDRWKAAGYKGEAIATSFPV-----RRTSPRIPTDI--EGQIGY--------YCNAAET-AISPGTWE-  126
                                          L3 Loop                                  L4 Loop
HDAC8   111  -YAAAIGGATITAAQCLIDGMCKVAINWSGG-WHHAKKDEASGFCYLNDAVLGILRLR-R-KFERILYVDLDLHHGDGVE  186
HDAC2   114  -FCQLSTGGSVAGAVKLNRQQTDMAVNWAGG-LHHAKKSEASGFCYVNDIVLAILELLKY--HQRVLYIDIDIHHGDGVE  189
HDAC4   125  GAARLAVGCVVELVFKVATGELKNGFAVVRPPGHHAEESTPMGFCYFNSVAVAAKLLQQRLSVSKILIVDWDVHHGNGTQ  204
HDAC7   636  NAARWAAGSVTDLAFKVASRELKNGFAVVRPPGHHADHSTAMGFCFFNSVAIACRQLQQQSKASKILIVDWDVHHGNGTQ  715
APAH    127  -AALSSMASAIDGADLIAAGHKAAFSLCRPP-GHHAGIDMFGGYCFINNAAVAAQRLLDK-GAKKIAILDVDFHHGNGTQ  203
          L4 Loop                  L5 Loop                  L6 Loop
HDAC8   187  DAFSFTSKVMTVSLHKFSP-GFFPGT-GDVSDVGLGKGRYYSVNVPI----QDGIQDEKYYQICESVLKEVYQAFNPKAV  260
HDAC2   190  EAFYTTDRVMTVSFHKY--GEYFPGT-GDLRDIGAGKGKYYAVNFPM----RDGIDDESYGQIFKPIISKVMEMYQPSAV  262
HDAC4   205  QAFYSDPSVLYMSLHRYDDGNFFPGS-GAPDEVGTGPGVGFNVNMAFTGGLDPPMGDAEYLAAFRTVVMPIASEFAPDVV  238
HDAC7   716  QTFYQDPSVLYISLHRHDDGNFFPGS-GAVDEVGAGSGEGFNVNVAWAGGLDPPMGDPEYLAAFRIVVMPIAREFSPDLV  794
APAH    204  DIFYERGDVFFASLHGD-PAEAFPHFLGYAEETGKGAGAGTTANYPM----GRGTPYSVWGEALTDSL-KRIAAFGAEAI  277
                      L7 Loop                                  L8 Loop
HDAC8   261  VLQLGADTIAGDP--MCSFNMTPVGIGKCLKYILQWQ-LATLILGGGGPNLANT----ARCWTYLTGVILGKTLSSEIPD  333
HDAC2   263  VLQCGADSLSGDR--LGCFNLTVKGHAKCVEVVKTFN-LPLLMLGGGGYTIRNV----ARCWTYETAVALDCEIPNELPY  335
HDAC4   284  LVSSGFDAVEGHPTPLGGYNLSARCFGYLTKQLMGLAGGRIVLALEGGHDLTAICDASEACVSALLGNELD-----PLPE  358
HDAC7   795  LVSAGFDAAEGHPAPLGGYHVSAKCFGYMTQQLMNLAGGAVVLALEGGHDLTAICDASEACVAALLGNRVD-----PLSE  869
APAH    278  VVSLGVDTFEQDP--ISFFKLTSPDYITMGRTIAASG-VPLLVVMEGGYGVPEI----GLNVANVLKGVAG---------  341
                                C-terminal Loop
HDAC8   334  HEFFTAYGPDYVLEITPSCRPDRNEPHRIQQILNYIKGNL----------KHVV  377
HDAC2   336  NDYFEYFGPDFKLHISPSNMTNQNTPEYMEKIKQRLFENL----------RML-  378
HDAC4   359  KVLQQRPNANAVRSMEKVMEIHSKYWRCLQRTTSTAGRSLIEAQTCENEEAETVT  413
HDAC7   870  EGWKQKPNLNAIRSLEAVIRVHSKYWGCMQRLAS---------------------  903
APAH         ------------------------------------------------------
```

B

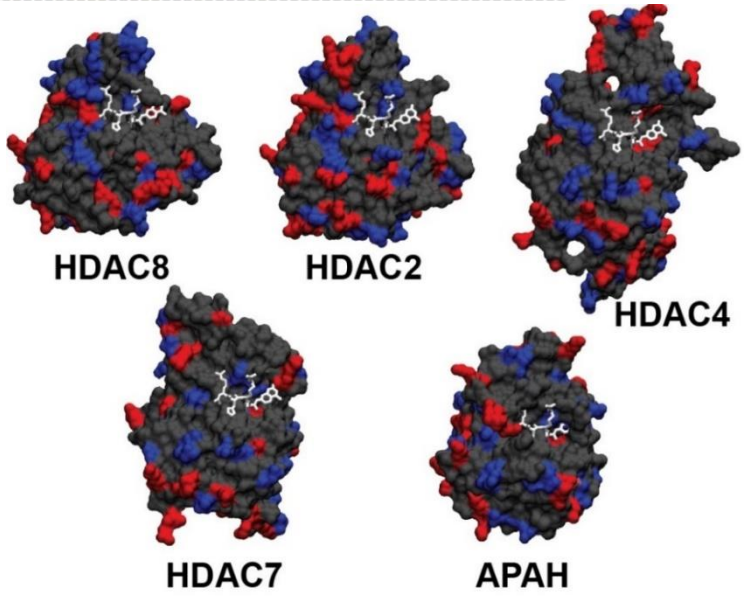

Figure 1-6: Structural comparison of HDACs

A. Aligned sequences of published HDAC crystal structures (111, 124-127). Residues in the loop regions and putative substrate binding region are yellow. Positively charged residues are red and negatively charged residues are green. Sequence alignment was performed with the constraint-based alignment tool for multiple protein sequences, COBALT (130). B. Surface visualizations of the crystal structures for HDAC2 (PDBID: 3MAX (125)), HDAC4 (PDBID: 2VQM (126)), HDAC7 (PDBID: 3C0Y (127)), HDAC8 (PDBID: 2V5W (111)), and APAH (PDBID: 3Q9B (124)). The Fluor-de-Lys substrate (white), from the HDAC8 structure, is superimposed on the structures. Positively charged residues Arg and Lys are red, and negatively charged residues Asp and Glu are blue. Structural visualizations were created using VMD and the figures are reproduced from (73) with permission from John Wiley and Sons.

Along with structural studies, peptide substrates have been useful for evaluating substrate motifs recognized by HDAC8. Reister and colleagues measured the activity of HDAC8 with a peptide library of the sequence Ac-X-Z-K(ac)-methylcoumarin, where X and Z were all amino acids except for cysteine (59). This work indicated that HDAC8 favors Pro, Met, Ala, Lys, Arg, Gln, Asp, Phe, and Ser at the -2 position and aromatic (Phe, Trp, and Tyr) and hydrophobic (Ile, Met, and Val) amino acids at the -1 position. However, the activity of HDAC8 in these assays was low, possibly due to the inclusion of the metal chelator EDTA in the assay. The Mrksich group developed a mass spectrometric assay to profile the local substrate specificities of HDACs (71). The activity of HDAC8 toward a peptide array of the sequence, Ac-G-X-K(ac)-Z-G-C-NH_2 where X and Z were any amino acid other than cysteine, showed that the most efficient substrate contains Arg and Phe at the X and Z positions, respectively (71). However, HDAC8 also catalyzes deacetylation of peptides containing the sequence X=Arg/Z= variable and X = variable/Z = Phe. HDAC8 selectivity was further screened using a peptide library with the following sequence: Ac-G-R-K(ac)-X-Z-C-NH_2 (60). These data demonstrated a preference for Arg or Phe at the X position. Furthermore, when X is Phe the identity of the Z position has only a modest effect on activity. These results suggest that specific positions and combinations of amino acids contribute significantly to the substrate recognition of small peptides, while other positions fine tune recognition.

The Mrksich group also demonstrated that distal sequences can modulate HDAC8 substrate specificity (61). Using peptides representing a partial sequence of the histone H4 tail acetylated at K12, they showed that adding a KRHR motif to the C-terminus (beginning 4 residues downstream of the acetyl-lysine) enhanced activity (61). A method for the preparation of singly-acetylated recombinant histone H3 was recently published (131), and we have used this to measure HDAC8-catalyzed deacetylation of full-length protein substrates. My dissertation demonstrates the importance of long-range interactions between HDAC8 and protein substrates in catalytic efficiency and substrate specificity.

Finally, the structure of the active site may also play a role in HDAC substrate specificity. HDAC2 and 8 have well defined 11Å channels leading to their active sites that easily accommodate an acetyl-lysine side chain, however, this tunnel is lacking in HDAC4

and 7 (111, 125-127) where only half of the channel is apparent. This modification in active site structure could suggest that HDAC4 and 7 catalyze deacetylation of alternate substrates, as proposed by Lombardi *et. al*. (124). Alternatively, these isozymes might need substrates that complement the active site to stabilize the binding of the acetyl-lysine moiety.

Catalytic mechanism and regulation of HDAC8 activity

The active site of HDAC8 contains a divalent metal ion coordinated to two aspartate and one histidine side chain (Asp178, Asp267, and His180) and one or two water molecules (Figure 1-7). The enzyme is proposed to catalyze hydrolysis using a metal-coordinated water nucleophile and general acid-base catalysis (GABC) with either one or two side chains, similar to typical metallohydrolase mechanisms, although His replaces the typical Glu/Asp GABC (Figure 1-7) (15, 105, 132, 133). The substrate binds to HDAC8 with the catalytic metal coordinating both the carbonyl oxygen of the acetyl-lysine substrate and a water molecule. In the first step of the mechanism, His143 functions as a general base to abstract a proton from the metal-bound water, as this nucleophile reacts with the carbonyl carbon to form a high energy tetrahedral intermediate. The oxyanion intermediate is proposed to be stabilized by coordination with the metal ion, hydrogen bonding with Tyr306, and electrostatic interactions with positively charged groups in the active site. Proton donation from an active site general acid to the amine leaving group accompanies breakdown of the tetrahedral intermediate to form acetate and deacetylated lysine (105, 132, 133). In the GABC mechanism originally proposed from the crystal structure of the homologous HDLP enzyme (132), His142 and protonated His143 are proposed to function as the general base and general acid, respectively. In the one GABC mechanism, H143 functions as both the general acid and general base catalyst and H142 acts as an electrostatic catalyst (105, 133), similar to the mechanism proposed for carboxypeptidase A (15). Subsequent studies utilizing mutagenesis and molecular dynamics simulations suggest a preference for the one base mechanism (68, 105, 133).

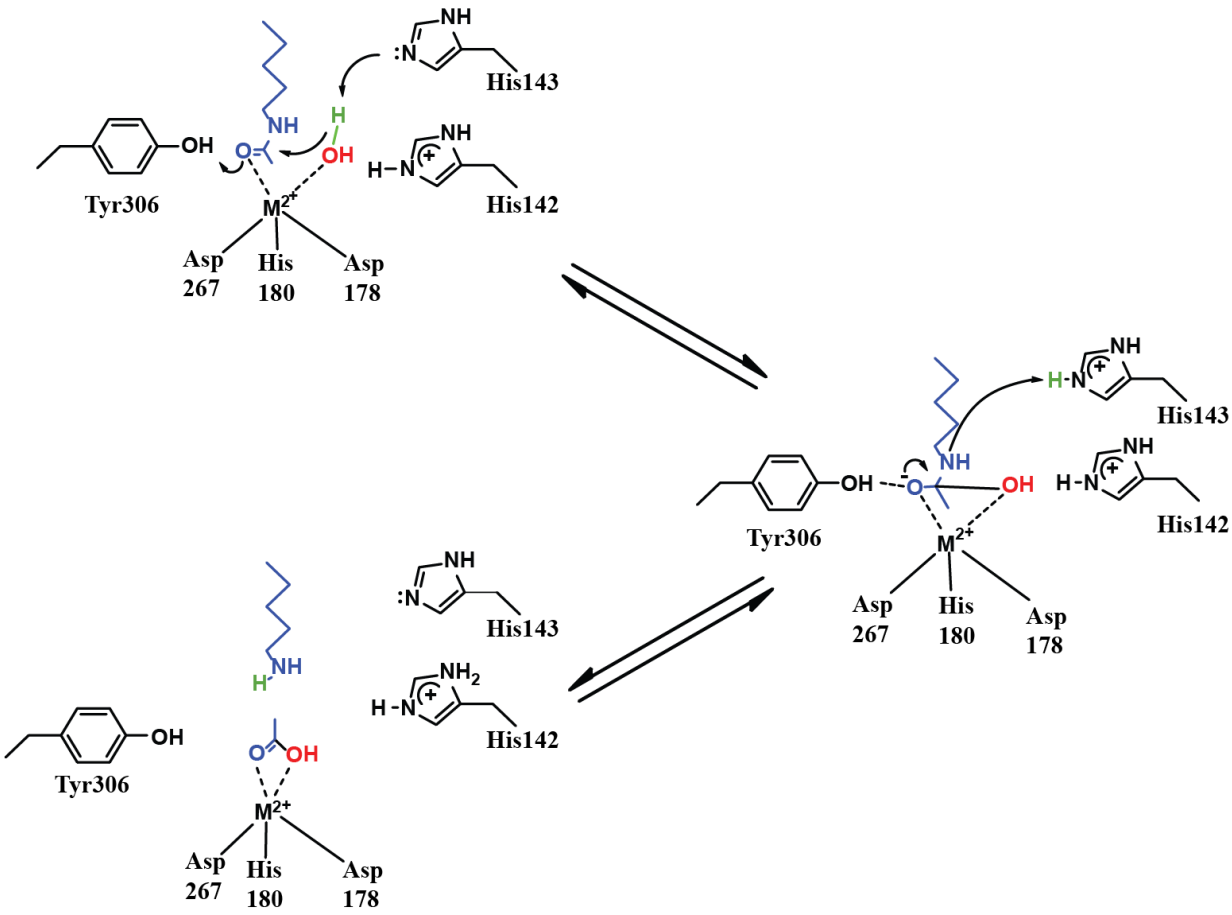

Figure 1-7: Scheme of proposed HDAC8 mechanism

Schematic of the one base mechanism for HDAC8. Blue is the acetyl-lysine substrate, while the nucleophilic water is green and red. For clarity, equilibration of exchangeable protons with solvent is not shown. The figure is adapted from (73) and reproduced with permission from John Wiley and Sons.

The HDAC8 crystal structure also contains two monovalent cation sites (18, 105, 111-114), suggesting that the activity of HDAC8 may be modulated by both the concentration and type of ions in solution. One monovalent cation site is 7 Å from the divalent catalytic metal ion and is coordinated by the side chain oxygens of Asp176 and Ser199 and the backbone carbonyl oxygens of Asp176, Asp178, His180, and Leu200. The second site is 21 Å from the divalent catalytic metal ion, and is ligated by two water molecules and the backbone carbonyl oxygens of Phe189, Thr192, Val195, and Tyr225.

The value of k_{cat}/K_M for HDAC8-catalyzed deacetylation has a biphasic dependence on the concentration of K^+ and Na^+ ions (89). In the absence of monovalent ions, the activity of HDAC8 is very low; addition of monovalent cations to Zn-bound HDAC8 increases activity with $K_{1/2,\ act}$ = 14 mM for K^+. At higher K^+ concentrations Zn-HDAC8 activity is inhibited with $K_{1/2,\ inhib}$ = 130 mM. Mutagenesis studies indicate a significant decrease in potassium inhibition in the His142Aala and Asp176Ala/Gln mutants indicating that the monovalent ion site near the active site is inhibitory. Potassium binding next to His142 has been proposed to lower the pK_a of this residue, decreasing the concentration of protonated His142, thereby lowering catalytic activity. Similar biphasic regulation has been measured for Na^+, but activation and inhibition require a five-fold and ten-fold higher concentration of Na^+ compared to K^+, respectively (89). At the 100 mM K^+ concentration within smooth muscle cells (134), HDAC8 activity is partially inhibited and sensitive to changes in the K^+ concentration.

HDAC8 is activated by a number of divalent metal ions, including Co^{2+}, Zn^{2+}, Ni^{2+}, and Fe^{2+} (67). When HDAC8 is purified under aerobic conditions, the bound metal ion is primarily Zn^{2+}. However, recombinant HDAC8 purified anaerobically from *E. coli* contains 8-fold more iron than zinc. Consistent with this, the recombinant HDAC8 activity in *E. coli* cell lysates is oxygen-sensitive (67). Additionally, although HDAC8 binds Zn^{2+} nearly 10^6-fold more tightly than Fe^{2+} (18), the affinities for both metal ions are comparable to the readily exchangeable metal concentrations estimated in living cells, suggesting that HDAC8 can bind either Fe^{2+} or Zn^{2+} *in vivo*. Furthermore, the identity of the bound metal ion alters the catalytic properties of HDAC8. When catalyzing deacetylation of the methylcoumarin-labeled p53 peptide, the k_{cat}/K_M value for Fe^{2+}-bound HDAC8 (2300 ± 160 $M^{-1}s^{-1}$) is almost three times larger than that of Zn^{2+}-HDAC8 (800 ± 50 $M^{-1}s^{-1}$). Interestingly, substitution of Fe^{2+} for Zn^{2+} also decreases the value of K_M for the substrate by five-fold and the K_I for SAHA by two-fold, suggesting that Fe^{2+} enhances ligand affinity (67). However, a comparison of the crystal structures of the hydroxamate-bound Fe^{2+}-HDAC8 and Zn^{2+}-HDAC8 shows no significant differences in the active site or the rest of the protein (18). These data suggest that either binding of the hydroxamic inhibitor stabilizes a common enzyme conformation, or that the bound metal ion affects protein dynamics that are not observable by crystallography. In this dissertation I demonstrate

that changing the identity of the active site metal ion affects HDAC8 substrate specificity toward non-fluorophore-conjugated peptides *in vitro*.

Comparison of the Zn^{2+}/Fe^{2+} metal affinities with the cellular concentrations of those metals suggests that HDAC8 could bind a combination of iron and zinc cofactors in eukaryotic cells (18). Furthermore, the cellular zinc concentration can change dramatically upon oxidative stress (135, 136) and metal toxicity (137) potentially altering the levels of readily exchangeable Fe^{2+}-HDAC8 and Zn^{2+}-HDAC8 based on cellular conditions. This provides a means by which the cell could couple HDAC8 activity to cellular stresses. This model can be expanded to propose that substrate selectivity is differentially regulated by stimuli. For example, scaffolding activators could preferentially enhance the binding of HDAC8 to a certain set of substrates. Similarly, alteration of the active site metal ion or bound monovalent ions could alter ligand specificity. For example, Fe^{2+}-HDAC8 binds the inhibitor SAHA 2-fold more tightly than Zn^{2+}-HDAC8 (89) even though Zn^{2+} is a stronger Lewis acid (reviewed in 138 pp. 337-341). This change in binding affinity suggests that the active site metal ion may contribute subtly to the structure, dynamics, and molecular recognition of HDACs.

HDAC8 localization

Most simply, protein localization may regulate HDAC8 substrate specificity by changing the effective substrate concentration. HDACs have been found to have a range of cellular locations. HDAC1 and 2 are exclusively nuclear, while HDAC6 is mostly cytoplasmic, and HDAC3, 4, 5, 6, 7, 9, 10, and 11 appear to shuttle in and out of the nucleus (139). Initially, HDAC8 was assumed to be nuclear because it has a nuclear localization sequence and was observed in the nucleus of NIH3T3 (56) and HEK293 cells (57). Upon further characterization, both nuclear and cytosolic HDAC8 have been observed. Microscopy demonstrated that HDAC8 localizes to both the cytoplasm and nucleus of embryonic smooth muscle cells, skin fibroblasts, NIH3T3 cells, and human myometrial cells (65, 83) although there remains some skepticism about this point. HDAC3, the closest HDAC8 human homologue (14), exists in both the cytoplasm and nucleus, and localization has been linked to the regulation and cellular function of this

enzyme. To what extent cellular localization plays a role in regulation of HDAC8 activity is currently unknown.

Determining the cell type-dependent expression of HDAC8 may provide interesting insights about its substrate specificity and biological function. In general, class I HDACs are ubiquitously expressed among the various cells of an organism, while class II HDACs are more cell-type specific (reviewed in 139, 140). HDAC8 (as well as the other class I HDACs) has been found in both normal epithelium and cancerous tissues from the stomach, esophagus, colon, and prostate, and has been found in breast, ovary, lung, pancreas, and thyroid carcinomas (141).

Phosphorylation of HDAC8

Post-translational modifications such as phosphorylation may also regulate HDAC8 activity. Results from a screen of three protein kinases, casein kinase II, protein kinase A (PKA) and protein kinase G (PKG), indicated that HDAC8 phosphorylation could be catalyzed by both PKA and PKG (142). PKA phosphorylation appeared to be predominant and this function was authenticated *in vivo* by incubation of cells with the PKA inhibitor H-89, which lowered HDAC8 phosphorylation levels (143). Based on consensus sequences, nineteen potential phosphorylation sites were identified in HDAC8. Phosphoamino acid analysis followed by two dimensional thin layer chromatography demonstrated modification of a serine residue (143) and, based on this information, Ser39 was identified as the only PKA phosphorylation site in the HDAC8 sequence (56, 143). A Ser39Ala HDAC8 mutant, which cannot be phosphorylated, negates phosphorylation of HDAC8 catalyzed by PKA, confirming this location as the primary phosphorylation site on HDAC8. Furthermore, phosphorylation of this site modulates HDAC8 activity. The specific activity of HDAC8 purified from cells treated with forskolin, a PKA activator, decreased by five-fold in an *in vitro* assay using purified histones as substrates (143). Furthermore, the specific activity of Ser39Glu HDAC8, a mutation that mimics phosphorylation, decreases to a level comparable to that of phosphorylated HDAC8, while the specific activity of the Ser39Ala mutant is similar to that of unmodified HDAC8. To examine whether *in vivo* effects of phosphorylation of HDAC8 correlate with the *in vitro* measurements, HDAC8-transfected HeLa cells were

treated with forskolin. These cells showed increased levels of acetylated histones H3 and H4, suggesting that the decreased deacetylase activity of phosphorylated HDAC8 led to increased histone acetylation *in vivo* (143).

Ser39 is located on the backside of the HDAC8 surface, 21Å from the catalytic metal ion (18, 105, 111-115) (Figure 1-8). Nonetheless, phosphorylation has the potential to affect the subcellular localization, protein-protein interactions, allosteric effects, and HDAC8 activity via conformational changes that propagate to the active site or enzyme-substrate interface. Ser39 lies near the junction with the L1 loop (18, 105, 111-115) that has been implicated in substrate recognition, and therefore phosphorylation at that position may alter enzyme-substrate interactions. Ser39 is located in a pocket on the enzyme surface surrounded by hydrophobic and acidic residues suggesting that phosphorylation of Ser39 could induce a drastic structural perturbation due to charge repulsion (112). Ser39 also is near the conserved Arg37 residue, which is proposed to be important for gating an acetate release channel in HDAC8 (104) (Figure 1-8). The Arg37Ala mutation decreases the k_{cat}/K_M value for Co^{2+}-HDAC8-catalyzed deacetylation of the Fluor-de-Lys substrate (R-H-Kac-Kac-fluorophore) by 530-fold (104). Based on the proximity of Ser39 to Arg37, phosphorylation at this position may affect HDAC8 activity.

.

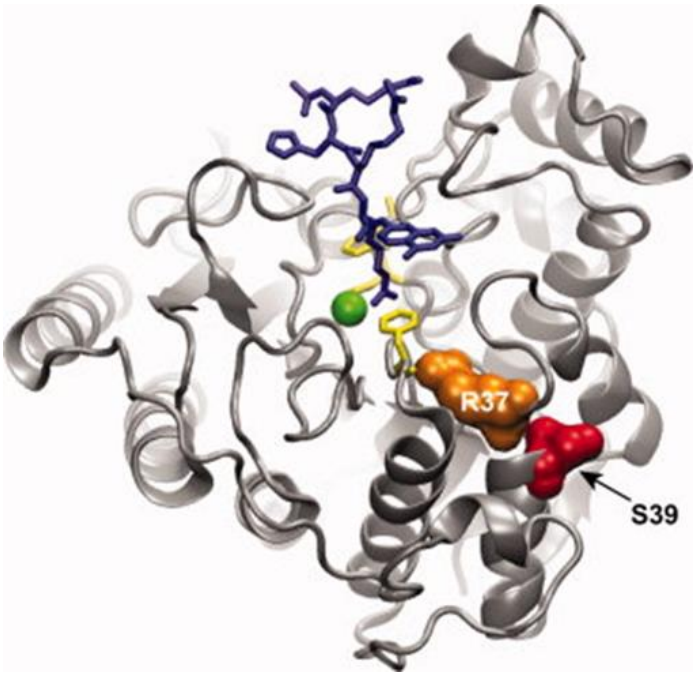

Figure 1-8: Ser39 in the HDAC8 structure

Phosphorylation of Ser39 may affect the active site structure and/or activity of HDAC8. PDBID: 2V5W (111). This structure shows that phosphorylation of Ser39 (red) is poised to potentially perturb the position and/or electrostatic environment of Arg37 (orange) and in turn, affect the active site residues (yellow). The Fluor-de-Lys substrate is blue and the active site metal is green. The structure was generated using VMD. Reproduced from (73) with permission from John Wiley and Sons.

Phosphorylation may also regulate HDAC8 through the modulation of protein-protein interactions. In the bacterial two-hybrid assay that identified fifteen HDAC8-interacting proteins (108) expression of PKA was necessary for the pulldown of six of these identified proteins, and suggests that these proteins interact solely with phosphorylated HDAC8. Two of these interactions, those between HDAC8 and hEST1B and between HDAC8 and Hsp70, were further observed by co-immunoprecipitation, showing that treatment of cells with forskolin led to increased amounts of phosphorylated HDAC8 and increased interactions (108). These data strongly suggest that HDAC8 phosphorylation regulates HDAC8 complex formation. Similarly, phosphorylation of HDAC1 and HDAC2 regulates association of these proteins with each other and complexes such as mSin3A, RbAp48 (NuRD subcomplex), and CoREST (142, 144, 145). Phosphorylation-dependent complex formation may also regulate the cellular localization of HDAC8. Fluorescence microscopy of myometrial cells shows that HDAC8 and phosphorylated HDAC8 both localize primarily to the cytosol, but cell fractionation data suggest that phosphorylated HDAC8 has increased association with the cytoskeleton compared to wtHDAC8 in this cell type (83). Phosphorylation is important for localization of other HDACs observed in both the nucleus and cytosol. HDAC4, HDAC5 and HDAC7 utilize a nuclear-cytoplasmic shuttle mechanism involving phosphorylation-dependent binding to 14-3-3 proteins (29-32). In the case of HDAC5, phosphorylation-dependent translocation is also kinase specific (146, 147). HDAC4 and HDAC5 localization is also modulated by cysteine oxidation (33-35). The mechanism through which phosphorylation potentially mediates HDAC8 localization is not known.

The Ser39 site is an interesting location for phosphorylation among HDACs. Ser39 is not conserved among class I HDACs; the residue in the corresponding position of other class I HDACs is arginine in HDAC1 and 2, and alanine in HDAC3. Also, HDAC8, HDAC5, and HDAC6 contain the only phosphorylation sites that are located within the HDAC catalytic domain (25, 35, 148, 149). In general, the effect of phosphorylation on the activity of other class I isozymes, HDAC1 and 2, is ambiguous and/or contradictory (142, 144, 145, 150, 151). For example, phosphorylation of HDAC1 had little to no effect on deacetylase activity using a synthetic histone H4 peptide (145, 150) but activity on isolated histones decreased using mutants that could not be phosphorylated (144).

Recent data demonstrate that HDAC2 is activated by phosphorylation in a residue-dependent manner (151). Therefore HDAC8 may be the most straightforward isozyme for examining the role of phosphorylation in regulating deacetylation. In this dissertation I present kinetic, structural, and simulation data for a phosphomimetic HDAC8 mutant. The phosphomimetic HDAC8 demonstrates altered substrate binding, decreased HDAC8-catalyzed deacetylation of peptides, and an increased rate constant for metal dissociation from the active site.

Many HDACs undergo additional post-translational modifications such as acetylation, ubiquitination, and sumoylation (reviewed in 25, 35), but additional *in vivo* modifications of HDAC8 have not yet been demonstrated. HDAC8 has a consensus motif for glycosylation at Asn136 that could be modified (56, 143); however the NetNGlyc 1.0 server does not predict N-glycosylation of this site due to the lack of a signal peptide (152). HDAC8 can be *S*-nitrosylated *in vitro*, and this has an inhibitory effect on catalysis (153). Acetylation was recently reported for HDAC2 (154) and has been observed at multiple sites on HDAC1 (155). Two of the HDAC1 sites are located in the deacetylase domain and four sites are near the C-terminus; acetylation of these sites inhibits HDAC1 deacetylase activity toward histones *in vitro* and corepressor function *in vivo* (155). The two sites in the deacetylase domain, Lys218 and Lys220, are located near the activating monovalent cation binding site, so decreased activity from acetylation of these residues may arise from alteration of monovalent cation binding (155). Sequence alignment by COBALT indicates that the Lys218 position in HDAC1 is conserved in the corresponding Lys221 position in HDAC8 (130). As this monovalent site activates HDAC8 allosterically (89), it is feasible that HDAC8 activity could be regulated by modification at this location. However, no modifications at this site have yet been observed and post-translational modifications of HDAC8 need to be further examined.

Concluding remarks

Due to the prevalence and critical functions of acetylation within the cell, enzymes that catalyze acetylation and deacetylation are regulated by an ever-growing collection of mechanisms. One mode of regulating HDAC activity is alteration of the substrate preferences for these enzymes, which in turn affects cellular processes. This regulatory

mechanism may allow the cell to finely tune the substrate preference for many HDACs simultaneously by allowing the same stimuli to differentially alter the activity, localization, and interactions of each HDAC isozyme. Understanding the relationships between diverse cellular stimuli and HDAC regulation will provide insight into the intricacies of cellular processes and disease formation. Even though HDAC8 has been extensively studied, there are vast areas of the field in need of further characterization, such as identification of HDAC8 substrates and binding partners, subcellular localization, and regulatory mechanisms. In light of the complicated HDAC regulation landscape, there are likely many factors affecting substrate recognition that have yet to be discovered. As we continue to investigate these factors, we enhance our understanding of the cellular function of HDACs as well as inform the broader field of cellular regulation by post-translational modifications.

Acknowledgements

The authors thank Dr. Patrick O'Brien for his useful insight into the paper's contents, Tony Mustoe for his help with visualization of molecules, Mark Taylor, Felicia Gray, Alison Tebo, and members of the Fierke Lab for their critical reading of this paper and discussion. This material was supported, in whole or in part, by the National Institutes of Health Grants NIGMS GM40602 (CAF), T32-GM-008353 (NAW), and 5-T32-GM-008597 (CAP). This material is based upon work supported by the National Science Foundation under Grant No. DGE0718128 (NAW).

Chapter 2

Histone deacetylase 8 recognizes histone substrates via both long and short range interactions[1,2]

Introduction

Histone deacetylases (HDACs) are a group of 18 enzymes that catalyze the hydrolysis of the acetyl moiety from acetyl-lysine residues in proteins (5, 156). The acetylation of proteins, catalyzed by KATs, alters a variety of protein properties (3) such as protein-protein and protein-ligand interactions and protein stability. These changes can lead to alterations in a number of downstream cellular events (9, 10). Regulation of acetylation by the respective activities of KATs and HDACs is important for effective cellular signaling and cellular homeostasis, and aberrant acetylation/deacetylation can result in diseases ranging from neurological disorders (157, 158) to cancers (8, 159). Identifying the specific substrate set for each HDAC isozyme should lead to both an enhanced understanding of the role of HDACs in disease progression and better treatments of these diseases.

Elucidating HDAC substrate specificity is challenging, at least partially because multiple HDACs may catalyze deacetylation of the same substrate. Additional complications for interpretation of the genetic studies are the difficulty in discerning whether the observed phenotypes are due to loss of a direct interaction between HDAC and another protein, inhibition of deacetylation of a substrate, or a downstream effect

[1] Reproduced from a manuscript in preparation: Pitcairn, C. A.*; Wolfson, N. A.*; Kuo, Y.-M.; Leng, K. R.; Andrews, A. J.; Fierke, C. A., Histone deacetylase 8 recognizes histone substrates via both long and short range interactions. *Co-first authors. *In preparation.*

[2] Noah A. Wolfson and Carol A. Fierke designed the study. Noah A. Wolfson designed the assays and performed the peptide and tetramer assays. Noah A. Wolfson, Carol Ann Pitcairn, and Katherine R. Leng purified proteins and performed octamer assays. Carol Ann Pitcairn and Katherine R. Leng assembled nucleosomes and performed nucleosome assays. Noah A. Wolfson, Carol Ann Pitcairn, and Carol A. Fierke analyzed the data. Yin-Ming Kuo performed and Andrew J. Andrews designed the histone mass spectrometry analysis. Noah A. Wolfson, Carol Ann Pitcairn, and Carol A. Fierke prepared the manuscript.

caused by perturbed acetylation of another HDAC substrate. Substrate identification is also difficult because HDAC-substrate interactions are weak (the Zn(II)-HDAC8 K_M for a commercial HDAC8 peptide substrate is 1.1 mM (67)), in contrast to higher affinity protein binding partners that frequently form complexes with HDACs, which make pulldown experiments to identify substrates difficult. To mitigate these difficulties, the HDAC field has sought to identify sequence motifs that define each isozyme's substrate specificity (59-61, 71). To date, most studies have utilized short peptides to determine HDAC recognition motifs. However, the validity of using peptides to mimic the recognition of proteins has not yet been established. The role of long-range interactions and secondary structural elements is still unexplored, as there has been little characterization of HDAC activity toward protein substrates.

Many HDACs are found in complexes where the protein binding partners may moderate substrate recognition (160). HDAC8 has historically been considered to act independently of a protein complex (18, 59-61, 67, 71, 89, 105), and therefore assays with HDAC8 should reflect *in vivo* activity. HDAC8 is the best understood HDAC, with numerous crystal structures (18, 44, 105, 111-115, 161), kinetic studies (67, 89), and peptide substrate specificity studies (59-61, 71). This background provides a good platform for further investigation of HDAC substrate recognition.

While a few putative HDAC8 substrates have been identified, such as ERRα (46) and SMC3 (47, 51), the protein substrate set for HDAC8 is currently unclear. Proteomic studies of HDAC8 have identified tens of substrates and/or binding partners (45-47, 65, 66, 81, 95, 108), and a combination of HDAC8-specific inhibitors with proteomic studies have led to a number of additional proposed substrates, including ARID1A (80). Many of the putative HDAC8 substrates are difficult to purify and generation of singly acetylated proteins for kinetic study has been challenging, precluding *in vitro* HDAC8 assays. As a result, previous studies of HDAC8 selectivity have assayed non-specifically acetylated protein substrates (56, 57). Kinetic parameters measured using these substrates provide little information about substrate preference, as these proteins contain multiple acetylation sites that are likely deacetylated at different rates.

HDAC8 is localized to both the cytosol and nucleus (56, 57, 66, 83, 139), and has been suggested to catalyze the deacetylation of histones. *In vivo* H3 acetylation levels differ modestly upon the overexpression of HDAC8 in HEK293 cells (58); and the HDAC8 inhibitor SAHA conjugated to pyrrole-imidazole polyamide (SAHA-PIP, also called Jδ) increased acetylated H3 levels and expression of HDAC8-regulated transcription factors in mouse embryonic fibroblasts (MEF) (162). HDAC8 can catalyze deacetylation of core histones and H3-based peptides in vitro (76, 143). However, H3 was not identified as a substrate in a proteomic study using an HDAC8-specific inhibitor (80). H3 can be prepared with singly acetylated lysines (131), and is amenable to mass spectrometric assays (163) so it is an interesting and practical target to study HDAC substrate specificity toward full-length proteins.

To elucidate HDAC8 substrate specificity and recognition of protein substrates, we present the first detailed kinetic study of HDAC-catalyzed deacetylation of singly acetylated full-length substrates. Singly acetylated lysine side chains are incorporated into H3 using unnatural amino acid incorporation (131, 164) and we directly compare HDAC8 activity toward peptide substrates and protein substrates with the same primary sequences. Furthermore, we analyze the effect of large histone complexes (histone core octamer and mononucleosome) on HDAC8-catalyzed deacetylation of Ac-H3. We demonstrate that deacetylation of acetylated full-length H3 tetramer and octamer complexes catalyzed by HDAC8 is significantly (> 10-fold) faster than that of acetylated peptides, although the addition of nucleic acid to form mononucleosomes yields activity comparable to that of peptides. HDAC8 recognizes H3 peptide tetramer substrates largely based on the six amino acids proximal to the acetyl-lysine. These results indicate substrate specificity is determined by both long-range contacts and short range contacts for H3 substrates.

Materials and methods

Reagents

Adenosine triphosphate (ATP), Coenzyme A, nicotinamide adenine dinucleotide (NAD^+), L-malic acid, citrate synthase, malate dehydrogenase, and propionic anhydride

were purchased from Sigma. Peptides were purchased from Peptide 2.0 Inc. Zinc used to reconstitute HDAC8 was purchased as an ICP standard (GFS Chemicals) or atomic spectroscopy standard (Fluka) and the acetic acid standard was purchased from Ricca Chemical Company. Chelex 100 resin was purchased from Bio-Rad. Acetyl-lysine was purchased from Chem-Impex Chemical International Inc. All other materials were purchased from Fisher or Sigma and were of a purity >95 % unless otherwise noted.

HDAC8 expression and purification

HDAC8 was expressed and purified using the method described previously (67, 72) with the following modifications. BL21 (DE3)pHD4-HDAC8-TEV-His6 *E. coli* were used to express HDAC8 in modified autoinduction-TB medium (12 g/L tryptone, 24 g/L yeast extract, 8.3g/L Tris-HCl, 4 g/L lactose, 1 g/L glucose, 10 mL/L glycerol, pH 7.4) supplemented with 100 µg/mL ampicillin and 200 µM $ZnSO_4$. The cells were grown overnight at 30°C and harvested 20 - 24 hours post inoculation (9,000 x g, 10 min, 4°C). Alternatively, BL21 (DE3)pHD4-HDAC8-TEV-His6 *E. coli* cells were grown in 2xYT at 37°C to an OD_{600} of 0.5. The temperature was reduced to 20°C and after one hour cells were induced with 0.5 mM IPTG and $ZnSO_4$ was added to a final concentration of 200 µM. Cells were harvested after 16 hours. The cell pellet was resuspended either in low salt DEAE buffer (50 mM HEPES, 200 µM $ZnSO_4$, 1 mM TCEP, 50 mM NaCl, 5 mM KCl, 1 µg/mL tert-Amyl methyl ether (TAME), 10 µg/mL PMSF, pH 7.8) or buffer A (30 mM HEPES pH 8, 150 mM NaCl, 5 mM KCl, 1 mM TCEP, 1 mM imidazole) and lysed using a microfluidizer (Microfluidics). In some cases, nucleic acids were precipitated by addition of 0.1% polyethylenimine (pH 7.9) followed by centrifugation (39,000 x g, 45 min, 4°C) and HDAC8 fractionated on a DEAE Sepharose column with a stepwise salt elution (50 mM HEPES, 200 µM $ZnSO_4$, 1 mM TCEP, 5 - 500 mM NaCl, 5 mM KCl, pH 7.8) and dialyzed against 50 mM HEPES, 100 mM NaCl, 25 mM imidazole, pH 7.8. HDAC8 with or without DEAE fractionation was further purified by metal affinity chromatography using Ni(II)-charged chelating sepharose fast flow (GE) and either a continuous (26 - 250 mM) or stepwise (50 mM/250 mM) imidazole gradient. Following TEV protease cleavage of the HIS tag during dialysis in Buffer A without imidazole, HDAC8 was separated from TEV

protease on a second Ni column. HDAC8 was then dialyzed against metal-free chelation buffer (25 mM MOPS pH 7.5, 1 mM EDTA, 1 mM TCEP, 5 mM KCl) overnight, followed by metal-free buffer (25 mM MOPS pH 7.5, 1 mM TCEP, 5 mM KCl). In some cases, the protein was further purified by size exclusion chromatrography prior to metal-free dialysis using a HiPrep 16/60 Sephacryl S200 HR column (GE) (30 mM HEPES pH 8, 150 mM NaCl, 1 mM TCEP). Finally, residual EDTA was removed with a PD-10 column (GE) (25 mM HEPES pH 8, 127 mM NaCl, 3 mM KCl, and 1 mM TCEP) and HDAC8 was concentrated, aliquoted, and stored at -80°C. HDAC8 activity was confirmed using the Fluor-de-Lys assay as described previously (67, 70, 165).

HDAC assay

Assays of deacetylation of acetylated peptides catalyzed by HDAC8 were performed using an enzyme-coupled assay, as previously described (72) with a few modifications. Briefly, depending on their solubility, peptides were dissolved in water, 50% acetonitrile, or 10% DMSO. The dissolved peptide solutions were chelated by incubation with Chelex resin at 4°C for more than three hours. Peptide concentrations were measured using the fluorescamine assay or absorbance at 280 nm, as previously described (72, 166). Peptides (0-100 µM) were incubated in HDAC8 assay buffer (50 mM HEPES, 137 mM NaCl, 3.7 mM KCl, pH 7.8) for 10 minutes at 30°C before initiating the reactions with the addition of 0.5 µM Zn(II)-HDAC8. Acetate formation was coupled to NADH formation measured by an increase in fluorescence (Ex = 340 nm, Em = 460 nm). Initial rates were fit to the linear portion of the time versus product curve.

Histone expression and purification

Recombinant H3 histones containing a single acetylated lysine were expressed and purified as previously described (131) with a few modifications. The acetyl-lysine is incorporated into expressed proteins at an amber codon site (TAG) using a tRNA-cognate tRNA synthetase pair encoded on the pAcKRS-3 plasmid (131). Amber codons were substituted for the K9, K14, and K56 codons in the His_6-tagged histone H3 sequence in

the PCDF PyLT-1 plasmid (generous gift from Jason Chin) (131, 164) using Quikchange PCR. BL21 (DE3) cells were transformed with the mutant or wild type PCDF PyLT-1 and pAcKRS-3 plasmids for H3 expression. Expression plasmids for preparation of recombinant H2A, H2B, and H4 *Xenopus* histones were generous gifts from Geeta Narlikar. BL21(DE3) cells were transformed with the respective plasmids and grown in LB or 2xYT supplemented with the proper antibiotic (kanamycin and streptomycin for H3, or ampicillin for H2A, H2B, and H4) at 37°C until reaching an OD_{600} of 0.7. To express full-length histone H3 proteins with a single acetyl-lysine residue 20 mM nicotinamide and 10 mM acetyl-lysine were added to the medium follow by induction of protein expression by the addition of 0.5 mM IPTG 30 minutes later. For expression of the other histones, the cells were induced with 0.5 mM IPTG. The cultures were harvested 3 - 4 hours after induction (5,053 - 9,000 x g, 10-15 min, 4°C). The cell pellets were stored at -80°C.

Histones were purified according to established protocols (167, 168). Cell pellets were resuspended in Phosphate Buffered Saline (PBS) supplemented with 20 mM nicotinamide and lysed using the M110L Microfluidizer (Microfluidics). The lysate was centrifuged (26,892 x g or 39,000 x g, 45 min, 4°C) and the supernatant was discarded. The pellets were resuspended and centrifuged twice in PBS with nicotinamide and 1% (v/v) Triton X 100 and twice in PBS with nicotinamide. The pellets were then macerated in DMSO and incubated at room temperature for 30 - 60 minutes. After incubation, 6 M guanidinium chloride, 20 mM Tris, and 2 mM dithiothreitol (DTT), pH 8 was added and incubated with shaking at 37°C for at least 1 hour. Subsequent purification of H3 was performed under denaturing conditions, as in (131) with the buffer modified to include 7 M urea and 1 mM TCEP, using two nickel columns as described for HDAC8: a first nickel column with elution by an imidazole gradient, followed by cleavage of the His-tag with TEV protease, and then a second nickel column to remove the protease (131). If the protease precipitated out of solution during dialysis, the second nickel column was omitted. For H2A, H2B, and H4 purification, the DMSO mix was centrifuged as above and dialyzed against 7 M urea, 100 mM sodium acetate (NaOAc), 20 mM Tris, 100 mM NaCl, pH 7.5 overnight at 4°C. The dialyzed protein extract was applied to an SP sepharose column, washed (7 M urea, 100 mM NaOAc, pH 5.2) and eluted stepwise with SP buffer (7 M urea, 100 mM NaOAc, pH 7.5) supplemented with 300 mM, 500 mM or 1 M NaCl.

The fractions containing H2A, H2B, and H4 (confirmed by SDS-PAGE) were collected and dialyzed at least twice in ultrapure water (Milli-Q, Millipore) containing 2 mM 2-mercaptoethanol (BME). After dialysis, the histones were lyophilized and stored at -80°C. Tetramer, octamer, and nucleosome were reconstituted as previously described (131, 167, 168). Tetramer and octamer were purified by size exclusion chromatography. Tetramer, octamer, and nucleosome were dialyzed with and without EDTA to remove contaminating metals. Octamer and nucleosome were subsequently treated with Chelex resin for at least 1 hour at 4°C to ensure metal removal. Nucleosome was stored in 20% glycerol, 20 mM HEPES pH 7.5 – 7.8, 1 mM TCEP.

Protein deacetylation assays

Apo-HDAC8 was reconstituted with stoichiometric Zn(II) for 1 hour on ice in HDAC8 assay buffer (50 mM HEPES, 137 mM NaCl, 3.7 mM KCl, pH 7.8) (67). Histone complexes were incubated in assay buffer (above) for 10 minutes at 30°C before initiating reactions by addition of 0 - 15 µM Zn(II)-HDAC8. The final concentration of NaCl in the assays with octamer was 137 or 239 mM NaCl. Reactions were quenched by addition of 25% trichloroacetic acid at varying times. The samples were incubated for 30 minutes on ice and then centrifuged (16,000 x g, 10 min, 4°C). The supernatant was removed and the pellet was washed 2 times with acetone and centrifuged after each wash. The pellet was dried in a SpeedVac System (Thermo Savant) and frozen at -80°C. The pellets were resuspended in 2 µL propionic anhydride and 6 µL ammonium hydroxide (NH_4OH) and incubated at 51°C for 1 hour. 30 µL of 50 mM NH_4HCO_3 was added to each tube, and the pH of each tube was adjusted to 7 – 9 using NH_4OH. Then 0.2 µg sequence grade trypsin (Promega) was added and incubated overnight at 37°C. Then 3.5 µL of 10% formic acid was added to each tube, and the tubes were centrifuged (16,000 x g, 10 min, 4°C). The supernatants were transferred to autosampler mass spectrometry vials and deacetylation was quantified by MS/MS mass spectrometry analysis in the lab of Andrew Andrews (Fox Chase Cancer Center) as previously described (169). The kinetic data were analyzed using a single exponential decay: $\frac{\text{Substrate}}{(\text{Substrate+Product})} = e^{-k_{obs} \times t}$. Nucleosome reaction initial

rate data were fit to a linear equation. Variation of mass spectrometry results between days was less than 20%. Data were fit using Prism (GraphPad Software, Inc.).

A concern with assaying octamer under low salt conditions (HDAC8 assay buffer and less than 240 mM NaCl) is that the octamer would disassemble into H3/H4 tetramer and H2A/H2B dimers. However the $K_{1/2,\ inactivation}$ for NaCl-dependent inhibition of HDAC8 (320 ± 140 mM for Co(II)-HDAC8) precluded higher salt concentrations (89). The observed kinetics for the tetramers and octamers are significantly different and suggest that the octamers, once assembled, remain intact during our assays.

Results

Sequence determines peptide specificity of HDAC8

To date, many papers determining HDAC substrate specificity have utilized acetylated peptides (60, 61, 71, 73), predicated on the assumption that HDAC8 uses the same interactions to recognize peptide and full-length protein substrates. To test the validity of this assumption, we examined the kinetics of deacetylation of peptides mimicking three biologically relevant acetylation sites on the putative HDAC8 substrate histone H3 for comparison to HDAC8 activity toward full-length proteins (Figure 2-1) and Table 2-1). We utilized histone H3 because histone H3 was shown previously to be amenable to non-natural acetyl-lysine incorporation (131). Two sites (H3K9ac and H3K14ac) are found within close proximity to each other on the N-terminal tail and share an unfolded secondary structure. Because these sites differ only in amino acid sequence, the role of primary sequence in HDAC8 substrate specificity can be probed. A third site (H3K56ac), located on an α-helix in the globular structure of H3 (Figure 2-1), allows the role of secondary structure in HDAC8 substrate recognition to be investigated. Peptides containing 7 amino acids (7-mer) representing the 3 amino acids upstream (-3) and downstream (+3) of the acetyl-lysines were synthesized. This complements the activity of HDAC8 with peptides containing 3 to 6 amino acids, which were used previously (60, 61, 71). The rates of HDAC8-catalyzed deacetylation of the H3K9ac, H3K14ac, and H3K56ac peptides were measured under multiple turnover conditions, using an assay coupling acetyl-lysine deacetylation to the formation of NADH (72). The initial rates were linearly

dependent on peptide concentration, indicating that the K_M values are higher than the peptide concentrations used in this assay (> 100 µM). The value of k_{cat}/K_M, the specificity constant, is the best parameter to compare the activity of HDAC8 toward multiple substrates (170-172). HDAC8 has the highest catalytic efficiency for catalyzing hydrolysis of the H3K56ac peptide (k_{cat}/K_M = 78 ± 8.0 $M^{-1}s^{-1}$), followed by the H3K9ac (56 ± 6.0 $M^{-1}s^{-1}$) and H3K14ac (8.0 ± 0.70 $M^{-1}s^{-1}$) peptide (Table 2-2).

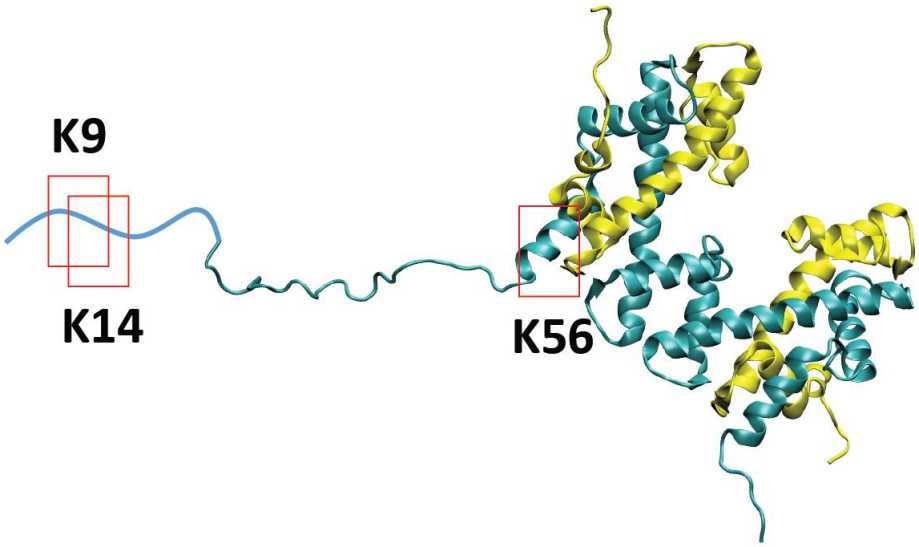

Figure 2-1: Structure of histone H3/H4 tetramer with highlighted acetylation sites

Structure of histone H3/H4 tetramer (167) with boxes around the sites which were acetylated. H3 is shown in blue and H4 in yellow. H3 residues 1 to 20 are shown in an extended conformation as they have no discrete fold within the crystal structure. The structure was generated from PDB ID 1AOI using VMD.

Table 2-1: Sequences of peptides used in this study

All peptides contained N-terminal acetylation and C-terminal carboxamide.

	7-mer peptide	13-mer peptide
H3K9ac	Ac-TARKacSTG-NH_2	Ac-TKQTARKacSTGGKA-NH_2
H3K14ac	Ac-TGGKacAPR-NH_2	Ac-RKSTGGKacAPRKQL-NH_2
H3K56ac	Ac-RYQKacSTE-NH_2	Ac-EIRRYQKacSTELLI-NH_2

Table 2-2: Catalytic efficiencies for deacetylation of histone substrates by HDAC8[a]

Substrate	7-mer Peptide	13-mer peptide	17-mer peptide	Tetramer	Octamer	Nucleosome
	k_{cat}/K_M ($M^{-1}\,s^{-1}$)			$k_{max}/K_{1/2}$ ($M^{-1}\,s^{-1}$)		
H3K9ac	56 ± 6	51 ± 3	120 ± 11	>24,000	3700 ± 100	28 ± 3
H3K14ac	8.0 ± 0.7	21 ± 4	-	2,500 ± 70	1,000 ± 200	-
H3K56ac	78 ± 8	100 ± 10	-	4,000 ± 600	-	-

[a] HDAC8 activity was measured and catalytic efficiencies were determined as described in the Experimental Procedures and the legend of Figures 2-4.

To probe the importance of amino acids further removed from the acetyl-lysine in determining substrate selectivity, longer peptides (13 and 17 amino acids) were assayed (Table 2-1). H3K9ac was assayed in the context of each peptide length and protein complex (tetramer, octamer, and nucleosome). The H3K14ac and H3K56ac sites were assayed as 7 and 13 amino acid peptides and select protein complexes for comparison. Increasing the length of the peptides from 7 to 13 amino acids had little to modest effects on catalytic efficiency (0.9 to 2.6-fold change) and did not affect the substrate specificity

trend of K56ac > K9ac > K14ac. A 17 amino acid peptide representing the H3K9ac site also showed less than a three-fold increase in k_{cat}/K_M compared to the 7-amino acid peptide (56 ± 6.0 $M^{-1}s^{-1}$ vs 120 ± 11 $M^{-1}s^{-1}$; Table 2-2). The modest differences in activity toward the longer peptides indicate that the primary sequence surrounding the acetylated lysine residue (+/- 3 of the acetyl-lysine) is the largest determinant of selectivity in peptide substrates, consistent with previously published data (59-61, 71).

HDAC8 catalyzes deacetylation of H3/H4 tetramers more efficiently than H3 peptides

To investigate the importance of long-range HDAC8-substrate interactions in substrate recognition, we compared the rates of peptide deacetylation to the rates of full-length protein deacetylation catalyzed by HDAC8. A major challenge in identifying HDAC substrates is determining the rates of deacetylation for individual acetyl-lysine sites, as HDAC substrates, such as histones, may have multiple acetylated lysine residues. We prepared proteins with single acetyl-lysine sites using the method of recombinant non-natural amino acid incorporation developed by Jason Chin's group. (131, 164) Q-TOF LC/MS of modified histone H3 demonstrated a mass change corresponding to an added acetylated lysine (data not shown). To stabilize H3, it was assembled into a H3/H4 tetramer. We measured HDAC8 activity toward the singly acetylated H3 proteins acetylated at the H3K9, H3K14, and H3K56 sites under single turnover (STO) conditions (3-15 μM HDAC8 and 0.5 μM acetylated H3/H4 tetramer) and assayed deacetylation by mass spectrometric analysis. STO was used to minimize the amount of singly acetylated H3/H4 tetramer. An exponential decay was fit to the reaction progress curves to generate the observed rate constants, k_{obs} (Figure 2-2A). The three sites showed differential dependence on the concentration of HDAC8. H3K9acH3/H4 tetramer has little dependence on HDAC8 concentration indicating that the enzyme concentration is above the $K_{1/2}$ for the reaction, even at the lowest concentration (3 μM). In contrast, H3K14acH3/H4 and H3K56acH3/H4 tetramers show hyperbolic and nearly linear dependence, respectively, on the HDAC8 concentration. Assuming rapid equilibration of the HDAC8-H3/H4 complex, a hyperbolic fit to these data yield values of $k_{max}/K_{1/2}$ equal to >24,000 $M^{-1}s^{-1}$, 2500 ± 70 $M^{-1}s^{-1}$, and 4000 ± 600 $M^{-1}s^{-1}$ for the H3K9ac, H3K14ac, and

H3K56ac tetramers, respectively (Figure 2-2B–D and Table 2-2). Each of these catalytic efficiencies is 10- to 100-fold faster than the corresponding peptide k_{cat}/K_M values. These specificity parameters can be directly compared assuming that product release is not rate limiting under multiple turnover conditions. Previous data suggest that the deacetylation step is likely the rate-limiting step (see discussion), also suggesting that $K_{1/2}$ and K_M reflect K_D (67, 76). These data demonstrate that interactions outside of short peptide sequences are important for enhancing HDAC8 substrate selectivity. The observed increase in catalytic efficiency is mainly due to a decrease in $K_{1/2}$ in the STO reaction relative to K_M for the peptides, suggesting enhanced binding of the protein substrates. While H3 peptides have K_M values higher than 100 µM, (data not shown) the H3K9ac/H4 tetramer has a $K_{1/2}$ value < 1 µM and the H3K14ac/H4 tetramer has a $K_{1/2}$ = 19 ± 1 µM. These differences suggest that long-range interactions enhance activity of HDAC8 toward full-length substrates.

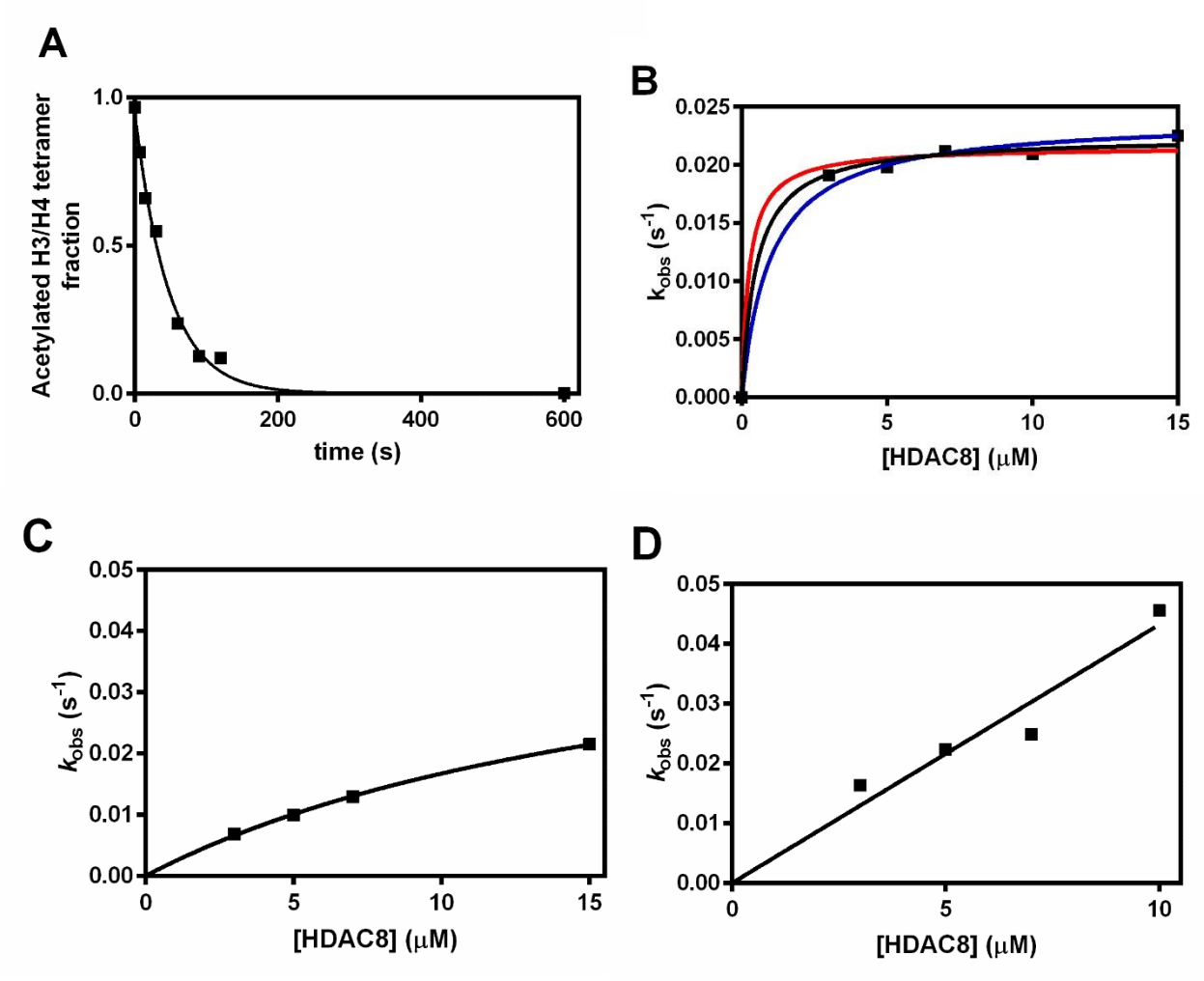

Figure 2-2: Single turnover deacetylation of singly acetylated H3/H4 tetramers

A. Sample data from deacetylation reaction with 7 μM HDAC8 and 0.5 μM H3K9ac/H4 tetramer (1 μM acetyl-lysine) measured using mass spectrometry. Data are best described by a single exponential. B. Dependence of apparent deacetylation rate constant of H3K9ac/H4 on the concentration of HDAC8. The k_{obs} is almost independent of [HDAC8]. Three separate hyperbolic fits bracket potential $K_{1/2}$ values: $K_{1/2}$ = 0.25 μM (red); $K_{1/2}$ = 0.5 μM (black); $K_{1/2}$ = 1 μM (blue). These fits demonstrate that the $K_{1/2}$ is < 1 μM and $k_{max}/K_{1/2}$ is > 24,000 $M^{-1}s^{-1}$. The data points are from multiple measurements in a single reaction at each HDAC8 concentration. C. Dependence of deacetylation rate of H3K14ac/H4 on the concentration of HDAC8. The data points are from multiple measurements in a single reaction at each HDAC8 concentration. A hyperbolic fit indicates that the $k_{max}/K_{1/2}$ is 2,500 ± 70 $M^{-1}s^{-1}$. D. Dependence of deacetylation rate of H3K56ac/H4 on the concentration of HDAC8. The data points are from multiple measurements in a single reaction at each HDAC8 concentration. A linear fit indicates that the $k_{max}/K_{1/2}$ is 4,000 ± 600 $M^{-1}s^{-1}$.

While the increased substrate length enhances substrate recognition in all three cases, the ratio of HDAC8 catalytic efficiency toward the protein versus peptide substrates is different for each acetylation site. The largest observed enhancement in catalytic efficiency is for the H3K9ac substrates (>400-fold increase with the tetramer substrate), followed by H3K14ac (~300-fold) and then H3K56ac (~50-fold). In particular, the modest selectivity of HDAC8 for catalyzing cleavage of H3K56ac peptide compared to H3K9ac peptides is not maintained in the tetramer substrates, as would be expected if sequence was the only determinant of substrate recognition. In the context of a full-length protein, the H3K9ac site on the H3 tail is more accessible than the H3K56ac site, which is within a helix, likely explaining the reversed preference of these two sites. The fact that H3K14ac is the least favorable substrate may be dictated by the amino acid sequence, since structurally it is expected to be similar to H3K9ac. Another explanation of decreased HDAC8 activity toward the H3K56/H4 site is that the binding surface of an α-helix is better characterized by the -3, 0, and +3 residues and therefore a linear peptide may not be a good representative of this site.

Octamer substrates fall between peptides and tetramers in substrate specificity profile

To further examine substrate selectivity, we measured the deacetylase activity of HDAC8 toward histone octamer complexes containing single acetylation sites at either H3K9ac or H3K14ac. Histone octamers were reconstituted with two copies of each core histone (H2A, H2B, H3Kac, and H4). The deacetylation rate catalyzed by HDAC8 was measured under single turnover conditions and analyzed as described above. The resulting k_{obs} values for H3K9ac octamer are linearly dependent on the HDAC8 concentration (Figure 2-3), yielding a $k_{max}/K_{1/2}$ value of 3700 ± 100 $M^{-1}s^{-1}$. Deacetylation of the H3K14ac octamer has a hyperbolic dependence on HDAC8 concentration leading to a value of $k_{max}/K_{1/2}$ of 1,000 ± 200 $M^{-1}s^{-1}$. This catalytic efficiency is decreased 3-fold compared to the H3K14ac/H4 tetramer and is ~45-fold faster than the deacetylation of H3K14ac peptides. These data suggest that the K14ac site is recognized similarly in the octamer and the tetramer by HDAC8. The catalytic efficiency for the H3K9ac octamer site, however, is decreased 12-fold compared to that of H3K9ac tetramer.

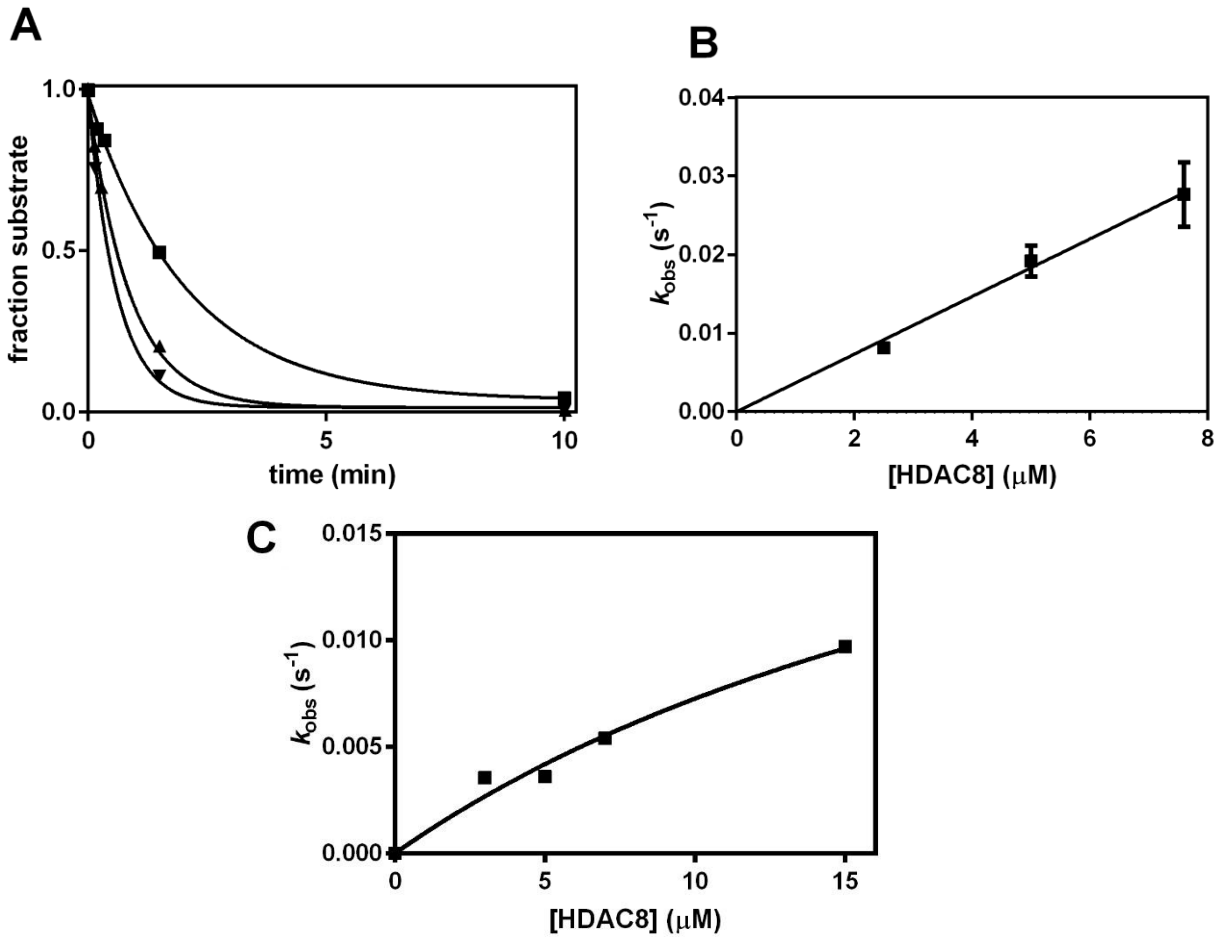

Figure 2-3: Single turnover deacetylation of singly acetylated H3 octamers

A. Reaction progress curves for deacetylation of H3K9ac octamer catalyzed by 2.5 μM (■), 5 μM (▲), and 7.5 μM (▼) HDAC8. Data points are from multiple measurements in a single reaction at each HDAC8 concentration, and a single exponential was fit to the data. B. Dependence of apparent deacetylation rate constant of H3K9ac octamer on the concentration of HDAC8. Data points are from multiple measurements in a single reaction at each HDAC8 concentration, and error bars on k_{obs} values represent errors calculated from the exponential fits. A linear fit of the data indicates that the $k_{max}/K_{1/2}$ is 3700 ± 100 $M^{-1}s^{-1}$. C. Dependence of apparent deacetylation rate constant of H3K14ac octamer on the concentration of HDAC8. The data points are from multiple measurements in a single reaction at each HDAC8 concentration. A hyperbolic fit indicates that the $k_{max}/K_{1/2}$ is 1,000 ± 200 $M^{-1}s^{-1}$.

HDAC8-catalyzed deacetylation of acetylated nucleosome is slow

HDACs involved in transcriptional regulation are likely to encounter nucleic acid-bound substrate proteins. To test the specificity for HDAC-catalyzed deacetylation of a larger substrate complex containing nucleic acid, we incorporated H3K9ac into recombinant mononucleosomes. These were assayed in the same manner as the tetramer and octamer substrates (Figure 2-4). Surprisingly, the addition of nucleic acid to the octamer to assemble nucleosomal substrates significantly decreased HDAC8 catalytic efficiency at this site, $k_{max}/K_{1/2}$ = 28 ± 3 $M^{-1}s^{-1}$. This is two-fold lower than the k_{cat}/K_M for the H3K9ac 7-mer peptide and ~900 fold slower than deacetylation of this site in the H3/H4 tetramer. Adding the DNA component of the nucleosome to an assay with the Fluor-de-Lys peptide resulted in only a 25% decrease in HDAC8 activity (data not shown); thus the 130-fold decrease in HDAC8 activity observed between octamer and nucleosome substrates is unlikely to be due to DNA inhibition of the enzyme.

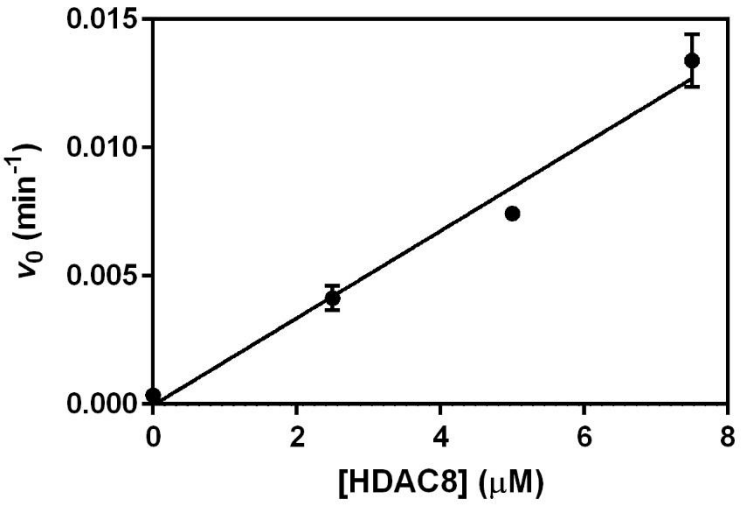

Figure 2-4: Single turnover deacetylation of singly acetylated H3 nucleosome

Progress curves for deacetylation H3K9ac nucleosome catalyzed by 0 – 7.5 μM HDAC8 were fit linearly to calculate initial rates. The data points are from multiple measurements in a single reaction at each HDAC8 concentration, and error bars represent errors calculated from the initial rate fits. A linear fit of the data indicates that $k_{max}/K_{1/2}$ 28 ± 3 $M^{-1}s^{-1}$.

Discussion

To understand the role of HDACs in cellular regulation, it is important to determine the substrate specificity and the molecular determinants of substrate recognition for each isozyme. Until now, HDAC recognition of protein substrates has largely been tackled by studying activity toward peptide substrates, which typically interact with less than an 8 Å x 20 Å area of an approximately 2025 $Å^2$ binding surface (111). Within this larger binding interface there may be many more HDAC8-protein substrate contacts, including potential recognition hotspots and negative interaction sites. With a peptide, a single interaction of 0.5 - 2 kcal/mol can alter the catalytic efficiency by 50-fold (72). With a larger substrate, the increased number of interaction sites could overcome the 2 kcal/mol of energy obtained from local interactions. There is a precedent for distal HDAC8-substrate interactions in recognition of a long peptide substrate; an upstream KRHR motif (based on histone H4) increases HDAC8-catalyzed deacetylation of an acetylated peptide (61). To investigate the role of long-range interactions on HDAC8 substrate recognition, we measured HDAC8-catalyzed deacetylation of substrates of increasing complexity, from peptide to full-length protein to protein-nucleic acid complex.

To analyze HDAC8-catalyzed deacetylation of peptide and protein substrates, we compared multiple turnover reactions (k_{cat}/K_M) of peptide substrates to single turnover ($k_{max}/K_{1/2}$) reactions of the protein substrates. This was due mainly to the challenge of preparing singly acetylated substrates. The apparent second order rate constants measured under these two conditions measure comparable reactions since a variety of data suggest that the hydrolytic step is the slowest step for peptide substrates preceded by rapid, equilibrium substrate binding. For example, HDAC8 catalyzes deacetylation of trifluoroacetate peptide substrates faster than non-fluorinated peptides (k_{cat}), ruling out product release as the rate-limiting step (76). Furthermore, the k_{cat}/K_M values for peptides are significantly slower than diffusion control (10^2-10^3 $M^{-1}s^{-1}$ vs 10^7-10^8 $M^{-1}s^{-1}$) and the K_M values are large (> 100 µM), suggesting that substrate association is also not rate-limiting. However, additional experiments will be done to further demonstrate that the single turnover and multiple turnover data are comparable.

The protein substrates have remarkably enhanced catalytic efficiency in comparison to the comparable peptide. Previous analysis of activity toward acetylated peptide substrates has shown that HDAC8 prefers substrates with aromatic amino acids on the C-terminal side of the acetyl-lysine (+1 position) (60, 71). Based on these empirical data, the mediocre catalytic efficiency of the histone H3-based peptides (10 to 10^2 $M^{-1}s^{-1}$) (Table 2-2) was predicted. The interactions between the 7-mer peptides and HDAC8 occur within a ~10 Å radius of the active site. HDAC8 catalyzed hydrolysis of the acetylated H3/H4 tetramers, which still lack an aromatic residue in the +1 position, is 50 - 400 times faster than the corresponding peptides. Thus, HDAC8-tetramer interactions that are absent with the peptide substrates enhance HDAC8 substrate recognition. The catalytic efficiency of the acetylated H3/H4 tetramer increased by 2-4 kcal/mol, lowering the activation energy[1] and demonstrating the importance of longer range interactions for protein substrate recognition by HDAC8. The H3K9ac/H4 tetramer has both the highest value of $k_{max}/K_{1/2}$ and the largest increase in activity compared to the corresponding peptide (>400-fold) that may be due to one or a few strong interactions or a number of weak interactions. However, the lower tetramer-induced enhancement values for deacetylation of H3K14ac (300-fold) and H3K56ac (50-fold) tetramers indicate that this is not a nonspecific protein-protein-interaction. The Mrksich group previously demonstrated that distal HDAC8-substrate interactions can have a significant effect on peptide deacetylation and proposed an exosite model which involves binding at the active site and at a second location elsewhere on the HDAC8 surface (61). Perhaps the slightly shifted interaction of HDAC8 with the K14ac and K56ac sites on the tetramer offers less rate enhancement due to a decrease in additional, non-active site binding interactions, and therefore these sites have limited full-length protein rate enhancement. Additionally, the different HDAC8 catalytic efficiencies likely reflect both variations in the interactions between HDAC8 and substrate residues surrounding the acetyl-lysine, as previously demonstrated (61) and differences in accessibility of the acetyl-lysine to the active site.

The crystal structure of HDAC8 is useful in visualizing the potential protein-protein interactions involved in full-length substrate recognition. In many crystal structures

[1] $\Delta\Delta G = RT*\ln((k_{cat}/K_{M1})/(k_{cat}/K_{M2}))$

HDAC8 forms a dimer at the substrate binding interface, as part of the fundamental crystal unit. The HDAC8 substrate binding interface is a flexible 45 Å x 45 Å surface containing multiple interaction sites, including 10 van der Waals interactions and 6 hydrogen bonds between the HDAC8 dimers (112, 115). The interactions observed between these two HDAC8 units provide a framework for explaining the differences in catalytic efficiency observed for peptide and full-length substrates. The 2-4 kcal/mol difference between the peptide and tetramer affinity could be explained by the van der Waals interactions and/or hydrogen bonds that are observed in the dimeric crystal structures. The dimer also visualizes repulsive charge-charge interactions. The attractive and repulsive protein-protein interactions likely work in concert to determine the HDAC8 substrate specificity. The HDAC8-substrate binding interface is mainly composed of flexible loops. Recent crystal structures have shown conformational changes in HDAC8 loops L1 and L2 upon binding of largazole analogs, as well as different L1 and L2 loop conformations between two monomers of the same crystal structure, demonstrating the adaptability and importance of these loops in HDAC8 inhibitor and substrate binding (44). These loops likely are important for conferring structural selectivity for large protein substrates.

Further increasing the size and complexity of the substrate protein complex in the histone octamer did not further enhance the catalytic efficiency. The H3K14ac histone octamer was deacetylated with a similar catalytic efficiency to the corresponding tetrameric substrate, suggesting that interactions with the tetramer are sufficient to explain HDAC8 substrate interactions in that case. In contrast, the H3K9ac octamer was deacetylated at least 12 fold slower than the tetrameric substrate. This is likely due to decreased accessibility of the acetyl-lysine to the HDAC8 active site, although other effects including protein-protein interaction, and allosteric effects could be involved in the recognition of these proteins. Addition of the nucleic acid component to form a nucleosome converted the most efficient substrate, the H3K9ac/H4 tetramer, to a substrate that is less efficiently deacetylated by HDAC8 than the corresponding peptide. The drastic decrease in $k_{max}/K_{1/2}$ for nucleosomal H3K9ac likely reflects decreased substrate accessibility due to precluded binding of the substrate to the distal HDAC8 binding interface, blocking the HDAC8 active site tunnel, or direct binding of the acetyl-lysine on the H3 tail by the nucleosome. One possibility is that the positively charged

histone H3 tail interacts with the negatively charged DNA in the nucleosome and is no longer accessible to HDAC8. The data are consistent with proteomic studies suggesting that histones are not physiological substrates for HDAC8 (80). However, the low activity observed for nucleosomal acH3K9ac does not completely preclude deacetylation by HDAC8 under all conditions. The chromatin structure can be altered by transcription factors, DNA binding proteins, chromatin remodeling factors and other proteins, possibly complexed with HDAC, to alter the accessibility of the acetylated lysines in the tail of H3.

This work presents a study of HDAC8 substrate recognition and the first report of detailed kinetics for HDAC8-catalyzed deacetylation of singly acetylated full-length protein substrates. HDAC8 catalyzes deacetylation of tetrameric protein substrates with catalytic efficiencies >10-fold greater than corresponding peptide substrates. Larger protein complex substrates have decreased catalytic efficiencies. The differences in catalytic efficiency represent the effects of HDAC8-protein substrate interactions which are absent in HDAC8-peptide interactions. This work provides a foundation for the study of full-length protein substrate specificity of HDACs.

Acknowledgements

We thank members of the Fierke laboratory for helpful discussions and comments on the manuscript. We thank Jeffrey E. López for collaborating on HDAC8 purification. We thank Dr. Jason Chin (Medical Research Council) for non-natural amino acid incorporation plasmids and Dr. Geeta Narlikar (University of California San Francisco) for histone expression plasmids. We thank the members of Geeta Narlikar's lab and Felicia Gray (University of Michigan) for histone purification and nucleosome assembly protocols and we thank Dr. Ted Huston and Dr. Lubomír Dostál (University of Michigan) for performing ICP-MS and the Ramamoorthy and O'Brien labs for use of their lyophilization instruments. We thank Brandon Ruotolo, and Yueyang Zhong for their determination of the histone tetramer stoichiometry.

We gratefully acknowledge that this work was supported in part by a National Science Foundation predoctoral fellowship (N.A.W.), National Institutes of Health Grant 5-R01-GM-040602 (C.A.F.), the University of Michigan Chemistry-Biology Interface (CBI) training program NIH grant 5T32GM008597 (C.A.P.), Rackham Graduate School (C.A.P.) and Cellular Biotechnology Training Program T32-GM008353 (N.A.W. and K.R.L.).

Chapter 3

Metal switching specificity: A novel regulatory mechanism for HDAC8[1,2]

Introduction

Protein lysine acetylation is an enzymatically reversible post-translational modification. Acetylation is catalyzed by twenty lysine acetyl transferases (KATs) while hydrolysis of the acetyl moiety is catalyzed by eighteen lysine deacetylases, including the metal-dependent histone deacetylases (HDACs) and the NAD(+)-dependent sirtuins (SIRTs). The balance of the enzymatic activities of HDACs and KATs is involved in many cellular processes (173). These enzyme families control the acetylation state of the >3800 acetylated sites in the mammalian proteome (1), and it is therefore important to understand the mechanisms by which the enzyme specificities are regulated (11, 174). Elucidating the determinants of HDAC substrate specificity is important for understanding the regulatory mechanisms of acetylation/deacetylation in the cell and for engineering selectivity in therapeutics.

HDAC8 is a member of the class I metal-dependent HDACs. HDAC8 is well understood biochemically, but its cellular role and regulation are still under investigation. It is primarily expressed in human smooth muscle cells and is found in both the nucleus and the cytoplasm (56, 65). The precise HDAC isozyme substrate sets remain largely undefined, but the list of putative HDAC8 substrates includes nuclear proteins, such as structural maintenance of chromosomes protein 3 (SMC3) (47, 51, 80, 175) and histone proteins (57), and several cytosolic substrates such as estrogen-related receptor alpha

[1] Reproduced in part from manuscript in preparation: Joseph, C. G.*; Pitcairn, C. A.*; Scholle, M. D.; Mrksich, M.; Fierke, C. A., Metal switching specificity: A novel regulatory mechanism for HDAC8. *Co-first authors. *In preparation*.

[2] Caleb G. Joseph performed the SAMDI high-throughput screen, Carol Ann Pitcairn performed the peptide assays in solution, Michael D. Scholle performed the MALDI mass spectrometry, and Milan Mrksich designed the SAMDI experiments. Caleb G. Joseph and Carol Ann Pitcairn analyzed the data, and Carol Ann Pitcairn, Caleb G. Joseph, and Carol A. Fierke wrote the manuscript.

(ERRα) (46, 73). HDAC8 is also sensitive to monovalent cation concentrations. The structure demonstrates two monovalent ion binding sites (18, 44, 105, 111-115); the site farther from the active site is activating, while the site near the catalytic metal is inhibitory (89). HDAC8 was originally proposed to be a zinc-dependent enzyme since zinc co-purified with the enzyme and was observed in the first HDAC8 crystal structure (115, 132), however several metal ions activate the enzyme and substrate specificity and inhibitor efficacy *in vitro* are dependent on the metal identity (67). The trend for k_{cat}/K_M values catalyzed by metal-substituted HDAC8 is Co(II) > Fe(II) > Zn(II) > Ni(II) > Mn(II) (67). Furthermore, the inhibition constant, K_i, of the T-cell lymphoma drug suberoylanilide hydroxamic acid (SAHA) follows a similar dependence on the identity of the metal bound to HDAC8 (Co(II) < Fe(II) < Zn(II)) (18).

Crystal structures of metal-substituted HDAC8 have not explained the differential activation and inhibition. Structures of HDAC8 bound to Fe(II), Co(II), Mn(II), and Zn(II) and hydroxamic acid inhibitors demonstrate a common penta-coordinate, square pyramidal geometry for the metal-substituted enzyme forms (18). These structures are a snapshot and do not show conformational changes or dynamic interactions that may occur when substrate is bound to the enzyme. Additionally, the hydroxamic acid inhibitor likely forces the active site into the metal coordination state observed in the crystal structure regardless of the identity of the bound metal ion.

Based on cellular metal concentrations and the affinity of HDAC8 for each metal, either Zn(II) or Fe(II) could activate the enzyme *in vivo*. Exchangeable Zn(II) is less available than Fe(II) in cells; although concentrations differ with cell type and subcellular location, the ranges are 5 pM – 2 nM exchangeable zinc and 0.2-12 μM exchangeable iron (136, 176-181). HDAC8 has a 10^6-fold higher affinity for Zn(II), at 5 ± 1 pM, compared to Fe(II) and is not activated by Fe(III) (18, 67, 182). Lysine deacetylase activity in both bacterial and mammalian cell lysates is oxygen sensitive, suggesting Fe(II)-dependent activity (67, 183). Moreover, immunopurified HDAC8 overexpressed in human tissue culture cells demonstrates oxygen-sensitive activity (183). Taken together, these data suggest that iron may play a role in cellular HDAC8 activation and regulation and demonstrate the importance of determining which metal/s activate HDAC8 *in vivo*.

Because cellular metal concentrations are dynamic, sometimes changing very rapidly (184), metalloproteins could be equipped to adapt to altered metal levels by either recognizing metal flux as a trigger for an alternate activity level or substrate set or by not exchanging metal ions rapidly and thus retaining the original metal. In bacteria there is a precedent for metal switching in UDP-3-O-((R)-3-hydroxymyristoyl)-N-acetylglucosamine deacetylase (LpxC) and N-acetyl-1-D-myo-inosityl-2-amino-2-deoxy-alpha-D-glucopyranoside deacetylase (MshB), which switch between Fe(II) or Zn(II)(185, 186), and a precedent for metal-dependent substrate and inhibitor specificity for the *E. coli* methionine aminopeptidase (*Ec*MetAP), which is activated by Co(II), Mn(II), Fe(II), or Zn(II) *in vitro* (187, 188). Similarly metal alteration in human HDAC8 may be a novel regulatory mechanism for this and other eukaryotic metalloenzymes.

Prompted by the enhanced activity of Fe(II)-HDAC8 and the oxygen sensitivity of this enzyme in cell extracts, we further investigated the role of the identity of the catalytic metal ion in regulating HDAC8 activity and substrate specificity *in vitro.* Here we show that the activity and substrate selectivity of HDAC8 is dependent on the metal ion in the active site; the specificity toward peptide substrates changes when the active-site metal ion is switched between Fe(II) and Zn(II). In cells, HDAC8 may switch metals with changing cellular availability of Fe(II) and Zn(II), potentially initiated by oxidative stress (18, 189). In our proposed model, HDAC8 is Fe(II)-bound in cells until a change in metal homeostasis increases the exchangeable Zn(II) concentration, yielding Zn(II)-HDAC8. This work suggests a new mechanism by which the specificity and activity of HDAC8 may be regulated.

Materials and methods

Metal free HEPES, NaCl, KCl, and NaOH are from Sigma, and TCEP is from GoldBio. All other reagents were purchased from Fisher unless otherwise specified.

HDAC8 purification

HDAC8 was prepared using the following method, modified from (67). HDAC8TEVHis6 was transformed into BL21DE3 Z competent cells and grown in 2xYT supplemented with 100 µg/mL ampicillin at 37°C and 170 rpm until OD_{600} 0.4 – 0.7. The temperature was decreased to 20°C for 45 – 60 minutes, followed by induction with IPTG (0.5 mM) and addition of $ZnSO_4$ (0.2 mM). Cells were harvested 15-16 hours post-induction by centrifugation (5,000 rpm, 15-20 minutes, 4°C) and resuspended in HDAC8 resuspension buffer (30 mM HEPES pH 7.8-8, 100-150 mM NaCl, 5 mM KCl, 1 – 16 mM imidazole, and 1 mM TCEP) supplemented with a cOmplete™ protease inhibitor cocktail tablet (Roche). Cells were lysed by microfluidizer, in some cases followed by nucleic acid precipitation with polyethyleneimine (pH 7.9). After centrifugation (26,000 – 27,000 x g, 45 min, 4°C), HDAC8 was loaded onto a Ni(II)-charged chelating sepharose (GE Healthcare) gravity column equilibrated with HDAC8 purification buffer (30 mM HEPES pH 8, 150 mM NaCl, 5 mM KCl, 1 mM TCEP) supplemented with 1 mM imidazole. The column was washed with 20 mM imidizole purification buffer and HDAC8 was eluted in a linear gradient (25 – 250 mM imidazole). The His6 tag was cleaved by His6-tagged TEV protease during overnight dialysis HDAC8 purification buffer to remove imidazole. A second, stepwise nickel column separated HDAC8 from the protease. HDAC8 was eluted in the flow through and 20 mM imidazole steps. HDAC8 was concentrated in 10k or 30k MWCO Amicon Ultra centrifugal concentrators at 2,800 – 3,2000 rpm and subjected to metal-free dialysis in metal-free buffer A (1 mM EDTA, 25 mM MOPS pH 7.5, 1 mM TCEP, 5 mM KCl) followed by metal-free buffer B (25 mM MOPS pH 7.5, 1 mM TCEP, 5 mM KCl). In some cases a PD-10 column (GE Healthcare) in either PD-10 buffer A (25 mM HEPES pH 7.4 - 7.8, 150 mM NaCl, 3 mM KCl, 1 mM TCEP) or PD-10 buffer B (25 mM MOPS pH 7.5, 1 mM TCEP) was used to remove residual EDTA. HDAC8 was aliquoted, flash frozen in liquid nitrogen, and stored at -80°C. Concentration was measured by absorbance at 280 nm using the extinction coefficient 52,120 $M^{-1}cm^{-1}$, which was determined empirically in (68).

High-throughput SAMDI mass spectrometric deacetylation assay

The specificity screens were performed using Self-Assembled Monolayers for MALDI-TOF Mass Spectrometry (SAMDI). The SAMDI assays were performed as previously published (60, 61, 71, 190). Peptides were transferred to an array plate having 384 gold islands, each having a monolayer presenting a maleimide group at a density of 10% against a background of tri(ethylene glycol) groups. In this way, the peptides underwent immobilization through the side chain of the terminal cysteine residue while the glycol groups play the important role of preventing non-specific adsorption of proteins to the monolayer. The array was treated with HDAC8 by distributing 3 µL portions of a solution (0.5 µM enzyme, 25 mM Tris pH 8.0, 147 mM KCl, 3 mM NaCl) using a 12-channel pipette. The solutions were kept at 37°C for 30 min and the reactions were then stopped by rinsing the array plate with ethanol. Separate controls were performed using ICP-MS to measure metal contamination in HDAC8 reactions from several SAMDI plates. Zn(II) was found at 0.5- to 1-fold the HDAC8 concentration, not including Zn(II) added for reconstitution.

Enzyme-coupled assay for in-solution peptide assays

Peptides (Peptide 2.0) had acetylated N-termini and carboxamide C-termini. Zn(II)- and Fe(II)-HDAC8 were reconstituted as described in (67, 182). Apo-HDAC8 (10 µM) was reconstituted with stoichiometric Zn(II) (Fluka) in peptide assay buffer (20-25 mM HEPES pH 8, 137 mM NaCl, 3 mM KCl) and incubated for 1 hour on ice. For Fe(II)-HDAC8, apo-HDAC8 was equilibrated in an anaerobic glove bag (Coy Laboratory Products) for one hour prior to reconstitution. Solid iron(II) chloride (Sigma), L(+)-ascorbic acid (Fluka), and peptide assay buffer were equilibrated in the anaerobic chamber at least overnight. Fe(II) (100 µM) in 5 mM ascorbate and assay buffer was prepared daily. Fe(II)-HDAC8 (10 µM) was reconstituted anaerobically with 5-fold excess Fe(II) in assay buffer and 2.5 mM ascorbate for 1 hour in a 0-4°C CoolBox (Biocision). Assays were performed aerobically within 2 hours, the effective working time for ascorbic acid to maintain Fe(II) (data not shown). The enzyme-coupled assay was performed as in (72). Fe(II)- and Zn(II)-HDAC8 and peptides in assay buffer were equilibrated to 30°C and reactions were initiated with

enzyme (1 µM HDAC8, 50 – 1200 µM substrate). Time points were quenched with hydrochloric acid, flash frozen in liquid nitrogen, and stored at -80°C. Assay workup was performed as in (72). Standards were prepared from acetic acid (Ricca Chemical Company). Time points were neutralized with sodium bicarbonate, and centrifuged (16,000 x g, 1 minute), and added to equilibrated coupled enzyme solution (50 mM HEPES pH 8**,** 0.4 to 9.4 mM ATP, 0.01 – 2.1 mM NAD^+, 30 – 730 µM CoA, 0.07 U/µL CS, 0.04 – 0.08 U/µL MDH, 50 µM ACS, 8 - 100 mM NaCl, 2.4 - 3 mM KCl**,** 33 - 100 mM MgCl, 2.5 - 46 mM L-malic acid, pH 8) in a 96-well plate (Corning #3686). The fluorescence of the resulting NADH was measured using a POLARstar fluorescence microplate reader (ex. filter = 340 nm, em. filter = 460 nm) and a linear equation was fit to the data to calculate initial rates.

Results and discussion

Mass spectrometry screen

As an initial screen to identify potential differences in specificity with different active site metals, we performed a high-throughput SAMDI screen of a 361-peptide array and showed that the substrate selectivity of HDAC8 is metal ion-dependent (71). The peptides were of the form GXK^{Ac}ZGC, where the flanking residues X and Z were varied across nineteen amino acids (all natural residues excluding cysteine). The monolayers were analyzed by matrix-assisted laser desorption-ionization mass spectrometry using the SAMDI method to observe the substrate and product of the reaction (Figure 3-1). The extent of deacetylation for each peptide was determined by the ratio of the deacetylated peak area to the sum of the peak areas for the substrate and product.

We prepared HDAC8 reconstituted with Fe(II) or Zn(II) and applied each of these enzyme forms to the peptide array. In both cases we observed deacetylation of multiple substrates. For Zn(II)-HDAC8, 172 of the peptides were non-substrates (< 3% deacetylation), 72 peptides were hydrolyzed with moderate activity (3-15% conversion) and 117 peptides showed high activity (> 15% conversion). Similarly, for Fe(II)-HDAC8 139 of the peptides were non-substrates, 62 peptides showed moderate activity and 160 peptides showed high activity. In total more peptides were substrates for Fe(II)-HDAC8 (222 peptides) than for Zn(II)-HDAC8 (189 peptides). The data are presented in heat maps for each Me(II)-HDAC8 (Figure 3-1A, B). The 0.5- to 1-fold Zn(II) contamination above the concentration of reconstituted HDAC8 concentrations could result in inhibition of Zn(II)-HDAC8 activity by up to 50% and Zn(II) displacement of Fe(II) in reconstituted Fe(II)-HDAC8 (18, 67), suggesting that these data are a lower limit for the alterations in metal-dependent selectivity. However, the significant specificity differences that were observed in this screen suggest that the plates used in these experiments likely contained less Zn(II) contamination.

To better visualize differences in relative activity of the two metal forms of the enzyme, we generated a specificity map with the ratios of Fe(II)-HDAC8 product conversion to Zn(II)-HDAC8 product conversion (Figure 3-1C). This heat map demonstrates that the peptide substrate selectivity of HDAC8 is dependent on the bound

metal ion. In the screen, Zn(II)-HDAC8 had higher activity (where the relative conversion was greater than seven-fold), than Fe(II)-HDAC8 for 11% of the peptides while 15% of the peptides were better substrates for the Fe(II) enzyme (by a factor of seven or more). Additionally, 34% of the peptides were comparably deacetylated (within a factor of two), and 40% of the peptides were non-substrates or demonstrated negligible deacetylation for both metal-substituted forms of HDAC8. In addition to Zn(II)/Fe(II) differences, the arrays suggest general peptide sequence specificity trends for HDAC8. For example, all but three of the peptides containing phenylalanine at the Z position were metal-insensitive substrates (deacetylated by both Me(II)-HDAC8), while methionine in the Z position was largely unfavorable to both enzyme forms and resulted in many non-substrate peptides. These data clearly demonstrate that the substrate selectivity varies with the identity of the active site metal ion.

.

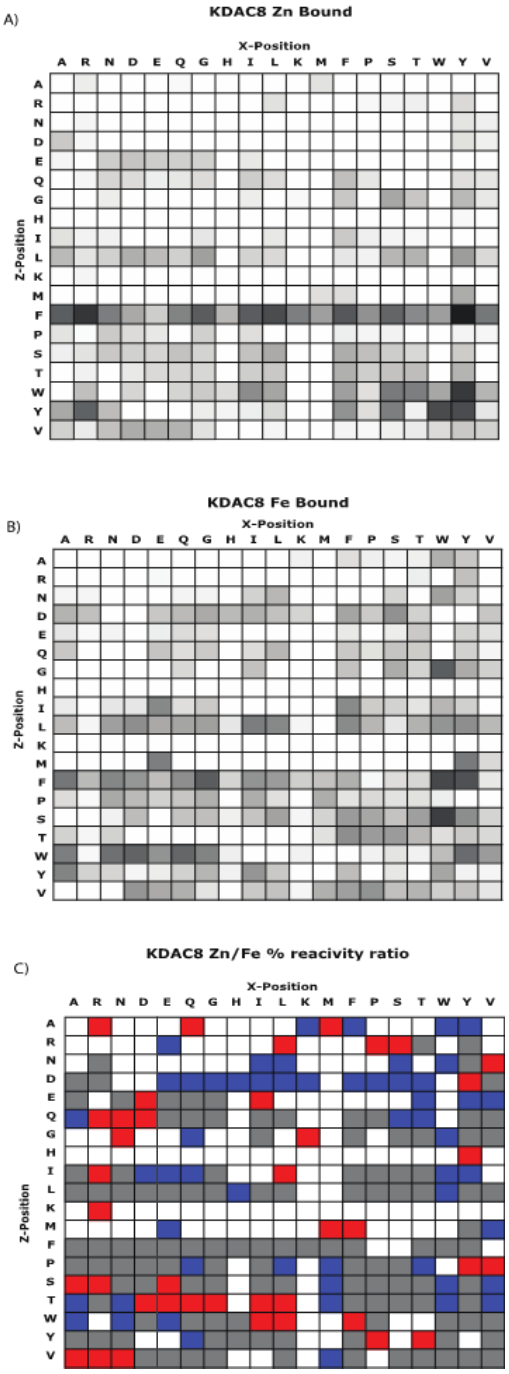

Figure 3-1: HDAC8 metal specificity screen

The specificities of Fe(II) and Zn(II)-bound HDAC8 were determined using an array of 361 peptides (GXK^{Ac}ZGC). A. The extent of peptide deacetylation by Zn(II)-HDAC8 is shown in a grey scale heat map. X and Z residues are on the axes. B. The extent of peptide deacetylation by Fe(II)-HDAC8 is shown in a grey scale heat map. X and Z residues are on the axes. C. A metal specificity heat map displaying the ratio of conversions for the Zn(II) and Fe(II) enzyme. Peptides having a greater than seven-fold activity for the Fe(II)-form are shown in blue and a Zn(II)-preference is shown in red. Non-substrates and metal-insensitive peptides are shown in white and gray, respectively.

Putative substrate peptides in solution

To further investigate these compelling metal-dependent specificity differences, we selected peptide substrates (listed in) based on putative *in vivo* substrates, as identified by proteomic and computational methods (80, 191), and measured HDAC8-catalyzed deacetylation under steady-state conditions. We obtained apparent k_{cat}/K_M (catalytic efficiency) values that were used to compare the Fe(II) and Zn(II)-substituted enzymes.

To measure deacetylation we used an acetate-NADH coupled assay that measures the conversion of acetate product to NADH by fluorescence (72, 192). The stopped assay was performed using Zn(II)- or Fe(II)-HDAC8 under multiple turnover conditions and initial rates of peptide deacetylation were used to calculate catalytic efficiencies. Representative peptide reaction data are presented in (

Figure 3-2). The catalytic efficiencies for the peptides ranged from 1.4 to 300 $M^{-1}s^{-1}$ for Zn(II)-HDAC8 and 8.3 to 1700 $M^{-1}s^{-1}$ for Fe(II)-HDAC8. In contrast to the array data, Fe(II)-HDAC8 exhibited greater catalytic efficiency toward deacetylation of all of the peptides tested in solution. Nonetheless, the ratio of k_{cat}/K_M values for the two metal-substituted enzymes varied widely, as predicted by the initial library screen. The ratios of Fe(II)- to Zn(II)-HDAC8 k_{cat}/K_M values ranged from 2 to 15 (Figure 3-3 and Table 3-1).

Table 3-1: Metal dependence of HDAC8 substrate specificity for peptides in solution[a]

Abbreviation	Protein name	Peptide sequence[a]	Fe(II)-HDAC8 $k_{cat}/K_{M,\ apparent}$[b] ($M^{-1}s^{-1}$)	Zn(II)-HDAC8 $k_{cat}/K_{M,\ apparent}$[b] ($M^{-1}s^{-1}$)	Fe/Zn ratio
H3K9 7mer	Histone H3	TARK(ac)STG	100 ± 10	50 ± 20	2.0 ± 0.9
ALDH5A1	Succinate-semialdehyde dehydrogenase, mitochondrial	FVK(ac)AFA	30 ± 4[c]	< 10[d]	3 ± 0.4
LARP1	La-related protein 1	LGK(ac)FRR	350 ± 40	110 ± 10	3.2 ± 0.6
SMC3 10mer	Structural Maintenance Of Chromosomes 3	RVIGAKK(ac)DQY	60 ± 9[e]	12 ± 4[e]	5 ± 2
ARID1A	AT Rich Interactive Domain 1A (SWI-Like)	KLISK(ac)FDKL	1700	301 ± 7	5.6 ± 0.1
CREB94	cAMP-responsive element-binding protein	CKDLK(ac)RLFS	8.3	1.4 ± 0.7	6 ± 3
CSRP2BP	CSRP2 binding protein	STPVK(ac)FISR	370 ± 20[e]	56 ± 6[e]	6.5 ± 0.8
H3K9 13mer	Histone H3	TKQTARK(ac)STGGKA	350 ± 7	37 ± 3	9.4 ± 0.8
CAD	CAD protein	LSK(ac)FLR	390 ± 50	37 ± 8	10 ± 2
THRAP3	Thyroid hormone receptor-associated protein 3	LGDGK(ac)MKS	27 ± 1	2 ± 1	13 ± 7
SMC3 9mer	Structural Maintenance Of Chromosomes 3	RVIGAKK(ac)DQ	119 ± 8	8 ± 3	15 ± 7

[a] Peptides were acetylated on the N-terminus with C-terminal amides.

[b] Unless otherwise noted, apparent $k_{cat}/K_{M,\ apparent}$ values were calculated from the initial rate of 100 – 200 μM peptide and 1 – 2 μM Me(II)-HDAC8 in assay buffer (20-25 mM HEPES pH 8, 137 mM NaCl, 3 mM KCl) at 30°C. Errors were calculated from a linear fit, when possible. If no error is reported, the initial rate was fit to two points. The error in the Fe/Zn ratio was propagated using the equation $\partial R = R \times \sqrt{\left(\left(\frac{\partial Fe}{Fe}\right)^2 + \left(\frac{\partial Zn}{Zn}\right)^2\right)}$, where δ is error, R is the ratio, and Fe and Zn are the apparent k_{cat}/K_M values.

[c] Peptide insolubility yielded ambiguous substrate concentration (< 100 μM), so $k_{cat}/K_{M,\ apparent}$ is estimated but relative Fe/Zn activity is accurate.

[d] Initial rate was below the detection limit of the assay.

[e] $k_{cat}/K_{M,\ apparent}$ determined by Michaelis-Menten fit of v_0/[E] versus [S] (0 - 500 μM S)

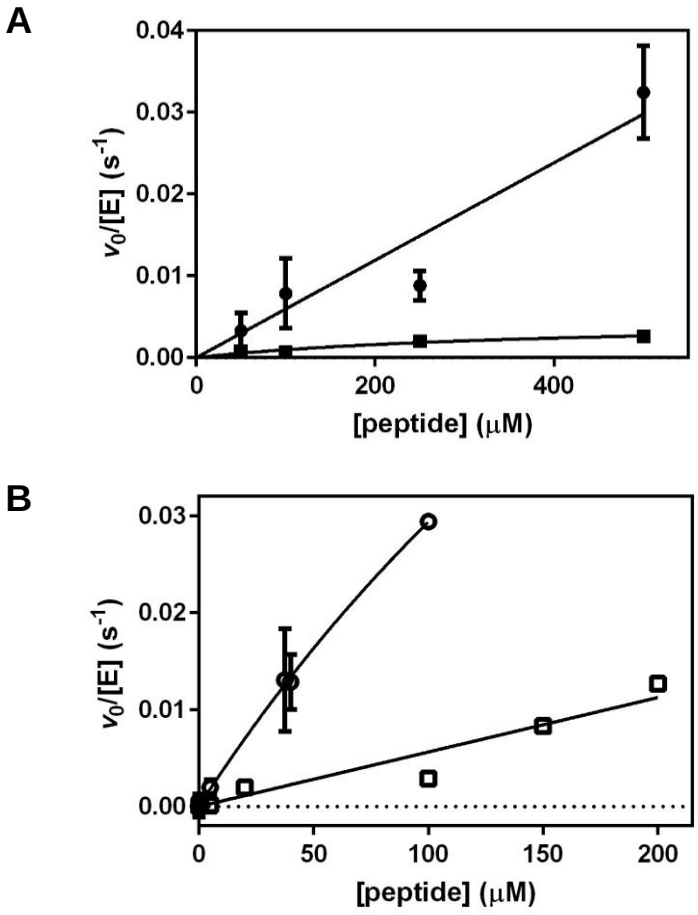

Figure 3-2: Metal-dependence of HDAC8 catalytic efficiency

A. The dependence of the initial rate on the substrate concentration for incubation of 1 – 1.5 μM Fe(II)-HDAC8 (●) or Zn(II)-HDAC8 (■) with 50 – 500 μM SMC3 10 amino acid acetyl-lysine peptide in 20-25 mM HEPES pH 8, 137 mM NaCl, 3 mM KCl at 30°C determined measuring production of acetate using an enzyme-coupled assay (72). The value of k_{cat}/K_M was calculated from a linear fit of the data. B. The dependence of the initial rate on the substrate concentration for incubation of 1 – 1.5 μM Fe(II)-HDAC8 (◯) or Zn(II)-HDAC8 (□) with 0 – 200 μM CSRP2BP acetyl-lysine peptide. The Michaelis-Menten equation was fit to these data.

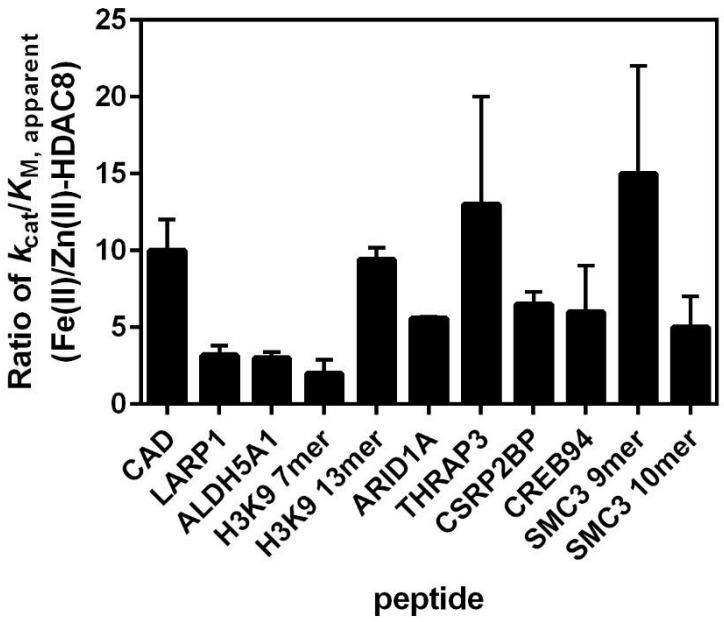

Figure 3-3: Fe(II)/Zn(II) HDAC8 substrate specificity ratios

The ratios of apparent catalytic efficiency for Fe(II)- and Zn(II)-bound HDAC8 are presented as a bar graph. Errors were propagated from the errors in $k_{cat}/K_{M, apparent}$.

The observed differences in Fe(II)- and Zn(II)-HDAC8 suggest several potential metal-dependent determinants of HDAC8 substrate specificity. The first is substrate length. For the H3K9ac peptides, increasing the peptide length from a 7-mer to a 13-mer had little effect on the catalytic efficiency on Zn(II)-HDAC8 but increased the Fe(II) activity 3.5-fold, resulting in an increase in the Fe/Zn specificity ratio. These data suggest that additional HDAC8-substrate interactions occur in the Fe(II)-bound enzyme. Length may not be the main determinant of metal selectivity, however, as three shorter peptides demonstrate higher Fe(II)/Zn(II) activity ratios than the 13mer H3K9ac peptide: CAD protein (6-mer), THRAP3 (8-mer) and SMC3 (9-mer). Furthermore, the SMC3 10-mer peptide exhibits a 3-fold decrease in Fe(II)/Zn(II) activity as compared to the 9-mer peptide.

A second substrate selectivity determinant is the sequence downstream of the acetyl-lysine. For example, a methylcoumarin fluorophore on the C-terminal side of the acetyl-lysine in the commercial Fluor-de-Lys substrates enhances HDAC8 activity (71, 72). The SMC3 peptides differ by the presence or absence of a tyrosine at the +3 position and this change leads to a 2-fold decrease in Fe(II)-HDAC8 catalytic efficiency with little effect on the Zn(II)-HDAC8 efficiency, therefore the Fe(II)/Zn(II) ratio decreases. This result suggests that the Fe(II)-HDAC8 may make enhanced interactions with the amino acid in the +3 position of peptides, conferring increased Fe(II)/Zn(II) selectivity, or that the k_{cat} for this substrate may be affected in a metal-dependent manner. Fe(II)-HDAC8 is also more active with the CREB94 peptide, which has a Phe at the +3 position, compared to Zn(II), although this peptide has low activity with both enzymes. These data suggest that +3 position aromaticity enhances the activity of Fe(II)-HDAC8.

The third factor affecting specificity is the overall peptide sequence where the entire sequence alters the Fe/Zn activity ratios. Peptides in the solution-based assay with Phe at the +1 position (Z-position) relative to the acetylated lysine (CAD, LARP1, ARID1A, CSRP2BP;) were predicted by the screen to have < 7-fold Fe(II)/Zn(II) HDAC8 activity preference. In general, the solution assays are consistent with this, although all four peptides have preference for Fe(II)-HDAC8 with Fe(II)/Zn(II) ratios of 3.2 ± 0.6 to 10 ± 2.

Interestingly, La-related protein 1 (LARP1) and CAD protein differ only at the -1 and +2 positions (both have a +1 Phe, -3 Leu, and +3 Arg), and while Fe(II)-dependent catalytic efficiency is nearly identical (and higher than for Zn(II)), the Zn(II) catalytic efficiency is 3-fold lower for the CAD peptide. Therefore, the Fe/Zn activity ratio for the CAD peptide of 10 ± 2 is increased compared to the LARP1 peptide. Based on the +1 (Z) and -1 (X) positions, the H3K9ac 7-mer was predicted as a zinc-specific substrate, however kinetic analysis using the solution assay indicates a slight preference for Fe(II)-HDAC8 (Fe(II)/Zn(II) = 2.0 ± 0.9). The H3K9ac 7mer data also show that characteristics of peptide sequence can switch HDAC8 substrate specificity in a metal-dependent manner, since placing a zinc-specific X and Y sequence [RK(ac)S] in the context of additional residues [TARK(ac)STG] in the H3K9 7mer peptide increased Fe(II) specificity. These data demonstrate that while the individual amino acids surrounding the acetyl-lysine alter the metal-dependent peptide specificity, the overall sequence of the peptide affects both specificity and metal-dependent selectivity which is difficult to discern from this data set.

Taken together, the data presented here demonstrate metal-dependent substrate specificity for HDAC8-catalyzed deacetylation. The Fe(II)/Zn(II) specificity varies with peptide substrate sequence. Residues throughout the substrate peptide sequence are synergistic in determining metal-dependent and sequence-dependent specificity for HDAC8. We suggest that either metallated form of HDAC8 could be a relevant deacetylase *in vivo*, and that manipulating the Me(II)-HDAC8 identity could regulate the pool of recognized substrates. This presents an intriguing link between cellular metal homeostasis and the acetylation/deacetylation process.

Remarkably, the difference between iron and zinc-HDAC8 activities varies greatly depending on the sequence of the substrate peptide. We showed previously that Fe(II)-HDAC8 had a higher $k_{cat}K_M$ than Zn(II)-HDAC8 for a commercial peptide (67), however it was not determined whether the difference in metal-dependent activation was substrate-dependent. Here we show that even among the short 6 amino acid peptides, which interact only with the active site and local substrate binding surface, there are significant differences in both catalytic efficiency and Fe(II)/Zn(II) specificity. If the ratio of Fe(II)/Zn(II) catalytic efficiency remained constant, it would suggest that the metal ion identity is a way to modulate level of HDAC8-catalyzed deacetylation in the cell. The

variability of the Fe(II)/Zn(II) specificity ratio lends itself to a more complicated hypothesis where the catalytic metal ion regulates the substrate specificity of HDAC8 toward its cellular targets.

The structural basis for the metal-dependent substrate specificity is unclear. Crystal structures of HDAC8 indicate that the substrate binding site is primarily composed of flexible loops which accommodate a range of substrates and also influence the enzyme's specificity (18, 44, 73, 105, 111, 112, 114, 115). The active site metal ligands may be oriented in part by these loops and their substrate-dependent interactions. Intrinsic properties of the metal ion, including Lewis acidity, size and geometric preferences, could influence the structure of the hydrophobic amino acids surrounding the metal ligands (193). These alterations could be propagated to alter the structure and dynamics of the loop regions thereby altering the binding interface presented to substrates and influencing substrate selectivity.

The range of catalytic efficiencies for Fe(II)-HDAC8 is much greater than that of Zn(II)-HDAC8 among the peptides tested, demonstrating that molecular recognition of Fe(II)-bound HDAC8 is more sensitive to the peptide sequence than Zn(II)-HDAC8. The ranges of activity may be even greater among full-length protein substrates, as it is known that moving from peptide to protein increased the range of Zn(II)-HDAC8 specificity in the context of histone H3 (Chapter 2; Fe not tested). Thus, in a cellular context, binding Zn(II) versus Fe(II) could have drastic effects on the selectivity for deacetylation of HDAC8 substrates. Compared to Fe(II)-HDAC8 (8.3 to 1700 $M^{-1}s^{-1}$), the Zn(II)-enzyme loses nearly an order of magnitude in efficiency (1 to 300 M-1s-1). This result suggests that switching from the Fe(II)-dependent HDAC8 to a Zn(II)-enzyme in the cell would significantly decrease the HDAC8-catalyzed deacetylation. Furthermore, the observed deacetylation would likely be less substrate-specific since the Zn(II)-enzyme does exhibits a narrower range of sequence-dependent substrate specificity.

The changes in HDAC8 catalytic efficiency may be due to changes in either K_M or k_{cat}. It was not possible to make these measurements for a majority of the peptide substrates as the value of K_M is too large, likely reflecting weak binding affinity. However, we anticipate changes in both parameters upon substituting the metal ion, as observed

for catalysis of coumarin-labeled peptides (67). Because the metal ion is directly involved in catalysis, the k_{cat} values are likely to reflect metal-dependent differences in activity. The hydrophobic shell around the active site is important for metal affinity and metal-specificity (193). These residues interact with the substrate, and may mediate specificity changes via the K_M as well.

These results suggest that HDAC8's metal-dependent specificity may be important for regulating deacetylation in the cell in response to changing metal homeostasis. This is plausible, given the dynamic nature of metal concentrations. For example, zinc is tightly buffered, but cellular zinc concentrations can change rapidly and drastically (184, 194). For example, zinc can be transported to the nucleus by metallothioneins when cells are stimulated by cytokines and nitric oxide (195), and zinc concentrations have been shown to increase in both the nucleus and cytoplasm under oxidative stress (196). The concentration of exchangeable Zn(II) is increased under redox stress as cellular zinc ligands are oxidized and release Zn(II) (reviewed in 189, 197). The dependence of Fe(II) concentration on the redox state of the cell is unclear, however Fe(II) and Fe(III) are likely involved in the cellular oxidative response as Fe(II) can generate free radicals via the Fenton reaction and the concentration of labile iron pools in mouse cancer cells correlates with increased DNA damage from hydrogen peroxide (reviewed in 198). We have shown previously that the metal-dependent bacterial deacetylase LpxC purifies with Zn or Fe based on the relative abundance of these metals in the growth conditions, and that the metal cofactor bound to LpxC metal switches from Fe(II) to Zn(II) under aerobic conditions *in vitro* (186). We propose a similar model for metal-dependent HDACs; Fe(II)-HDAC8 (K_D for Fe(II) = 0.2 – 1 μM) (18, 182) may exist in a resting state, but upon increased exchangeable Zn(II) concentration HDAC8 would exchange the Fe(II) cofactor for Zn(II), which has a picomolar K_D for Zn(II) (18, 182), maintaining HDAC8 activation but altering the activity level and substrate specificity.

Although peptides that react more readily with Zn-HDAC8 were observed in the high-throughput screen, the universal trend among the longer, more physiologically relevant peptides was higher Fe(II)-dependent catalytic efficiency (k_{cat}/K_M) and therefore greater Fe(II) specificity for the enzyme. One possible explanation for these differential results is that the two screens reflect different kinetic parameters; the high-throughput

screen may reflect values for k_{cat} rather than k_{cat}/K_M since the substrate is on a solid surface rather than in solution. The higher Fe(II)-dependent HDAC8 activity suggests that the enzyme is activated, at least in part, by Fe(II) in the cell. A complementary hypothesis is that peptides with a high ratio of iron to zinc activity may represent *in vivo* substrates while peptides with a ratio nearer to 1 may not be HDAC8-specific substrates *in vivo*. This is bolstered by the fact that peptides corresponding to proteins recently identified as potential HDAC8 substrates in a proteomics screen (80) have Fe/Zn substrate specificity ratios of 5 – 10, however this conclusion is complicated by the drastic effects of sequence-dependent specificity (for example SMC3 Fe/Zn ratio drops from 15 to 5 upon the addition of 1 residue at the C-terminus). Likewise, despite *in vitro* activity, cellular inhibitor studies are beginning to suggest that histones may not be *in vivo* HDAC8 substrates (80, 199, 200) and the H3K9ac 13-mer had an Fe/Zn ratio of 10, although the shorter peptide has a ratio of 2. Thus the metal-dependent specificity of peptide substrates is too sensitive to length and local sequence to be a strong indicator of *in vivo* substrates at this point. An alternative model is that the metal-dependent substrate specificity ratio is not a predictor of substrates versus non-substrates, but rather distinguishes substrates by cellular priority. The proteins that are not highly affected by metal switching may be constitutively deacetylated substrates acted upon at a basal level regardless of the bound metal ion, while substrates that are highly activated by Fe(II) binding to HDAC8 would be deacetylated under specific, iron-favored cellular conditions.

Another possibility is that the metal-dependence is related to subcellular HDAC8 location, particularly due to the wide range of metal concentrations reported for cytosol, nuclei, and organelles. Analysis of acetylated proteins identified experimentally and computationally in 2009 parsed some localization-dependent sequence specificity surrounding the acetylation sites (9, 174, 201). Nuclear, cytosolic, and non-histone acetylated lysine sites had similarities among their sequences, while mitochondrial and histone sites differed. Glycine in the -1 position of nuclear substrates was prevalent in both the experimental and computational studies and tyrosine at the +1 position was the most common amino acids among the mitochondrial, nuclear, and cytosolic sites identified by Choudhary *et al*. (9). My data demonstrate a range of Fe/Zn selectivity for peptides with small aliphatic amino acids at the -1 position, however these ratios tend not

to be as large as the ratios that are observed for lysine and serine at that position. As most of the substrates examined are nuclear and the Fe/Zn selectivity ranges from 2 - 15, our data does not provide support for localization-dependent selectivity at this point.

In conclusion, this study is the first to demonstrate that the sequence-dependent substrate specificity of HDAC is dependent on the identity of the active site metal ion. The SAMDI peptide screen enabled a broad survey of enzyme specificity, and the enzyme assays in solution demonstrate a range of Fe/Zn specificities toward substrates of physiological relevance. *In vivo* evidence consistent with the hypothesis of metal switching regulation is still needed, however the data presented here allude to the possibility that cellular conditions dictate the active site metal ion as a means of modulating the deacetylation of specific target proteins.

Acknowledgements

We thank Eric D. Sullivan for collaborating on protein purification. We thank the National Institutes of Health Grant 5-R01-GM-040602 (C.A.F.), the University of Michigan Chemistry-Biology Interface (CBI) training program NIH grant 5T32GM008597 (C.A.P.), and Rackham Graduate School (C.A.P.) for funding.

Chapter 4

Investigation of the effect of HDAC8 phosphorylation on activity, metal dissociation, and substrate specificity[1]

Introduction

Phosphorylation, acetylation, and methylation are general cellular regulatory mechanisms of increasing interest (2). These ubiquitous PTMs are enzymatically appended to and removed from proteins throughout the cell and are part of the larger cellular phenomenon known as post-translational modification crosstalk, which has been observed among histone and non-histone proteins (reviewed in 6, 202, 203). In the complicated system of cellular function, post-translational modifying enzymes can also be modified themselves. HDACs can undergo post-translational modification, with modifications including phosphorylation, acetylation, and ubiquitination affecting enzyme activation, protein-protein interactions, and localization (5, 25). Understanding the ways that PTMs regulate enzymatic function and signal transduction is important for characterizing normal and diseased cellular processes.

Phosphorylation is common among HDACs; HDACs 1 through 9 are phosphorylated on at least one site, and the modifications regulate their protein-protein interactions, protein complex formation, and subcellular localization (25, 35). Of these, only HDAC5, HDAC6, and HDAC8 have a phosphorylation site within the deacetylase domain of their protein structure. HDAC8 is phosphorylated at S39 (142, 143). This site is not conserved among the closely related class I HDACs (arginine in HDAC1 and HDAC2, alanine in HDAC3). HDAC4, 5, 7, and 9 have a nearby serine based on

[1] Carol Ann Pitcairn wrote the manuscript and performed *in vitro* HDAC8 experiments. Dr. Christophe Decroos (University of Pennsylvania) performed crystallography and related methods, analyzed structural data, and wrote text regarding crystal structure. Dr. Shozeb Haider (University College London) performed molecular dynamics simulations, analyzed that data and wrote corresponding text. Jeffrey E. López collaborated on metal affinity experiments and Noah A. Wolfson helped with the substrate specificity assay using the NADH-coupled assay.

sequence alignment, though the local sequence environment is different (126). Ser39 is conserved among HDAC8 homologs in several species, but is not conserved in HDAC8 from Schistosome, a parasite for which HDAC8 is a druggable target. The uniqueness of this HDAC8 phosphorylation site makes it an interesting target of investigation as it may be an isozyme-specific regulatory mechanism.

S39 phosphorylation on HDAC8 was first reported in 2004 (143). The site was identified by phosphoamino acid analysis, thin layer chromatography, immunoblotting, and mutagenesis (143). HDAC8 was identified as a substrate of cyclic AMP dependent protein kinase A (PKA) by process of elimination (CK2 and PKC do not generate radiolabeled HDAC8 (142)), and by the observed changes in phospho-HDAC8 levels upon activation or inhibition of PKA (143). Phosphorylation of HDAC8 by other kinases and/or at other sites *in vivo* has not been determined; however PKG can catalyze formation of radiolabeled phospho-HDAC8 (142). Additionally, a phosphorylation prediction server (Group-based Prediction Server ver 3.0) predicts additional kinase recognition motifs in the HDAC8 sequence and suggests that other kinases may catalyze phosphorylation at S39 (204).

Ser39 is ~20 Å from the active site metal (18, 105, 111-115) yet phosphorylation affects catalysis. Immunopurified Flag-HDAC8 from PKA-activated cells, producing phosphorylated HDAC8, was inhibited in its ability to catalyze deacetylation of core histones H3 and H4 (143). Additionally, histones isolated from forskolin-treated HeLa cells (adenylyl cyclase activator to stimulate PKA) expressing Flag-HDAC8 demonstrated increased acetylation over controls with either no HDAC8 overexpression, no forskolin, or expression of S39A-HDAC8, indicative of PKA-mediated HDAC8 inhibition (143). The mechanism by which this inhibition occurs has not been studied, but one hypothesis is that perturbation of the position of R37, located near S39 (Figure 4-1), distorts hydrogen bonding in the HDAC8 internal channel (104). R37 is critical for high catalytic efficiency of HDAC8 (104). Additionally, S39 is at the base of the L1 loop, which is important for HDAC8-substrate interactions, and structural perturbations upon adding a phosphate at this site are predicted (112).

HDAC8 phosphorylation affects both protein-protein interactions (108) and subcellular localization (83). Phosphorylation increases association with Human Est1p-like protein B (hEST1B) and Hsp70 (108). Phosphorylation may affect HDAC8 subcellular localization, or HDAC8 may be phosphorylated to different extents depending on the cell type or cellular location. There is a precedent for this, as class II HDACs demonstrate phosphorylation-dependent mechanisms of translocation between the nucleus and cytosol (29-32, 146, 147). HDAC8 is observed in both the nucleus and the cytoplasm (65, 66, 83). In myometrial cells, phosphorylated HDAC8 co-localizes almost entirely with the cytoskeleton while unmodified HDAC8 is observed in the cytoplasmic, cytoskeletal, and nuclear fractions (83). Intriguingly, phosphorylated HDAC8 levels (but not overall HDAC8 expression) are increased in the myometrial cells of pregnant women (83). This suggests there is a functional relationship between phosphorylation, HDAC8 localization, and HDAC8 protein interactions that needs to be explored further.

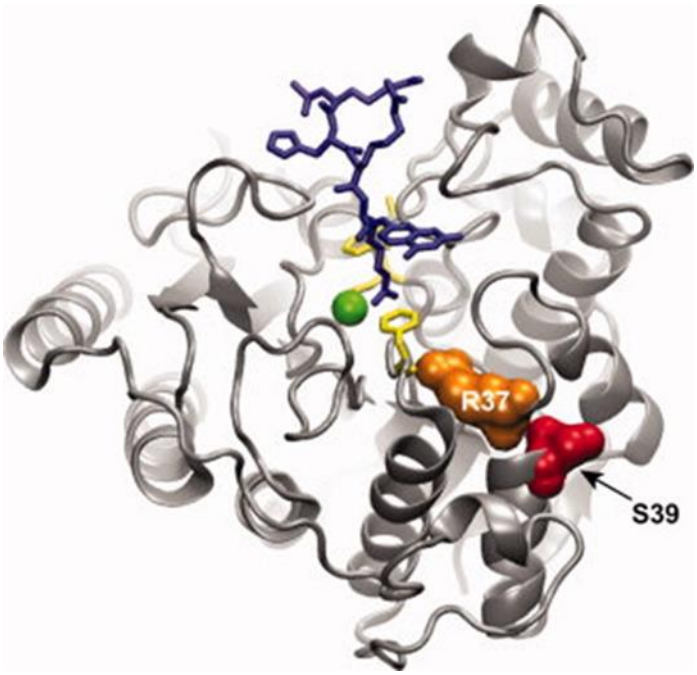

Figure 4-1: Ser39 and HDAC8 structure

HDAC8 structure (PDBID: 2V5W) (73, 111) showing Ser39 (red) in relationship to Arg37 (orange) and the active site residues (yellow). The Fluor-de-Lys substrate is blue and the active site metal is green. The structure was generated using VMD and the figure is reproduced (73)from with the permission of John Wiley and Sons.

Structurally, phosphorylation is poised to have a significant impact on the substrate binding site and on the active site. The L2 loop of HDAC8 is very flexible, and typically the electron density for this loop is less resolved than the rest of the crystal structure (44). These structures show that the L1 and L2 loops of HDAC8 interact via residues K33 and D101 and this is likely important for substrate recognition and/or binding affinity (44). D101 has been reported as a critical residue for positioning peptide substrates (105). S39 is located such that perturbing its size and charge would distort the α2 helix and could impact K33 positioning and the K33-D101 interaction, thereby affecting substrate binding affinity or specificity.

Phosphorylation on HDAC8 is unique regarding residue location and catalytic effect, compared to other class I HDACs. HDAC1 and HDAC2 phosphorylation has been suggested to activate these enzymes (142, 144, 145, 150, 151), while decreased activity was observed for phospho-HDAC8 (143). Phosphorylation also plays a role in complex formation for HDAC1 and HDAC2, but the evidence is conflicting (142, 144, 145). HDAC8 is the most amenable HDAC to study *in vitro* because activity does not depend on formation of a protein complex and it is well-characterized biochemically. Phosphorylation of HDAC8 presents a distinctive mode of HDAC regulation. Here we provide, using the S39E phosphomimetic mutant, a combination of structural and kinetic data demonstrating that phosphorylation of HDAC8, although on the surface of the protein, modulates its function via changes in catalytic activity, metal binding, and substrate specificity.

Materials and methods

Reagents

Most reagents used for buffers or crystallization were purchased from Fisher or Sigma, unless otherwise specified. The HDAC inhibitor 4-(4-chloro-2-methylphenoxy)-*N*-hydroxybutanamide (Droxinostat) was obtained from Sigma Aldrich and was used without further purification.

Expression and purification of S39E HDAC8 for crystallization

The S39E mutation was introduced into the HDAC8-6His-pET20b construct (105) using Quickchange site directed-mutagenesis kit protocols (Agilent Technologies, Inc.). Primers used for PCR mutagenesis are as follows: forward, 5'-GCT AAA ATC CCG AAA CGT GCA gag ATG GTG CAT TCT TTG ATT GAA G-3'; and reverse, 5'-C TTC AAT CAA AGA ATG CAC CAT ctc TGC ACG TTT CGG GAT TTT AGC-3'. Incorporation of desired mutations was confirmed by DNA sequencing at the University of Pennsylvania Perelman School of Medicine. Recombinant S39E HDAC8 was expressed in BL21(DE3) *Escherichia coli* cells and purified according to a previously published procedure (86).

Expression and purification of wild type and S39E-HDAC8 for assays[2]

The S39E mutation was introduced into the pHD4 (HDAC8-TEV-His) plasmid using custom primers (Integrated DNA Technologies) via Quikchange site directed mutagenesis. The primer sequences were: forward, 5'-CCC GAA ACG TGC Aga GAT GGT GCA TTC TTT GAT TGA AGC ATA TG-3'; and reverse, 5'-CAT ATG CTT CAA TCA AAG AAT GCA CCA TCt cTG CAC GTT TCG GG-3'. Incorporation of the mutation was confirmed by DNA sequencing performed by the University of Michigan DNA Sequencing Core and the corresponding mass of the purified S39E-HDAC8 was confirmed via Q-TOF HPLC-MS (Agilent). WT and S39E-HDAC8 were expressed and purified as in (67, 191). BL21(DE3) cells were grown in Tris auto-TB media (12 g/L tryptone, 24 g/L yeast extract, 8.3g/L Tris-HCl, 4 g/L lactose, 1 g/L glucose, 10 mL/L glycerol, pH 8.3) supplemented with 0.2 mM $ZnSO_4$ and 100 µg/mL ampicillin at 30°C overnight with shaking at 170 rpm. Alternatively, 2xYT media was used and cells were grown at 30-37°C until OD_{600} of at least 0.4, followed by a temperature decrease to 20°C for 45-60 minutes and induction with IPTG (0.5 mM) and supplementation with 0.2 mM $ZnSO_4$. At 15-17 hours post-induction, cells were harvested by centrifugation at least 5000 rpm for at least 15 min at 4°C. Cells pellets were resuspended in either DEAE low salt buffer (30 mM HEPES pH 8, 10 µM $ZnSO_4$, 1 mM TCEP, 100 mM NaCl, 10 µg/mL PMSF, and 1 µg/mL TAME) or

[2] Several batches of enzyme were used for these experiments. One preparation of S39E-HDAC8 was performed by rotation student Oleta Johnson.

Nickel buffer A (30 mM HEPES pH 8, 100-150 mM NaCl, 1 mM imidazole, 1 mM TCEP, 5 mM KCl) which in some cases included cOmplete™ protease inhibitor cocktail tablets (Roche), and lysed using a microfluidizer (microfluidics). In some cases, nucleic acids were precipitated by PEI pH 7.9 for 10-15 minutes stirring on ice. Lysate was cleared by centrifugation (26,900 – 38,700 x g, 4°C, for at least 40 min). Cleared lysate was loaded onto a 100 mL DEAE column and purified as in (191) or a 15 mL Ni(II)-charged chelating sepharose fast flow (GE Healthcare) column and purified as in (67). Following the nickel column, HDAC8 was incubated with 6His-TEV protease during overnight dialysis in 25-30 mM HEPES pH 8, 100-150 mM NaCl, 1 mM TCEP, and 5 mM KCl at 4°C. In one case TEV protease was added following dialysis and incubated for 4 hours. HDAC8 was purified from 6His-TEV on a second nickel column, concentrated in 30k MWCO Amicon centrifuge filters at 3200 rpm, and dialyzed against metal-free chelation buffer (25 mM MOPS pH 7.5, 5 mM KCl, 1 mM EDTA, 1 mM TCEP) at least overnight, If necessary, the enzyme was further purified by size exclusion chromatography on an S200 column in chelation buffer. The enzyme was then dialyzed in metal-free buffer (25 mM MOPS pH 7.5, 1 mM TCEP, 5 mM KCl) at 4°C at least overnight. Residual EDTA was removed using a PD-10 column (GE Healthcare) in metal-free buffer or assay buffer.

Fluor-de-Lys assay

The Fluor-de-Lys assay (70, 165) (Enzo Life Sciences) was performed as in (67). Enzyme was reconstituted for 1 hour on ice with stoichiometric Zn(II) (Fluka Zinc Atomic Spectroscopy standard #96457) or Fe(II) (iron(II)chloride, Sigma). Reactions were performed at 30°C using the Fluor-de-Lys HDAC8 substrate (Enzo Life Sciences). Enzyme was used to initiate reactions in 0.5 or 1X HDAC8 assay buffer (1X assay buffer: 20-25 mM HEPES or Tris pH 8.0, 137 mM NaCl, 3 mM KCl) with p53-based commercial fluorophore-conjugated peptide substrate. Enzyme and substrate were equilibrated for at least 5 min at 30°C prior to the assay. For iron assays, solid iron(II)chloride (Sigma), solid ascorbic acid (Fluka), and HDAC8 assay buffer were equilibrated overnight in an anaerobic chamber (Coy Laboratory Products). The enzyme was equilibrated in the anaerobic chamber for 1 hour prior to reconstitution and substrate was equilibrated 1 hour

prior to the assay. Iron assays which were performed outside the anaerobic chamber were completed within 2 hours, the effective working timespan for ascorbic acid to maintain Fe(II) (data not shown). Enzyme concentrations were 0.5 to 1 µM and substrate concentrations were 10 to 500 µM. Time points were quenched using a combination of trypsin developer and trichostatin A (TSA) solution. After at least fifteen minutes of incubation at room temperature, fluorescence of product (ex. 340 nm, em. 450 nm) and substrate (ex. 340 nm, em. 380 nm) were measured using a PolarStar fluorescence plate reader. The ratio of product to substrate fluorescence was used to calculate HDAC8 activity using a standard curve. K_{cat}/K_M values were generated by fitting v_0/[E] versus [S] to the Michaelis-Menten equation (equation 1).

Equation 1: $$\frac{v_0}{[E]} = \frac{k_{cat}}{K_M}\left(\frac{[S]}{\left(\frac{[S]}{K_M}+1\right)}\right).$$

Enzyme-coupled HDAC8 assay

Non-fluorophore conjugated peptides were assayed by coupling deacetylation of acetyl-lysine residues to the formation of NADH. Hydrolysis of acetyl-lysine forms acetate, which is converted to NADH via acetyl-CoA synthetase, citrate synthase, and malate dehydrogenase, and NADH is measured by fluorescence, as described in (72, 192). Peptides (Peptide 2.0) were N-terminally acetylated (N-terminal acetylation is not hydrolysable by HDAC8) with C-terminal amides. The enzyme-coupled HDAC8 assay was performed as in (72). The concentration of substrate was 120 µM and the concentration of HDAC8 was 2.4 µM. Reaction time points were quenched into hydrochloric acid. Coupled enzyme solution reagents were purchased from Sigma, with the exception of HEPES (Fisher) and acetyl-CoA synthetase, which was expressed and purified as in (72). Neutralized time points (60 µL) were loaded into wells of a black 96-well plate (Corning #3686) containing coupled enzyme solution (10 µL) and allowed to equilibrate protected from light. The fluorescence of the resulting NADH was measured (ex. = 340 nm, em. = 460 nm) and converted to product concentration using an acetate standard curve. Initial rates of reaction were used to calculate the apparent catalytic

efficiency using equation 1 under the assumption that the substrate concentration was well below the K_M.

Determination of metal ion dissociation rate constants (k_{off})

The divalent metal off rate constants for HDAC8 were determined by measuring the time-dependent decrease in activity upon incubation with EDTA as described in (182). HDAC8 was reconstituted with stoichiometric Zn(II) or Fe(II) for activity assays. Fe(II)-HDAC8 was reconstituted in the glove bag in the presence of ascorbic acid. A stock of 500 µM Fe(II) in 5 mM ascorbic acid was prepared and used for a final enzyme reconstitution of 100 µM Fe(II)-S39E-HDAC8 in 1 mM ascorbic acid and 1X assay buffer. After at least one hour on ice or coolbox in the glove bag, the enzyme was diluted into assay buffer containing 1 mM EDTA at 30°C. At each time point (0–60 min), the enzyme in EDTA was diluted 4-fold into 1X assay buffer containing 250 µM Fluor-de-Lys HDAC8 substrate, and initial rates of deacetylation were measured using the Fluor-de-Lys assay (70, 165). Reaction time points were quenched by adding them to TSA and trypsin developer as described above. The initial rate for product formation was determined for reactions at each EDTA incubation time. Control reactions without EDTA were incubated for the same times at 30°C and the initial rate of the EDTA reaction was divided by the non-EDTA reaction for each incubation time to yield the activity retained. The k_{off} was determined by fitting the normalized activity retained (fraction activity/y-intercept of single exponential) to a single exponential (Equation 2). In the equation, ΔA is the normalized fraction activity, A is the normalized fraction activity at time zero, t is time, and k_{off} is the dissociation rate constant.

Equation 2: $\Delta A = A \times \exp^{(-k_{off} \times t)}$

Determination of Zn(II) affinity (K_D)

The K_D values were measured using the anisotropy of fluorescein suberoylanilide hydroxamic acid (flSAHA), synthesized as in (182). The flSAHA assay was performed as described (182). HDAC8 was reconstituted with NTA-buffered Zn(II) and incubated at

25°C for 30 minutes. The NTA buffer (1 mM nitrilotriacetic acid (NTA), 137 mM NaCl, 3 mM KCl, 10 mM MOPS, pH 7) maintained concentrations of free Zn(II). The concentration of free metal ion was calculated from the total metal content using the software program MINEQL (Environmental Research Software). Final concentrations were $[Zn(II)]_{free}$ = 0 - 4.5 nM ($[Zn(II)]_{total}$ = 0 – 1 mM) and 1 μM S39E-HDAC8. Zn(II)-HDAC8 was added to a 96-well half-area black plate (Corning) and mixed with flSAHA (50 nM). Anisotropy of flSAHA (ex = 485 nm, em = 535 nm) was measured using a TECAN plate reader. The K_D values were obtained by fitting the data (GraphPad Prism) to a binding isotherm (Equation 3), where r is anisotropy, Δr is the change in anisotropy, X is the $Zn(II)_{free}$ concentration, K_D is the metal affinity equilibrium constant, and C is the amplitude (fit by the software).

Equation 3: $\frac{r}{\Delta r} = \left(\frac{X}{X+K_D}\right) + C$

Molecular dynamics simulations

The coordinates for the HDAC8-substrate complex for the simulations were taken from PDB ID: 2V5W (111). The spatial positions of K^+ ions and Zn^{+2} were retained in the simulation from the original PDB. Three sets of simulations were carried out. (a) WT HDAC, (b) HDAC8 with phosphorylated S39 and (c) HDAC8 with S39E mutation.

The modified phosphorylated protein was made using the Forcefield PTM server (www.selene.princeton.edu/FFPTM). The AMBER forcefield parameters for post-translations modifications were taken from Khoury et al. (205, 206). The S39E mutant was obtained from the crystal structure. The missing loops were constructed using 2V5W structure as the template. The substrate was introduced in the HDAC enzyme after superimposition with 2V5W structure. A total of six simulations were carried out, with and without substrate.

The parameters for substrate were generated via the Antechamber module of the AMBER software using Generalized AMBER force field (207, 208). The charges were assigned to the substrate using the AM1-BCC method (209). The systems were set up using xleap module of AMBER14 (210). K^+ ions were used for neutralization and TIP3P water molecules were used for solvation. AMBER-adapted Joung and Cheatham

parameters specific for TIP3P waters and K^+ ions (radius 1.593 Å and well depth 0.4297054 kcal mol^{-1}) were used (211). The system was solvated in a periodic box whose boundaries extended at least 10 Å from any solute atom. The periodic boundary conditions were defined by the PME algorithm and non-bonded cut-off was set to 10 Å (212). All chemical bonds involving hydrogen atoms were restrained using SHAKE, allowing for stable simulations with a 2 fs time step (213). Simulations were carried out using an NPT ensemble, using the Berendsen algorithm to control temperature and pressure (214). Standard equilibration protocols were used for initial minimization of the structure (215). The final MD simulations were carried out for 400 ns using ACEMD and the frames were collected every 10 ps using a timestep of 4fs (216). Analyses of the trajectory were performed using the GROMACS 4.5 tools (217, 218). The programs ICM, VMD and PyMOL were used for visualization (219-221).

Crystallization and data collection.

Crystals of the S39E HDAC8-Droxinostat complex were prepared by cocrystallization at 21°C in sitting drops using the vapor diffusion method. A 500 nL drop containing 5.0 mg/mL S39E HDAC8, 50 mM Tris (pH 8.0), 150 mM KCl, 5% glycerol, 1 mM dithiothreitol, 2 mM Droxinostat, and 0.03 M glycylglycylglycine was added to a 500 nL drop of precipitant solution and equilibrated against a 100 μL reservoir of precipitant solution. The precipitant solution consisted of 100 mM BisTris (pH 6.5), 6% (w/v) PEG 8,000 (Hampton Research), and 4 mM tris-(2-carboxyethyl)phosphine.

Crystals typically appeared within 1 day. Crystals were flash-cooled in liquid nitrogen after transfer to a cryoprotectant solution consisting of precipitant solution supplemented with 25% glycerol. X-ray diffraction data were collected on beamline X29 at the National Synchrotron Light Source (NSLS, Brookhaven National Laboratory, New York). Data collection statistics are recorded in Table 4-1. Data were indexed, integrated and scaled using HKL2000 (222).

Phasing, model building, and structure refinement

Crystals belonged to space group $P2_1$, with 2 molecules in the asymmetric unit. The crystal structure was solved by molecular replacement using PHENIX (223) with the atomic coordinates of the H143A HDAC8–tetrapeptide substrate complex (PDB accession code 3EWF) (105) less substrate, metal ions, and solvent molecules used as a search probe for rotation and translation function calculations. The model was refined with iterative cycles of refinement in PHENIX (223) and manual model rebuilding in COOT (224). Solvent molecules and inhibitors were added after initial rounds of refinement. Translation Libration Screw (TLS) refinement was performed in the late stages of refinement. TLS groups were automatically determined using PHENIX. Final refinement statistics are recorded in Table 4-1.

Portions of the N-terminus, the C-terminus, and the L1 and L2 loops were characterized by missing or broken electron density. These segments appeared to be disordered and were excluded from the final model as follows: M1-S13 (monomers A and B), A32-I34 (monomer B), G86-D89 (monomer A) G86-E95 (monomer B), I378-H389 (monomer B), and E379-H389 (monomer A). Likewise, side chains of residues that were partially or completely disordered were excluded from the model as follows: L14 (monomers A and B), K33 (monomer A), I34 (monmer A), K52 (monomer B), K58 (monomer B), K60 (monomers A and B), K81 (monomers A and B), Q84 (monomer A), E85 (monomer A), I94 (monomer A), E95 (monomer A), Y100 (monomer B), E106 (monomer B), K132 (monomers A and B), K221 (monomer B), E238 (monomer B), Q253 (monomers A and B), E358 (monomer B), K370 (monomer A), V377 (monomer A), and I378 (monomer A).

Occasional ambiguous electron density peaks were observed in the structure. These peaks were usually elongated and potentially corresponded to disordered PEG fragments or other molecules present in the crystallization buffer. However, since these electron density peaks were not confidently interpretable, they were left unmodeled. Similarly, ambiguous electron density was observed around W141 in monomer A, possibly corresponding to alternative conformations. However, since such conformations

were not confidently interpretable, the W141 side chain was modeled in only one primary conformation.

Results

Crystal structure of S39E HDAC8

Because the phosphorylated enzyme is difficult to obtain in large quantities and purity for crystalization, we used the S39E-HDAC8 mutant, which mimicks phosphorylation at this site. The mutant was crystalized in an inhibitor-bound state. This is the first crystal structure of an HDAC isozyme complexed with Droxinostat, a selective HDAC3, HDAC6, and HDAC8 inhibitor (225). The structure of the S39E HDAC8-Droxinostat complex shows how the phosphorylation of S39, as mimicked by the S39E substitution, might influence inhibitor binding in the enzyme active site. Residue S39 is located in helix A2, ~20 Å away from the catalytic Zn^{2+} ion. The structure of the S39E HDAC8–Droxinostat is similar to that of the wild-type HDAC8–M344 complex (PDB accession code 1T67) (112) with an r.m.s. deviation of 0.49 Å for 356 Cα atoms and 0.47 Å for 350 Cα atoms, for monomer A and B, respectively. Although the S39E substitution does not cause any large-scale change in the HDAC8 structure (Figure 4-2), local structural changes are observed in the vicinity of S39E that propagate through to the active site via changes in the structure of Loop 1. These structural changes may similarly be triggered by phosphorylation of S39 in the wild-type enzyme.

In the wild-type HDAC8 structure, the hydroxyl group of S39 donates a hydrogen bond to the carboxylate group of D29, which is located in the adjacent helix A1. In S39E-HDAC8, the E39 side chain is oriented toward solvent and does not interact with any surrounding residues, including positively charged K36. Similarly, E39 does not perturb the nearby residue R37, the “gatekeeper” for the internal channel (104). However, the S39E mutation induces a slight shift of D29 (0.6 Å for the Cα atom). The carboxylate side chain of D29 undergoes a conformational change away from E39, presumably to minimize electrostatic repulsion with the carboxylate side chain of E39 (Figure 4-2).

The conformational change of D29 causes the L1 loop to reorganize. The L1 loop (L31-P35) connects helices A1 and A2 and is adjacent to the active site. The L1 loop is important, along with the L2 loop, for substrate and inhibitor binding (73). Alternative conformations are often observed for these loops in HDAC8 structures as they accommodate the binding of different ligands. Although more data is needed to definitively state that the mutation of S39 significantly alters loop L1 beyond the normal flexibility, there is evidence that the L1 loop in the S39E-HDAC8 structure is more disordered than usually observed in HDAC8 complexes. These observations are the higher thermal B factors, along with missing electron density for the side chains of K33 and I34 in monomer A, and weak electron density in monomer B that did not allow modeling of the A32-I34 segment.

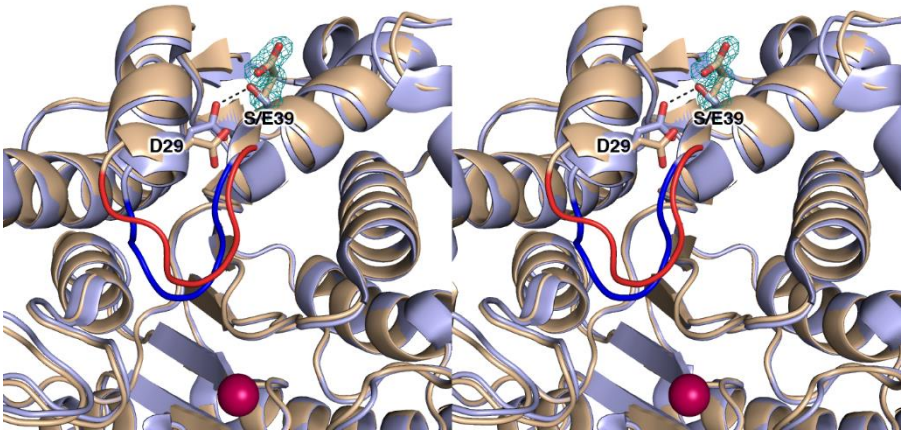

Figure 4-2:

Stereoview of Superimposition of S39E-HDAC8-Droxinostat and WT-HDAC8-M344

Stereo view superimposition of the S39E HDAC8-Droxinostat complex (monomer A: C = wheat, N = blue, O = red, Zn^{2+} = magenta sphere) and the wild-type HDAC8-M344 complex (PDB 1T67, color-coded as above except C = light blue). In the wild-type structure, S39 donates a hydrogen bond (black dashed line) to D29. Upon substitution to a glutamate (simulated omit map contoured at 4.0σ showing the E39 side chain), this interaction is not conserved and causes local rearrangement. The L1 loop adopts a different conformation as highlighted in red and blue for the S39E HDAC8-Droxinostat complex and the wild-type HDAC8-M344 complex, respectively.

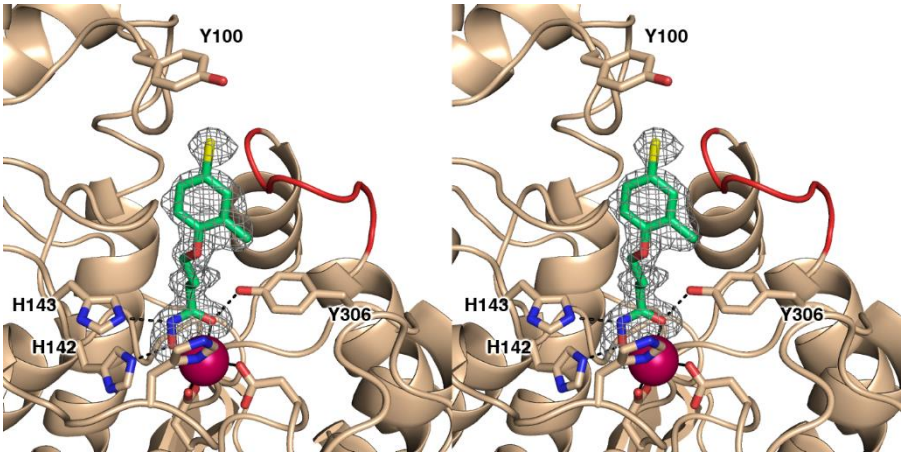

Figure 4-3:

Stereoview of simulated annealing omit map of S39E-HDAC8-Droxinostat

Simulated annealing omit map of Droxinostat bound in the active site of S39E HDAC8 (monomer A, contoured at 3.0σ). Atomic color codes are as follows: C = wheat (protein, monomer A), or green (inhibitor), N = blue, O = red, Zn^{2+} = magenta sphere. Metal coordination and selected hydrogen bond interactions are shown as solid black or dashed black lines, respectively. As in Figure 4-2, the L1 loop of S39E-HDAC8 is highlighted in red.

Table 4-1: Data collection and refinement statistics for the S39E-HDAC8-Droxinostat complex

Unit cell	
space group symmetry	$P2_1$
a, b, c (Å)	53.4, 84.4, 94.6
α, β, γ (deg)	90, 99.4, 90
Data collection	
wavelength (Å)	1.075
resolution limits (Å)	43.0-1.59
total/unique reflections	819616/110604
R_{merge}[a,b]	0.080 (0.605)
$I/\sigma(I)$[a]	19.3 (4.7)
redundancy[a]	7.4 (7.1)
completeness (%)[a]	100 (100)
Refinement	
reflections used in refinement/test set	110567/5539
R_{cryst}[c]	0.142
R_{free}[d]	0.160
protein atoms[e]	5648

water molecules[e]	777
ligand molecules[e]	2
Zn^{2+} ions[e]	2
K^+ ions[e]	4
glycerol molecules[e]	2
R.m.s. deviations from ideal geometry	
bonds (Å)	0.010
angles (°)	1.3
dihedral angles (°)	12
Ramachandran plot (%)[f]	
allowed	91.1
additionally allowed	8.9
PDB accession code	5BWZ

[a] Values in parentheses refer to the highest shell of data. [b] $R_{merge} = \sum|I_h - \langle I\rangle_h|/\sum I_h$, where $\langle I\rangle_h$ is the average intensity for reflection h calculated from replicate reflections. [c] $R_{cryst} = \sum||F_o| - |F_c||/\sum|F_o|$ for reflections contained in the working set. $|F_o|$ and $|F_c|$ are the observed and calculated structure factor amplitudes, respectively. [d] $R_{free} = \sum||F_o| - |F_c||/\sum|F_o|$ for reflections contained in the test set held aside during refinement. [e] Per asymmetric unit. [f] Calculated with PROCHECK version 3.4.4.

This disorder appears to propagate through to the active site; the 4-chloro-2-methylphenoxyl capping group of the hydroxamate inhibitor Droxinostat is characterized by somewhat weaker electron density and higher thermal B factors. The hydroxamate moiety of Droxinostat coordinates to the active site Zn^{2+} ion, forming a five-membered ring chelate, as typically observed in all HDAC8-hydroxamate crystal structures (18, 86, 105, 111, 112, 115). The coordination distances to the Zn^{2+} ion are 2.0 Å and 2.2 Å for the hydroxamate hydroxyl and carbonyl groups, respectively. The Zn^{2+}-bound hydroxamate is also stabilized by hydrogen bond interactions with Y306, H142, and H143 (Figure 4-3). The capping group of Droxinostat does not make significant interactions with residues at the mouth of the active site. A contact is made between the chlorine atom of Droxinostat and the hydroxyl group of Y100 in the L2 loop (the Cl---O distance in monomer A is 3.2 Å; the side chain of Y100 is disordered in monomer B). However, Y100 is poorly oriented to consider this interaction as a hydrogen bond. The interaction may be a halogen bond.

S39E mutation decreases Co(II)- Fe(II)- and Zn(II)-dependent catalytic efficiency

While inhibition of HDAC8 activity by phosphorylation or the S39E-HDAC8 phosphomimetic mutant had been observed for core histone deacetylation, detailed kinetic parameters for either of these enzymes had not been determined (143). Using the Fluor-de-Lys assay, S39E-HDAC8 was assayed with Zn(II), Fe(II), and Co(II) bound to the active site to compare the catalytic efficiency to that of wild type HDAC8. Consistent with previous reports, S39E-HDAC8 activity was decreased compared to WT-HDAC8 in all cases tested (Table 4-2, Figure 4-4). Fe(II)-dependent catalytic efficiency (k_{cat}/K_M) was 6-fold lower for the mutant, Zn(II)-dependent catalytic efficiency was 12-fold decreased, and Co(II)-dependent catalytic efficiency was 7-fold decreased. The K_M and k_{cat} values can also be compared for the Fe(II) enzymes, and they reveal that the decrease in k_{cat}/K_M is due to both a 2-fold increase in K_M and a 3-fold reduction in k_{cat}. This indicates that mutation of S39 to E39 minimally affects both substrate recognition and hydrolysis. Phosphorylation on HDAC8 may be a modulator of HDAC8 activity.

Table 4-2: Kinetics of S39E-HDAC8 toward Fluor-de-Lys peptide[a]

HDAC8	k_{cat}/K_M ($M^{-1}s^{-1}$)	K_M (μM)	k_{cat} (s^{-1})
Fe(II)-S39E	440 ± 60	170 ± 30	0.077 ± 0.005
Fe(II)-WT	2800 ± 700	90 ± 30	0.25 ± 0.02
Zn(II)-S39E	50 ± 40	> 400[b]	> 0.05[b]
Zn(II)-WT	580 ± 90	1100 ± 50[c]	0.90 ± 0.03[c]
Co(II)-S39E	1100 ± 400	> 1700[b]	> 2[b]
Co(II)-WT	7500 ± 300[c]	160 ± 6[c]	1.2 ± 0.2[c]

[a] Reactions consisting of 0.5 to 1 μM HDAC8 and 10 to 500 μM substrate in 20-25 mM HEPES or Tris pH 8.0, 137 mM NaCl, 3 mM KCl at 30°C.
[b] K_M and k_{cat} are poorly defined by this data set. More data is needed.
[c] Values reported in (67).

A

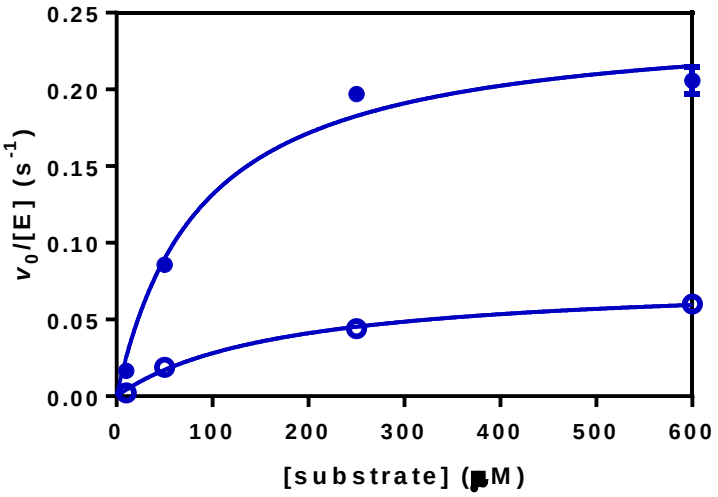

B

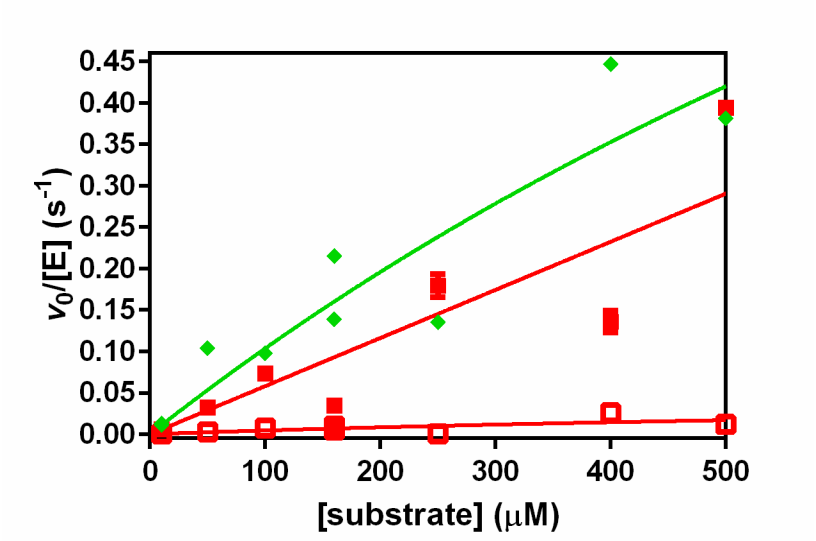

Figure 4-4: S39E-HDAC8 catalytic activity toward Fluor-de-Lys peptide substrate

A. Dependence of initial rates for deacetylation of the Fluor-de-Lys peptide substrate on the substrate concentration catalyzed by Fe(II)-S39E-HDAC8 (open blue circles) and Fe(II)-WT-HDAC8 (closed blue circles). The Michaelis-Menten equation was fit to the data. B. Substrate concentration dependence of the initial rate for deacetylation catalyzed by Zn(II)-WT-HDAC8 (■), Zn(II)-S39E-HDAC8 (□), and Co(II)-S39E-HDAC8 (♦). The data are a combination of three experiments, with error bars (colored to match the symbols) representing errors calculated from fits of initial rates, and the Michaelis-Menten equation (S39E-HDAC8) or a linear slope (Zn(II)-WT-HDAC8) was fit globally to the data.

S39E-HDAC8 activity is decreased toward unlabeled peptide substrates

To investigate whether S39 alteration affects substrate specificity of the enzyme or simply reduces activity towards all substrates, we measured the apparent catalytic efficiency of Zn(II)-S39E-HDAC8 and Zn(II)-WT-HDAC8 toward two peptides that do not contain a fluorophore. The methylcoumarin fluorophore on the Fluor-de-Lys peptide enhances activity and substrate affinity to HDAC8 (71, 72). The two peptides tested were a 13 amino acid peptide representing the H3K9ac acetylation site on histone H3, Ac-TKQTARKacSTGGKA-NH_2, and a peptide representing an acetylation site on SMC3, a putative *in vivo* HDAC8 substrate, of the sequence Ac-RVIGAKKacDQY-NH_2. An assay which couples the formation of acetate to a fluorescent NADH readout was used (72). The decrease in activity observed for S39E-HDAC8 was comparable to the decrease observed for S39E-HDAC8 toward the methycoumarin-conjugated Fluor-de-Lys peptide substrate (12-fold decrease), at 13- and 16-fold lower apparent catalytic efficiency for H3K9ac and SMC3, respectively (Figure 4-5 and Table 4-3). These data suggest that the S39E mutation mainly decreases activity and not substrate selectivity. More data is needed, however, as the fits of three time points may underestimate the initial rates for WT-Zn(II)-HDAC8.

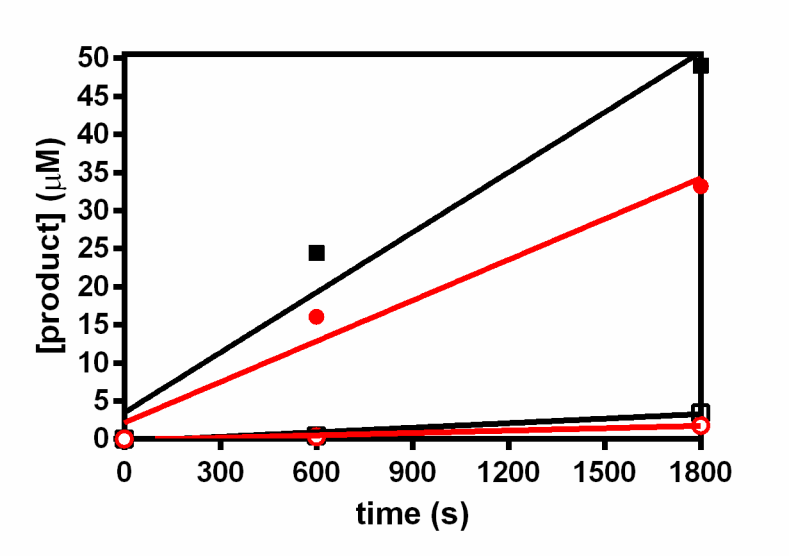

Figure 4-5: S39E-HDAC8 catalytic activity toward unlabeled peptides

Dependence of HDAC8-catalyzed product formation on time for deacetylation of SMC3 (red circles) and H3K9ac (black squares) peptides by WT-Zn(II)-HDAC8 (● for SMC3, ■ for H3K9ac) and S39E-Zn(II)-HDAC8 (○ for SMC3, □ for H3K9ac). A linear slope was fit to the data to measure initial rates of reaction (3 time points) over 1800 seconds for 120 μM peptide and 2.4 μM Zn(II)-HDAC8, using the NADH-coupled acetate assay. Data points are from single measurements and data was fit using GraphPad Prism.

Table 4-3: S39E-HDAC8 apparent catalytic efficiency for unlabeled peptides

HDAC8	H3K9ac peptide $k_{cat}/K_{M,\ app}$ ($M^{-1}s^{-1}$)	SMC3 peptide $k_{cat}/K_{M,\ app}$ ($M^{-1}s^{-1}$)
WT-Zn(II)-HDAC8	92 ± 5	60 ± 30
S39E-Zn(II)-HDAC8	7 ± 3	4 ± 2
fold decrease	13	16
The $k_{cat}/K_{M,\ apparent}$ values were calculated from the linear initial rates of reaction (3 time points) over 1800 seconds for 120 μM peptide and 2.4 μM Zn(II)-HDAC8, using the NADH-coupled acetate assay.		

S39E-HDAC8 metal dissociation is faster than wild type

To explore the effect of phosphorylation on the active site metal ion, the dissociation rate constants for the catalytic metal (Fe(II) or Zn(II)) were determined. The dissociation rate constants for both Fe(II)- and Zn(II)-S39E HDAC8 increased more than 10-fold (Figure 4-6), indicating that metal dissociation is much more rapid for this mutant compared to WT-HDAC8. However, similar to wild type, the dissociation rate constants for the two metal ions are comparable. This dramatic increase in metal k_{off} indicates that an alteration within the S39E structure facilitates rapid metal dissociation.

Table 4-4*:* Metal ion dissociation rate constants for S39E and WT HDAC8

Enzyme	Fe(II) k_{off} (min^{-1})	Zn(II) k_{off} (min^{-1})
S39E-HDAC8	0.48 ± 0.05	0.57 ± 0.07
WT-HDAC8	0.03 ± 0.004[a]	0.04 ± 0.003[a]
The k_{off} values are calculated by a global fit of an exponential decay equation to data from replicates on different days. [a]Values reported in (182).		

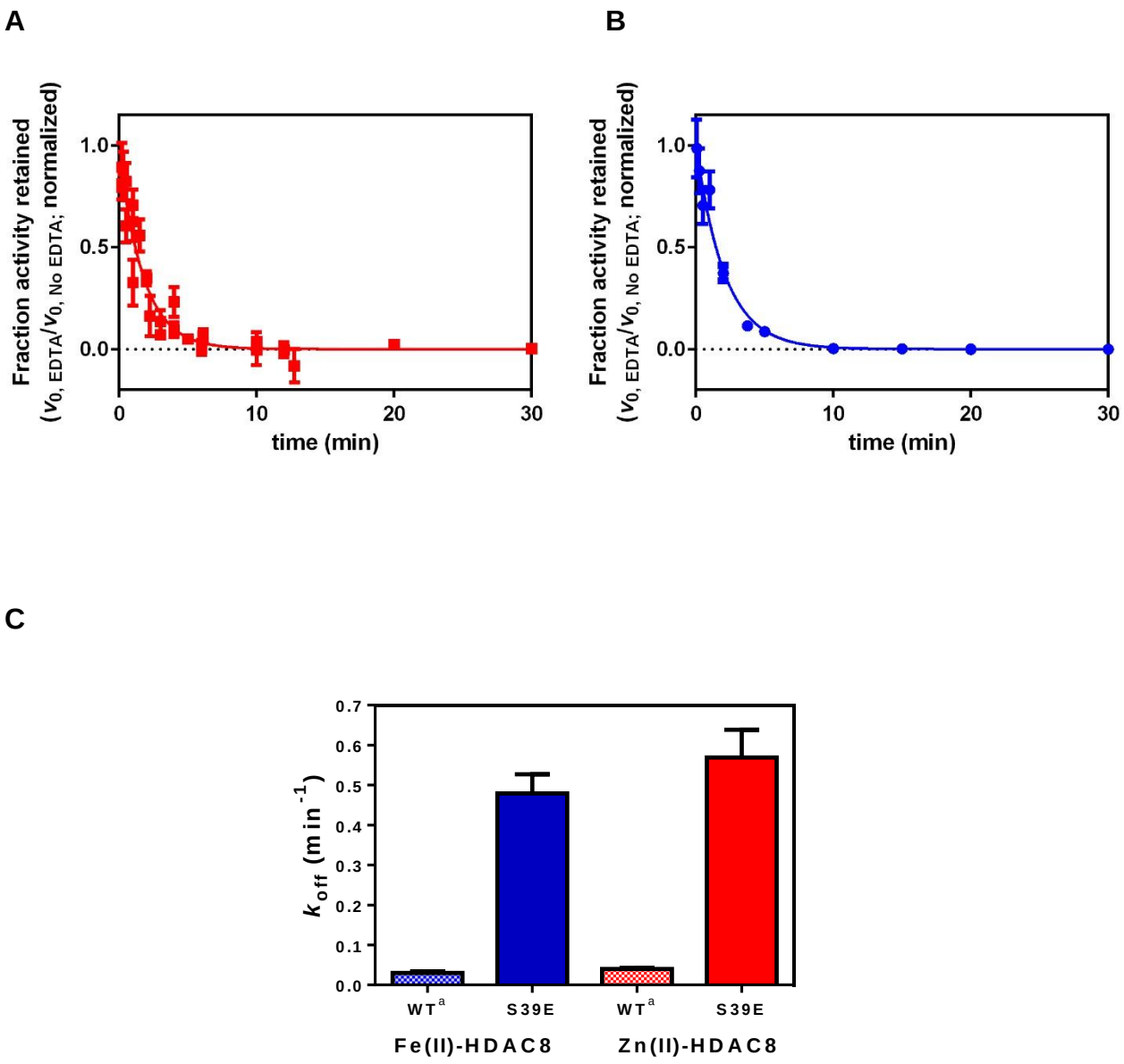

Figure 4-6: Metal ion off rates for Fe(II)- and Zn(II)-S39E HDAC8

A and B. Initial rates for Zn(II)-S39E-HDAC8 (A, red squares) and Fe(II)-S39E-HDAC8 (B, blue circles) deacetylation activity as a function of time as measured using the Fluor-de-Lys assay after addition of 1 mM EDTA. The fraction activity is determined by dividing this activity by the activity of HDAC8 incubated in the absence of EDTA. The exponential equation, Y=Amp*exp(-k_{off}*time, was fit to all of the data, and replicates from multiple days are shown. C. Graphical representation of k_{off} values demonstrates the significant difference between WT and S39E metal ion off rates. [a]Values reported in (182).

Zn(II) affinity of S39E-HDAC8

Intrigued by the effect of S39E on the dissociation rate constants for the catalytic metal ion bound to HDAC8, we measured the metal affinity equilibrium constant using a fluorescein-SAHA anisotropy assay (182). The resulting K_D value for the S39E mutant was 2 ± 2 pM, which is comparable to the WT value of 6 ± 1 pM (182), however more data is needed to precisely determine the K_D and draw conclusions comparing mutant and wild type HDAC8 Zn(II) binding. A complicating factor for these data is that in addition to the expected increase in anisotropy at low metal concentrations due to binding of fluorescein-SAHA to the enzyme, there is a decrease in anisotropy at the highest zinc concentrations. One possible explanation for this result is that at higher zinc concentrations the mutant binds multiple zinc ions that complete with fl-SAHA binding at the active site and as a result the observed anisotropy decreases.

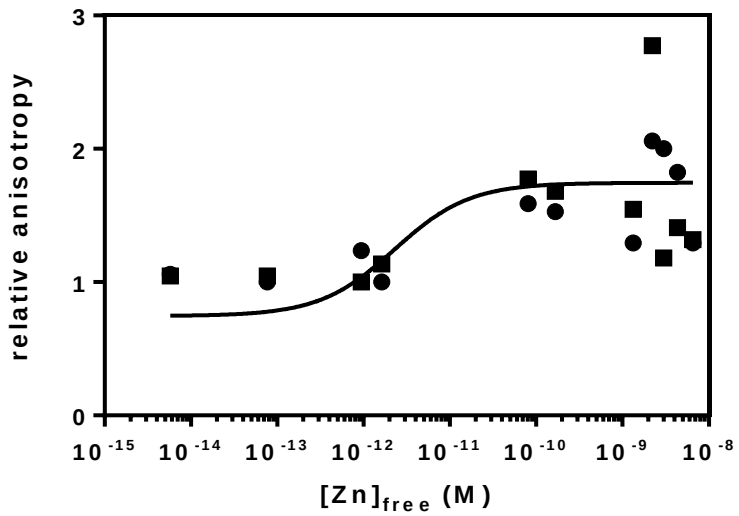

Figure 4-7: Zinc affinity for S39E-HDAC8

Global fit of two replicate K_D experiments. Different symbols represent different days. Equation 3 was fit to the data.

Molecular dynamics simulations suggest possible phospho-HDAC8 structural changes

The crystal structure provides a snapshot of inhibitor-bound S39E-HDAC8. To investigate the effects of phosphorylation on substrate-HDAC8 interactions, molecular dynamics simulations were used, starting with an HDAC8-peptide substrate complex crystal structure (PDBID: 2V5W (111)). We compared the substrate binding dynamics of phosphorylated HDAC8 (pS39-HDAC8, modeled), S39E-HDAC8 (with substrate modeled), and WT-HDAC8. By simulating phosphorylation on the WT structure, we were able to predict the structure and dynamics of residues in the L1 loop that were not resolved in the S39E crystal structure and validate the S39E mutation as a mimic of phospho-HDAC8. While the mutant was crystalized in complex with an inhibitor, the simulations predict the structure of pS39-HDAC8 with and without peptide substrate bound. In the first set of simulations (Figure 4-8), WT-HDAC8 is modeled with and without the Fluor-de-Lys p53-based peptide substrate, to compare with the pS39 simulations. Relevant residue conformations surrounding S39 are highlighted in Figure 4-8, with the most important being that of substrate, Y306, and K33. Figure 4-9 shows the results of simulation of pS39-HDAC8, and Figure 4-10 shows a comparison of pS39- and S39E-HDAC8 with and without bound substrate. These simulations indicate that modification of S39 leads to a disruption of the interaction between Y306 and K33, which perturbs substrate binding. The interaction between S39 and D29 is also disrupted by the addition of negative charge at position 39; D29 instead interacts with K36. The K36-D29 interaction and altered Y306-K33 interaction preclude binding of substrate at the wild-type position, instead the peptide binds in a channel between K33 and Y306 where it is not optimally positioned for deacetylation by the active site metal-water nucleophile. These simulations provide insight into the basis for decreased pS39- and S39E-HDAC8 activity, and although the D29-K36 contact is not noticeable in the S39E crystal structure, the altered orientation of D29 is consistent with the 0.6 Å shift for D29 that was observed in the crystal structure.

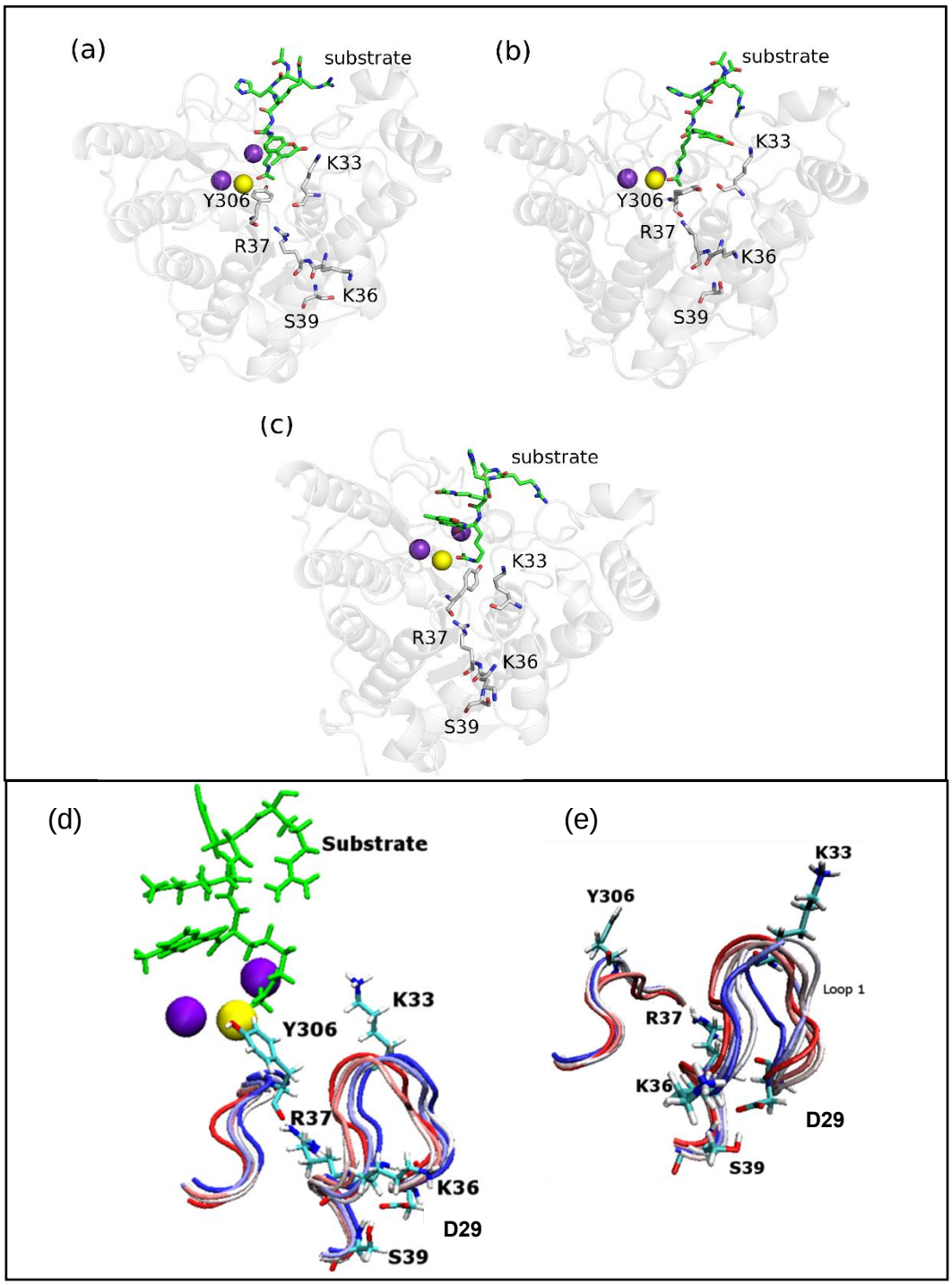

Figure 4-8: Simulations of WT-HDAC8 binding to substrate

The top panel shows the orientation of key residues in WT-HDAC8 at the (a) start, (b) 204 ns and (c) 400 ns of the substrate binding simulation. S39 is solvent-exposed. Y306 bends at 90° toward K33, and the Hε of Y306 forms a hydrogen bond with the carbonyl of K33 (b). This opens the tunnel for substrate interaction with the active site, which is otherwise blocked by Y306. Yellow and purple spheres represent Zn^{+2} and K^{+} ions respectively. The bottom panel shows a representation of the key residues and loops with (d) and without (e) substrate. The K33 side chain interacts with a substrate oxygen. Spheres represent metal ions as above.

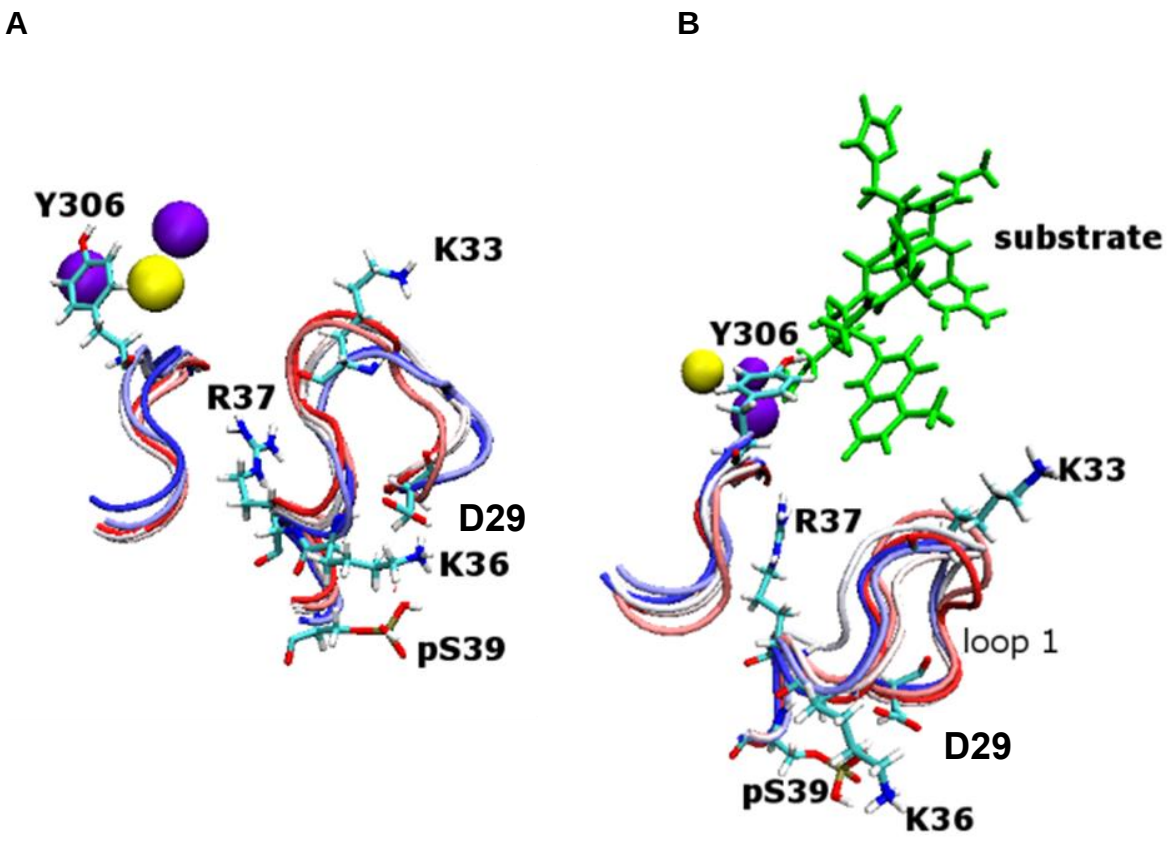

Figure 4-9: Simulation of substrate binding to pS39-HDAC8

Representation of key residues in HDAC with phosphorylated S39 (A) without and (B) with substrate. RMSF of K33 is equivalent in both the simulations. As the –OH group of pS39 is unavailable, in (B) K36 interacts with D29 directly. The substrate does not gain full access to catalytic site and instead goes into the channel between K33 and Y306. Yellow and purple spheres represent Zn(II) and potassium ions respectively.

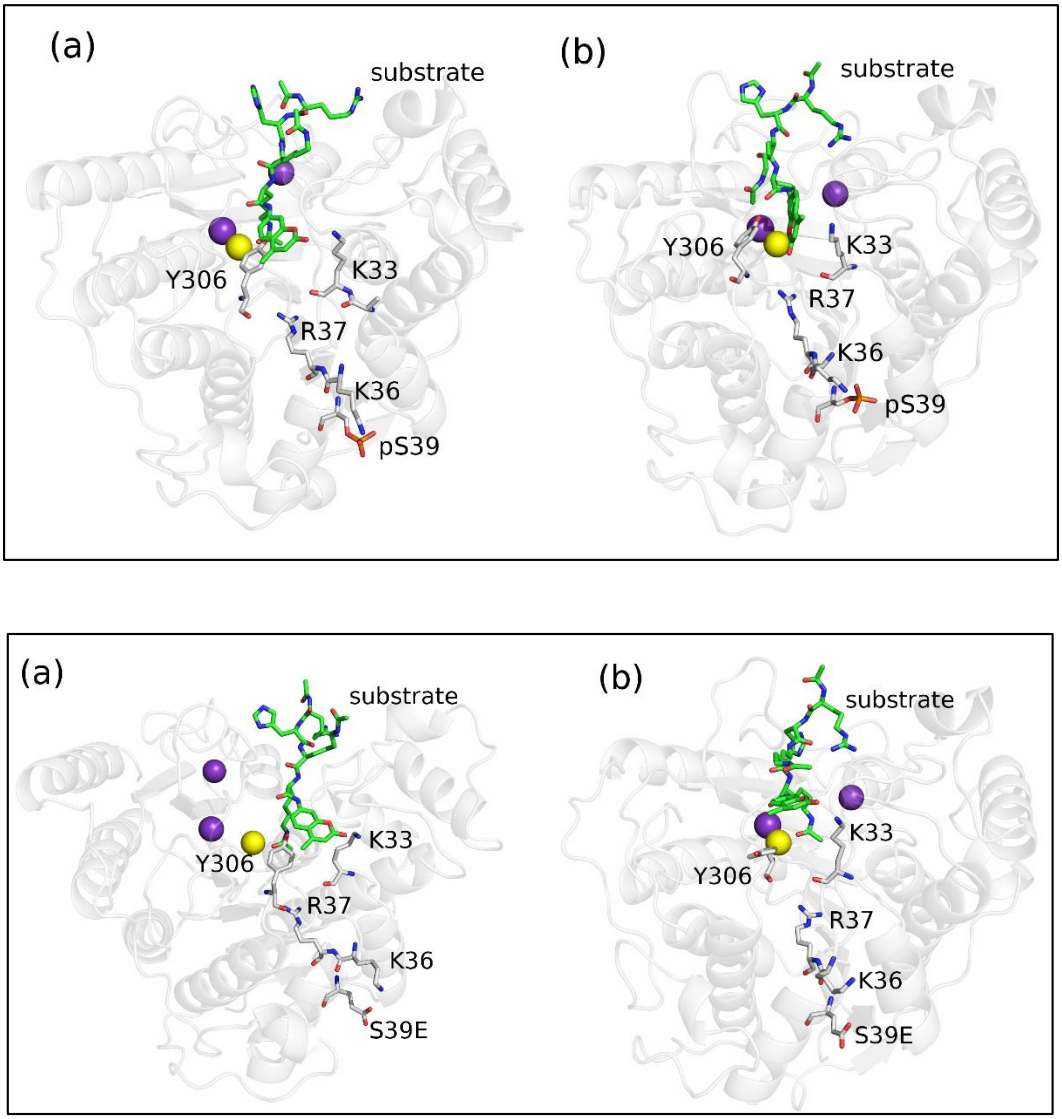

Figure 4-10: Simulations of pS39 and S39E bound to substrate

In simulations, the S39E mutant behaves similarly to the pS39-HDAC8, validating this phosphomimic. In the top panel (pS39 modeled on WT-HDAC8), two snapshots (start (a) and 400 ns (b)) during the simulation demonstrate that the substrate is shifted in the active site between K33 and Y306 compared to WT-HDAC8 (Figure 4-8A–C). Y306 interacts with substrate but does not interact with K33. The bottom panel (S39E-HDAC8 with modeled substrate) is a representation at the start (a) and 400 ns (b) of the simulation of key residues in S39E-HDAC8 and demonstrates that the enzyme behaves similarly to pS39-HDAC8. The L1 loop is distorted, Y306 and K33 do not interact (unlike in WT-HDAC8 (Figure 4-8B) where Y306 forms a hydrogen bond with the carbonyl oxygen of K33), and Y306 does not interact with substrate in this simulation. Substrate access to the active site is altered.

Discussion

The mechanistic and functional roles of phosphorylation on HDAC8 are important facets of HDAC8 regulation that have not been well studied up to this point. To examine the effect of addition of a bulky negative charge at S39, the S39E mutant HDAC8 was used as a phosphomimic. The validity of the mimic was bolstered by the fact that the S39E- and phospho-HDAC8 behave similarly in assays while the S39A-HDAC8 behaves like the wild type enzyme (143). Previously, crystal structures of the S39D-HDAC8 has been solved, and the structure of this mutant is reported to be essentially the same as the wild type (44, 111). The S39E mutant, however, is a more appropriate mimic of phosphorylation (143) and the S39E-HDAC8-Droxinostat structure visualizes noticeable differences from the wild type structure. The structure of S39E-HDAC8-Droxinostat reveals that the L1 loop is distorted and the interaction between S39 and D29 is disrupted by the glutamate substitution. Loop L1 is important for HDAC8 substrate and inhibitor interactions (44), so this structural perturbation likely contributes to the decreased catalytic efficiency. It is important to note that a structure of WT-HDAC8 complexed with Droxinostat has not been solved. Comparing S39E-HDAC8-Droxinostat directly to WT-HDAC8-Droxinostat would be useful to eliminate the possibility of structural changes induced by the identity of the inhibitor.

Interestingly, the position of R37 is not altered in either the inhibitor-bound crystal structure or the phosphorylation simulation. R37 is critical for activity (104) and, due to its proximity to S39E, distortion of this residue would not have been surprising. Additionally, an electrostatic interaction between K36 and E39 had been anticipated but was not evident in the structure. Instead the relevant changes are in the perturbed interactions between Y306, substrate, and K33, the loss of a hydrogen bond between the hydroxyl of S39 and the carboxylate of D29 (which bridges the α1 and α2 helices) and the gain of an interaction between D29 and K36. Regarding the lost D29-S39 hydrogen bond, the inhibitor bound structure shows that this change is correlated with a distortion of the L1 loop. The pS39 HDAC8 simulation reveals that this lost interaction alters the position of the bound substrate. In this simulation, K36 interacts with D29 and the side chain of K33 is shifted (part of the L1 loop). Substrate binding is typically oriented in part by Y306 and K33, however in the absence of the hydrogen bond interaction between Y306 and the

K33 backbone carbonyl, the substrate is shifted in the active site between these residues. This was the most significant difference observed in the simulations. The inhibitor-bound crystal structure does not show this altered Y306/K33 interaction and the inhibitor is positioned in the typical Zn(II)-bound orientation such that the carbonyl forms a hydrogen bond with Y306 (Figure 4-3). The fact that the crystal structure and the simulation provide somewhat different visualizations of ligand-bound S39E-HDAC8 may be due to several factors. Mainly, the inhibitor is small and interacts primarily with the active site, limiting interactions with the HDAC8 peptide binding groove outside of the active site tunnel. The interaction between Droxinostat and Y100 is not even close enough to be characterized as a hydrogen or halogen bond. Additionally, some residues (*e.g.* K33) cannot be directly compared to the simulated structure because they were not resolved in the crystal, suggesting significant mobility. Finally, while the S39E structure demonstrates structural difference and mimics phosphorylation, glutamate is not identical to phosphoserine and thus some differences between E39 and pS39 are expected.

S39E-HDAC8 exhibits a decrease of 6- to 16-fold in catalytic efficiency compared to WT. The simulations and crystal structure suggest that the decrease in catalytic activity that accompanies the mutation and phosphorylation arise from the consequent reordering of and/or disorder in the L1 loop flanking the active site cleft. Structural differences in this loop presumably influence its affinity for substrates and inhibitors binding to the active site. The increase in K_M observed for Fe(II)-S39E-HDAC8 over WT-HDAC8 is consistent with perturbation in the L1 loop affecting substrate affinity, since K_M is proposed to reflect K_D for peptide deacetylation (67). Assuming that the mutation does not change the kinetic mechanism of this enzyme, the k_{cat} effect indicates that hydrolysis of the acetyl-lysine is decreases. This may be due to a direct effect on the reactivity of the metal-water nucleophile via structural changes propagated by the altered D29-S39 interaction, but it is more likely due to the altered site of the bound peptide that leads to incorrect positioning of the acetyl-lysine amide bond relative to the metal-water. However, the k_{cat} value was only accurately determined for the Fe(II)-bound enzyme while the structure and simulations used Zn(II)-HDAC8; and activity data demonstrate that both S39E-HDAC8 and WT HDAC8 (67) are activated to different extents depending on the identity of the catalytic metal ion. Additionally, we have shown that the substrate specificity of Zn(II)-

S39E-HDAC8 toward three peptides was comparable to wild type activity (*i.e.* the mutation decreased activity by the same fold difference in each case). Further study using a larger library of peptides is needed to further evaluate substrate specificity effects.

The dissociation rate constants for the catalytic metal surprisingly reveal a greater than 10-fold increase in k_{off} for the catalytic metal ion which is 21 Å away from the mutation. The structural and simulation data do not readily explain the significant effect of the S39E mutation on metal dissociation. The effect on metal dissociation may be indicative of decreased protein stability, partially due to the loss of D29-S39 hydrogen bonding between the α1 and α2 helices. Monovalent cation stability of HDAC8 may also be affected, however it is not clear how modification at S39 would propagate an effect to the monovalent sites. Since no perturbation of R37 was observed, that residue and the internal HDAC8 channel are not likely to be involved in the metal dissociation difference.

The significant increase in the dissociation rate constant means that there should also be either a significant increase in the K_D values (decreased metal affinity), a significant increase in the k_{on} values, or changes in both K_D and k_{on}. Preliminary K_D measurements indicate a Zn(II) K_D of approximately 2 pM, comparable to the wild-type enzyme. Assuming a single step metal binding, the apparent k_{on} should be at the diffusion controlled limit (5×10^9 $M^{-1}s^{-1}$). However, the comparable values measured for k_{off} for Zn(II) and Fe(II) despite the large differences in K_D values argue for at least a two-step metal binding mechanism, possibly consisting of a rapid metal binding association step followed by a unimolecular rearrangement step. In the case of the wild type enzyme, the k_{off} values and the affinities for Fe(II) ($K_D = 0.2 \pm 0.1$ μM) and Zn(II) ($K_D = 6 \pm 1$ pM) are such that the metal association was predicted to be a one-step mechanism for Zn(II) ($k_{on}^{app} = 1 \times 10^8$ $M^{-1}s^{-1}$) and a two-step mechanism for Fe(II) ($k_{on}^{app} = 3 \times 10^3$ $M^{-1}s^{-1}$) (182). A similar metal association scheme is predicted for S39E- (and phospho-) HDAC8.

Taken together, these data provide insight into the residue interactions (i.e. S39/D29) that lead to perturbation of the kinetic properties by S39 phosphorylation. Further study is needed to parse how the metal-dependence, phosphorylation, and substrate specificity of HDAC8 are interconnected. The role and regulation of phospho-HDAC8 in the cell is unclear, and elucidating some of these factors will help us to

understand the regulation of deacetylation and will inform drug discovery, as phosphorylation-dependent protein-protein interactions may present druggable targets for small molecule therapeutics.

Accession Code

The atomic coordinates and the crystallographic structure factors of S39E HDAC8 in complex with Droxinostat have been deposited in the Protein Data Bank (www.rcsb.org) with accession code 5BWZ.

Acknowledgements

We thank the NSLS for access to beamline X29 for X-ray crystallographic data collection. We thank Drs. Ted Huston and Lubomír Dostál for performing ICP-MS. We thank Jeffrey E. López for collaborating on the metal affinity measurements and Dr. Ningkun Wang and Oleta T. Johnson for collaboration on protein purification. We thank the National Institutes of Health Grant 5-R01-GM-040602 (C.A.F.), the University of Michigan Chemistry-Biology Interface (CBI) training program NIH grant 5T32GM008597 (C.A.P.) and Rackham Graduate School (C.A.P.) for funding.

Chapter 5
Conclusions and future directions

Overview

This dissertation presents an investigation into several facets of the inherently complex system of HDAC regulation. HDAC8 is part of a large family of enzymes that catalyze the same chemical reaction, hydrolysis of acetate from acetyl-lysine, but which serve in distinct and diverse roles throughout the cell. Because HDACs are involved in an elaborate web of critical cellular processes, it is not surprising that their regulatory modes are proving to be equally intricate. Narrowing the focus to 6% (1 out of 18) acetyl-lysine deacetylase enzymes still offers several avenues of HDAC regulation that require further elucidation, including metal switching, substrate recognition determinants, and phosphorylation, which I have discussed here. Despite over a decade of kinetic and cell-based research, including recent studies aimed at revealing endogenous HDAC8 substrates (80), parsing HDAC8-inhibitor interactions (44), and illuminating HDAC8's role in disease (51), there is still much to be uncovered regarding how this metallo-hydrolase contributes to normal and disease-related cellular function.

In the HDAC field, very little is known about the kinetics of deacetylation on biological substrates. We have performed the first detailed kinetic study of HDAC-catalyzed deacetylation of a full-length protein acetylated at a single site, and provides new information regarding determinants of HDAC8 substrate recognition. For the first time, HDAC8 substrate specificity toward peptides is compared directly to the substrate specificity for protein substrates. This method would be useful for assaying other HDACs as well, to glean more information about how HDACs recognize physiological substrates.

The metal-dependent substrate specificity findings I have presented here suggest a potential regulatory mechanism for HDAC8, as well as other metal-dependent deacetylases. In particular, HDACs 1, 2, and 3 (class I), which are the most similar to

HDAC8 (14), may be activated by Fe(II) and may also be regulated by metal switching in the cell. Metal-dependent HDACs are currently described in the literature as Zn(II)-dependent, but our Fe(II)-HDAC8 data challenges this paradigm. Additionally, there is some data to suggest iron-related HDAC1 behavior in cells. In the rat hippocampus, iron deficiency was recently linked to an increase in HDAC1 binding to the *bdnf*-IV (brain-derived neurotrophic factor) promotor, and iron deficiency was correlated to decreased H4 acetylation levels (226). The altered acetylation was linked to the interdependence of histone methylation and acetylation (226), but iron-dependent HDAC1 activity could be involved. Thus, investigating the relationship between HDAC8 metal-dependence and substrate specificity is important to enhance our understanding of HDAC8 regulation as well as to further our understanding of the metal-dependent regulation of other HDACs in the cell.

Post-translational modifications on HDACs, phosphorylation in particular, are important for the cellular regulation of HDACs, modulating protein-protein interactions, localization, and activity (25, 35). HDAC1 and HDAC2 may be activated by phosphorylation (142, 144, 145, 150, 151), and they exhibit phosphorylation-dependent protein-protein interactions (142, 144, 145). HDAC4, 5, and 7 exhibit phosphorylation-dependent localization and translocation (29-32, 146, 147). Studies of HDAC8 phosphorylation demonstrate effects on localization, protein-protein interactions, and activity inhibition, but do not make clear conclusions regarding the physiological role of phosphorylation on HDAC8 nor the mechanism by which this modification regulates HDAC8 function (83, 108, 143). The investigation I have presented here, studying the effect of phosphorylation on HDAC8 kinetic properties and substrate interactions, is important for elucidating how HDAC8 is regulated by phosphorylation and how this regulatory mode may differ from that of phosphorylation on other HDACs.

Substrate recognition: peptide and protein substrates

Considerable data have been amassed regarding HDAC8 peptide substrate specificity, and recently full-length proteins have been investigated as well (191). The work presented here measures the kinetics for deacetylation of singly acetylated full-

length protein substrates in multi-protein complexes and a protein-nucleic acid complex, which is a significant jump for the field in terms of biologically relevant substrate recognition. Remarkably, full-length proteins demonstrate significantly greater catalytic efficiency than corresponding peptides, and show that peptide substrate specificity does not fully represent HDAC8 specificity toward physiological (full-length) substrates. The determinants of HDAC8 substrate recognition include local substrate sequence and long-range contacts, as demonstrated and discussed in the previous chapters and in (61). Interestingly, HDAC8 exhibits varied selectivity among acetylation sites in the same protein and protein complex, suggesting that increased activity toward proteins over substrates is not due mainly to non-specific interactions. As *in vivo* HDAC8 substrates continue to be identified, they are typically characterized using representative peptides *in vitro* (80). While this does provide a prediction of HDAC8 activity and substrate specificity, our work suggests that these measurements may not provide the best representation of HDAC8 selectivity *in vivo*. To accurately capture HDAC substrate specificity, the kinetics of full-length substrates must be measured. Additionally, Zn(II)-HDAC8 activity toward histone substrates was examined here; Fe(II)-HDAC8 substrate specificity may be different as well, and a next step is to compare the full-length substrate specificity of the two Me(II)-bound HDAC8 enzymes.

To further elucidate the determinants of HDAC8 substrate selectivity as it pertains to full-length proteins, substrates with *in vivo* validation such as SMC3 (47, 51, 80) should be examined. The challenges of purifying and assaying physiologically relevant proteins *in vitro* (such as SMC3 in the cohesin complex) point toward a need for *in vivo* deacetylase assays such as the mass spectrometry-based substrate identification assay described in Olson *et al* (80). HDAC8 substrate recognition in the cell is likely to be more complicated than simply HDAC8-substrate contacts. Binding partners and chaperones may be involved in this process, as suggested by pull-down experiments (81). Using a more global approach can also tackle substrate specificity determinants such as metal switching and HDAC8 phosphorylation.

Metal switching

HDAC8 is curiously poised within cellular metal homeostasis such that it could be activated by iron(II) or zinc(II) *in vivo*. Previous work has shown that the enzyme is activated by both metals and exhibits metal dependent inhibitor efficacy *in vitro* (67). Mammalian and *E. coli* lysates, and immunopurified HDAC8 overexpressed in HeLa cells have demonstrated oxygen-sensitive deacetylase activity, suggesting iron(II)-dependent catalysis (67, 183). The data presented here add to this evidence by demonstrating metal-dependent substrate specificity toward a high throughput library of short peptides as well as a library of peptides based on putative physiological substrates. Here I have presented three key concepts regarding HDAC8, metal-dependence, and metal switching. The first is that HDAC8 is more active with Fe(II) than with Zn(II) toward all substrates tested in solution. The second is that the range of catalytic efficiencies observed for iron is an order of magnitude greater than the range of activity observed for the zinc-activated enzyme. The third observation is that the ratio of Fe/Zn catalytic efficiency varies in a range of 2 to 15. This demonstrates that not only is Fe(II)-HDAC8 is more active than Zn(II)-HDAC8 under the conditions tested, the substrate specificities of Fe(II)- and Zn(II)-HDAC8 are different. These results lead to several questions which will guide future study.

The first question is: do the peptide substrate specificities and the preference for Fe(II) remain true for protein substrates of HDAC8? In light of the histone data presented in chapter 2, which shows that full-length protein substrates contain additional contacts that enhance binding affinity relative to peptides, it is likely that the peptide substrate specificities for Fe(II)- and Zn(II)-HDAC8 do not directly correlate to that of proteins. The relative ratios of Fe/Zn substrate specificity may change for full-length protein substrates, but this does not undermine the fact that these distinct metal-dependent differences in specificity exist. We have shown that the sequence, length, and complex of protein substrates are indeed important for determining substrate specificity, but we then add to that the identity of the HDAC8 catalytic metal ion. The important next step is to examine iron- and zinc-dependent substrate specificity using full-length protein substrates, to investigate how the different metal-bound forms of HDAC8 behave and further elucidate the determinants of substrate specificity in the cell.

Another lingering question is which metal binds to HDAC8 *in vivo.* HDAC8's metal affinities combined with cellular metal concentrations present conditions where HDAC8 could modulate its activity and specificity by switching metal ion cofactors. We propose that the Fe(II)-enzyme would switch to a Zn(II)-enzyme under cellular stimuli that increase highly regulated exchangeable zinc concentrations. If endogenous cellular HDAC8 is indeed sensitive to the flux of iron and zinc metal ions in the cell, this adds a layer of complexity to an enzyme that is involved in both nuclear and cytosolic processes, such as regeneration of the cohesin complex during the cell cycle (47) and cellular contractility (66). We have been working to develop an assay to quantify the metals bound to cellular HDAC8. We use pull downs from mammalian tissue culture cells combined with inductively coupled plasma mass spectrometry (ICP-MS) to measure the metal content of HDAC8. This method is currently being optimized and will be a novel and versatile way of identifying metal(s) bound to cellular metalloenzymes. An additional method we have sought to optimize is that of top-down mass spectrometry to identify metals bound to HDAC8. The goal of this method would be its potential application to human tissues. Mass spectrometry has been used previously to identify metallated species of superoxide dismutase (227), however HDAC8 is more than 2-fold larger than SOD, which is prohibitory for current mass spectrometry methods. Using high resolution mass spectrometry such as Fourier transform ion cyclotron resonance (FT-ICR) MS, the top down identification of Me(II)-HDAC8 from cells and tissues may be attainable.

Third, as I have discussed, is the question of the *in vivo* plausibility of metal switching. Metal concentrations and cellular metal homeostasis are dynamic and the metal switching hypothesis depends on this fluctuating cellular landscape, but this makes identifying HDAC8's role *in vivo* challenging. An area that remains to be studied is to pull down HDAC8 from human cells following manipulation of cellular metal concentrations and redox state to assay metal content. To investigate metal switching, tissue culture cells expressing HDAC8 will be exposed to conditions such as supplemental Fe^{2+} and Zn^{2+}, nitric oxide-generating compounds to induce oxidative stress, and iron chelators to alter metal homeostasis. The role of iron chaperone proteins is an additional avenue we can pursue in this manner, by expressing the iron chaperone human poly (rC) binding protein 1 (PCBP1) (228, 229). HDAC8-bound metals will be analyzed using the pull down/ICP-

MS method we are optimizing. Comparing these data to HDAC8-bound metals under resting cellular conditions will provide a clear picture of what metal(s) HDAC8 utilizes *in vivo*.

Finally, the direction in which this project will go is toward simultaneous identification of substrates, substrate specificity, and metal-dependent specificity *in vivo.* The recent proteomic work of our collaborators has demonstrated a method for identification of specific HDAC8 substrates in the cell (80), and further proteomic study can be applied to the question of metal-dependent specificity. This versatile method can be used to probe other HDACs for metal-dependent specificity and activity as well, using several HDAC-specific inhibitors. In addition to broad substrate identification, we can use proteomics to look at target proteins, such as those which had large Fe/Zn ratios here, under the various cellular conditions stated above. A proteomic study of the acetylation state of specific substrates following induction of metal switching in cells would elucidate this regulatory HDAC mechanism and is within the scope of current technologies.

Phosphorylation and HDAC8

HDAC8 is positioned within the network of post-translational modifications as both a modifying enzyme and a substrate protein. Elucidating how phosphorylation regulates HDAC8 is important for determining how HDAC8 fits into normal and diseased cellular function. I have demonstrated here, using a phosphorylation mimicking mutant, that phosphorylation of HDAC8 decreases HDAC8 activity toward non-histone peptide substrates *in vitro* and that phosphorylation changes the metal dissociation properties of HDAC8. We have shown with crystal structure and molecular dynamics data that phosphorylation at S39 perturbs substrate binding to HDAC8, decreases catalytic efficiency toward non-histone as well as histone substrates *in vitro*, and increases the catalytic metal dissociation rate constant. However, there is still more to uncover regarding how phosphorylation of HDAC8 affects substrate specificity, metal-binding, protein-protein interactions, and ultimately, the role of HDAC8 in disease.

I am investigating the effect of phosphorylation on HDAC8 substrate specificity using a peptide library representing putative and predicted *in vivo* substrates (80, 191).

Structural data predicts that pS39 will affect substrate recognition. I expected to observe differences for phosphorylation-dependent specificity as were observed for metal-dependent specificity, although this was not observed for the small peptide library examined. HDAC8 is promiscuous, ubiquitous, and localizes to both the nucleus and cytosol, so the fact that we are uncovering complicated modes of regulating substrate specificity is not surprising. In addition to *in vitro* substrate specificity, it is imperative to understand the effect of phosphorylation on HDAC8 substrate recognition *in vivo.*

Alteration of acetylated histone levels in HeLa cells upon activation of PKA to phosphorylate HDAC8 were observed by Lee *et al* (143). In light of the ambiguity of histones as HDAC8 substrates, and the recent availability of high-quality proteomic techniques (80), I propose subsequent studies to analyze global cellular acetylation states of proteins (particularly the set of new putative *in vivo* HDAC8 substrates, such as SMC3 and ARID1A) to monitor changes upon phosphorylation of HDAC8 using proteomics. Additionally, I expect that controlling for the phosphorylation state of HDAC8 during *in vivo* substrate identification experiments will effectively add to the growing list of physiological HDAC8 substrates. For example, we know that HDAC8 associates with actin (65, 83), but the actin structure-related proteins that were identified in a proteomic substrate screen did not demonstrate sufficient changes in acetylation levels to be considered above the experimental threshold (80) and no HDAC8-specific actin interactions were observed in recent binding partner pulldowns (81). One imaging study demonstrates that HDAC8 is increasingly associated with actin upon phosphorylation (83). Thus, using the pulldown and mass spectrometry methods to look for phospho-HDAC8 substrates may explain why some predicted substrates have not been observed above background in global analyses.

Phospho-HDAC8 specific binding partners also failed to appear in a proteomic interactome study (81). Phosphorylation is known to affect protein-protein interactions and HDAC complex formation (reviewed in 25, 35). Based on this precedent and the location of S39 on the surface of HDAC8, away from the active site, a role in protein-protein interactions is expected. Consistent with this, Hsp70 has been demonstrated to co-immunoprecipitate only with phospho-HDAC8 (108), and, as discussed above, actin-HDAC8 co-localization is increased upon phosphorylation of HDAC8 (83). Despite this

evidence, recent identification of the HDAC “interactome” did not report HDAC8-specific interactions with these proteins (81). The absence of these interactions in the pulldown may be due to the pulldown method or cell line-specific complexes. Lysis disrupts the cytoskeleton, and actin was observed as a non-specific interaction (81). The GFP fusion protein increases the effective size of HDAC8 and may alter HDAC8-protein binding. Another possibility is that the proteins are not observed due to the fact that these pS39-specific interactions account for only a small population of HDAC8 and are thus overshadowed by the other binding partners. There is a need for proteomic studies that select for phospho-HDAC8 or use cells that contain significant levels of phospho-HDAC8. These experiments may confirm binding partners and/or substrates such as actin and Hsp70.

The effect of phosphorylation on HDAC8 metal affinity is intriguing and had not been studied prior to the work presented here. There is a possibility that phosphorylation facilitates the metal switching proposed in the previous section. The hypothesis is that upon a cellular stimulus, HDAC8 is phosphorylated and the bound metal ion dissociates rapidly. Because both Fe(II) and Zn(II) dissociation rate constants are approximately the same, phosphorylation may be a way for Zn(II)-HDAC8 to switch to Fe(II)-HDAC8 despite the much stronger affinity for Zn(II). Further study of phospho-HDAC8 metal affinity is needed.

Finally, phosphorylation of HDAC8, as it relates to disease states, is of great importance. For example, I have shown that phospho-HDAC8 activity toward an SMC3 peptide is decreased significantly from that of WT-HDAC8. If this disparity is maintained *in vivo*, then phosphorylation of HDAC8 would affect the function and dissociation of cohesin in the cell cycle. A percentage of CdLS cases display mutations in HDAC8, and it is possible that abnormal regulation of the PKA pathway is responsible in some cases as well. We need to investigate the effect of HDAC8 phosphorylation in cellular processes such as the cohesin cycle and cytoskeleton dynamics in normal and disease states.

Concluding remarks

The HDAC field is at an exciting stage, moving increasingly toward *in vivo* assays and an informed picture of HDACs in healthy cells as well as cells and patients of clinical pathologies. In a fascinatingly unfortunate paradox, the more we learn about HDACs, and HDAC8 in particular, the more complicated the study becomes. For example, consider the status of HDAC8 in a given cell. If the regulatory mechanisms of HDAC8 are limited to the determinants we currently know, then HDAC8 can be Fe(II)-bound, Zn(II)-bound, or apo; saturated with monovalent metal ions at either or both the activating or inhibitory sites (described in (89)); and unmodified or phosphorylated. From a purely mathematical standpoint, that yields 12 possible HDAC8 states, each potentially with a different level of catalytic activity and specificity, and capable of changing upon cellular stimulus. That does not include the potential (and likely) effects of phosphorylation-dependent binding partners or subcellular localization. Thus, future HDAC8 studies need to be very specific and elucidate HDAC8 behavior under various defined cellular conditions/states. I look forward to the developments the next decade will uncover, and I have a feeling the story of human HDAC8 is going to become more intricate before it becomes truly clear.

Bibliography

1. Khoury GA, Baliban RC, Floudas CA. Proteome-wide post-translational modification statistics: frequency analysis and curation of the swiss-prot database. Scientific reports. 2011;1. Epub 2011/10/29. doi: 10.1038/srep00090. PubMed PMID: 22034591; PMCID: 3201773.

2. Verdin E, Ott M. 50 years of protein acetylation: from gene regulation to epigenetics, metabolism and beyond. Nat Rev Mol Cell Biol. 2015;16(4):258-64. doi: 10.1038/nrm3931.

3. Glozak MA, Sengupta N, Zhang XH, Seto E. Acetylation and deacetylation of non-histone proteins. Gene. 2005;363:15-23. doi: DOI 10.1016/j.gene.2005.09.010. PubMed PMID: ISI:000234166700002.

4. Kovacic P. Novel electrostatic mechanism for mode of action by N-acetylated proteins: cell signaling and phosphorylation. Journal of receptor and signal transduction research. 2011;31(3):193-8. Epub 2011/05/31. doi: 10.3109/10799893.2011.577784. PubMed PMID: 21619447.

5. Yang XJ, Seto E. The Rpd3/Hda1 family of lysine deacetylases: from bacteria and yeast to mice and men. Nat Rev Mol Cell Biol. 2008;9(3):206-18. Epub 2008/02/23. doi: nrm2346 [pii] 10.1038/nrm2346. PubMed PMID: 18292778; PMCID: 2667380.

6. Yang XJ, Seto E. Lysine acetylation: codified crosstalk with other posttranslational modifications. Mol Cell. 2008;31(4):449-61. doi: 10.1016/j.molcel.2008.07.002. PubMed PMID: 18722172; PMCID: 2551738.

7. Workman JL, Kingston RE. Alteration of nucleosome structure as a mechanism of transcriptional regulation. Annu Rev Biochem. 1998;67:545-79. Epub 1998/10/06. doi: 10.1146/annurev.biochem.67.1.545. PubMed PMID: 9759497.

8. Glozak MA, Seto E. Histone deacetylases and cancer. Oncogene. 2007;26(37):5420-32. Epub 2007/08/19. doi: 1210610 [pii] 10.1038/sj.onc.1210610. PubMed PMID: 17694083.

9. Choudhary C, Kumar C, Gnad F, Nielsen ML, Rehman M, Walther TC, Olsen JV, Mann M. Lysine Acetylation Targets Protein Complexes and Co-Regulates Major Cellular Functions. Science. 2009;325(5942):834-40. doi: 10.1126/science.1175371.

10. Zhao S, Xu W, Jiang W, Yu W, Lin Y, Zhang T, Yao J, Zhou L, Zeng Y, Li H, Li Y, Shi J, An W, Hancock SM, He F, Qin L, Chin J, Yang P, Chen X, Lei Q, Xiong Y, Guan KL. Regulation of cellular metabolism by protein lysine acetylation. Science. 2010;327(5968):1000-4. Epub 2010/02/20. doi: 327/5968/1000 [pii] 10.1126/science.1179689. PubMed PMID: 20167786; PMCID: 3232675.

11. Haberland M, Montgomery RL, Olson EN. The many roles of histone deacetylases in development and physiology: implications for disease and therapy. Nat Rev Genet. 2009;10(1):32-42. Epub 2008/12/10. doi: nrg2485 [pii] 10.1038/nrg2485. PubMed PMID: 19065135; PMCID: 3215088.

12. Kazantsev AG, Thompson LM. Therapeutic application of histone deacetylase inhibitors for central nervous system disorders. Nat Rev Drug Discov. 2008;7(10):854-68. Epub 2008/10/02. doi: nrd2681 [pii] 10.1038/nrd2681. PubMed PMID: 18827828.

13. Drummond DC, Noble CO, Kirpotin DB, Guo Z, Scott GK, Benz CC. Clinical development of histone deacetylase inhibitors as anticancer agents. Annu Rev Pharmacol Toxicol. 2005;45:495-528. Epub 2005/04/12. doi: 10.1146/annurev.pharmtox.45.120403.095825. PubMed PMID: 15822187.

14. Gregoretti IV, Lee YM, Goodson HV. Molecular evolution of the histone deacetylase family: functional implications of phylogenetic analysis. J Mol Biol. 2004;338(1):17-31. Epub 2004/03/31. doi: 10.1016/j.jmb.2004.02.006. PubMed PMID: 15050820.

15. Hernick M, Fierke CA. Zinc hydrolases: the mechanisms of zinc-dependent deacetylases. Arch Biochem Biophys. 2005;433(1):71-84. Epub 2004/12/08. doi: S0003-9861(04)00450-3 [pii] 10.1016/j.abb.2004.08.006. PubMed PMID: 15581567.

16. Frye RA. Phylogenetic classification of prokaryotic and eukaryotic Sir2-like proteins. Biochemical and biophysical research communications. 2000;273(2):793-8. Epub 2000/06/30. doi: 10.1006/bbrc.2000.3000S0006-291X(00)93000-6 [pii]. PubMed PMID: 10873683.

17. Milne JC, Denu JM. The Sirtuin family: therapeutic targets to treat diseases of aging. Curr Opin Chem Biol. 2008;12(1):11-7. Epub 2008/02/20. doi: S1367-5931(08)00011-2 [pii] 10.1016/j.cbpa.2008.01.019. PubMed PMID: 18282481.

18. Dowling DP, Gattis SG, Fierke CA, Christianson DW. Structures of metal-substituted human histone deacetylase 8 provide mechanistic inferences on biological function. Biochemistry. 2010;49(24):5048-56. Epub 2010/06/16. doi: 10.1021/bi1005046. PubMed PMID: 20545365; PMCID: 2895166.

19. Lombardi PM, Cole KE, Dowling DP, Christianson DW. Structure, mechanism, and inhibition of histone deacetylases and related metalloenzymes. Current opinion in structural biology. 2011;21(6):735-43. Epub 2011/08/30. doi: 10.1016/j.sbi.2011.08.004. PubMed PMID: 21872466; PMCID: Pmc3232309.

20. Boyault C, Sadoul K, Pabion M, Khochbin S. HDAC6, at the crossroads between cytoskeleton and cell signaling by acetylation and ubiquitination. Oncogene. 0000;26(37):5468-76.

21. Yao YL, Yang WM. Beyond histone and deacetylase: an overview of cytoplasmic histone deacetylases and their nonhistone substrates. Journal of biomedicine & biotechnology. 2011;2011:146493. Epub 2011/01/15. doi: 10.1155/2011/146493. PubMed PMID: 21234400; PMCID: 3014693.

22. Gregoire S, Tremblay AM, Xiao L, Yang Q, Ma K, Nie J, Mao Z, Wu Z, Giguere V, Yang XJ. Control of MEF2 transcriptional activity by coordinated phosphorylation and sumoylation. The Journal of biological chemistry. 2006;281(7):4423-33. Epub 2005/12/17. doi: 10.1074/jbc.M509471200. PubMed PMID: 16356933.

23. Zhao X, Sternsdorf T, Bolger TA, Evans RM, Yao TP. Regulation of MEF2 by histone deacetylase 4- and SIRT1 deacetylase-mediated lysine modifications. Mol Cell Biol. 2005;25(19):8456-64. Epub 2005/09/17. doi: 10.1128/mcb.25.19.8456-8464.2005. PubMed PMID: 16166628; PMCID: Pmc1265742.

24. Gao C, Ho CC, Reineke E, Lam M, Cheng X, Stanya KJ, Liu Y, Chakraborty S, Shih HM, Kao HY. Histone deacetylase 7 promotes PML sumoylation and is essential for PML nuclear body formation. Mol Cell Biol. 2008;28(18):5658-67. Epub 2008/07/16. doi: 10.1128/mcb.00874-08. PubMed PMID: 18625722; PMCID: Pmc2546935.

25. Brandl A, Heinzel T, Kramer OH. Histone deacetylases: salesmen and customers in the post-translational modification market. Biology of the cell / under the auspices of the European Cell Biology Organization. 2009;101(4):193-205. Epub 2009/02/12. doi: 10.1042/BC20080158. PubMed PMID: 19207105.

26. Segre CV, Chiocca S. Regulating the regulators: the post-translational code of class I HDAC1 and HDAC2. Journal of biomedicine & biotechnology. 2011;2011:690848. Epub 2011/01/05. doi: 10.1155/2011/690848. PubMed PMID: 21197454; PMCID: Pmc3004424.

27. Wu Y, Song SW, Sun J, Bruner JM, Fuller GN, Zhang W. IIp45 Inhibits Cell Migration through Inhibition of HDAC6. Journal of Biological Chemistry. 2010;285(6):3554-60. doi: 10.1074/jbc.M109.063354.

28. Jensen ED, Schroeder TM, Bailey J, Gopalakrishnan R, Westendorf JJ. Histone deacetylase 7 associates with Runx2 and represses its activity during osteoblast maturation in a deacetylation-independent manner. Journal of bone and mineral research : the official journal of the American Society for Bone and Mineral Research. 2008;23(3):361-72. Epub 2007/11/14. doi: 10.1359/jbmr.071104. PubMed PMID: 17997710; PMCID: Pmc2669158.

29. Wang AH, Kruhlak MJ, Wu J, Bertos NR, Vezmar M, Posner BI, Bazett-Jones DP, Yang XJ. Regulation of histone deacetylase 4 by binding of 14-3-3 proteins. Mol Cell Biol. 2000;20(18):6904-12. Epub 2000/08/25. PubMed PMID: 10958686; PMCID: 88766.

30. Grozinger CM, Schreiber SL. Regulation of histone deacetylase 4 and 5 and transcriptional activity by 14-3-3-dependent cellular localization. Proceedings of the National Academy of Sciences of the United States of America. 2000;97(14):7835-40. Epub 2000/06/28. doi: 10.1073/pnas.140199597. PubMed PMID: 10869435; PMCID: 16631.

31. Li X, Song S, Liu Y, Ko SH, Kao HY. Phosphorylation of the histone deacetylase 7 modulates its stability and association with 14-3-3 proteins. The Journal of biological chemistry. 2004;279(33):34201-8. Epub 2004/05/29. doi: 10.1074/jbc.M405179200. PubMed PMID: 15166223.

32. Kao HY, Verdel A, Tsai CC, Simon C, Juguilon H, Khochbin S. Mechanism for nucleocytoplasmic shuttling of histone deacetylase 7. The Journal of biological chemistry. 2001;276(50):47496-507. Epub 2001/10/05. doi: 10.1074/jbc.M107631200. PubMed PMID: 11585834.

33. Ago T, Liu T, Zhai P, Chen W, Li H, Molkentin JD, Vatner SF, Sadoshima J. A redox-dependent pathway for regulating class II HDACs and cardiac hypertrophy. Cell. 2008;133(6):978-93. Epub 2008/06/17. doi: 10.1016/j.cell.2008.04.041. PubMed PMID: 18555775.

34. Haworth RS, Stathopoulou K, Candasamy AJ, Avkiran M. Neurohormonal Regulation of Cardiac Histone Deacetylase 5 Nuclear Localization by Phosphorylation-Dependent and Phosphorylation-Independent Mechanisms. Circulation Research. 2012;110(12):1585-95. doi: 10.1161/circresaha.111.263665.

35. Eom GH, Kook H. Posttranslational modifications of histone deacetylases: Implications for cardiovascular diseases. Pharmacology & Therapeutics. 2014;143(2):168-80. doi: http://dx.doi.org/10.1016/j.pharmthera.2014.02.012.

36. Mottamal M, Zheng S, Huang TL, Wang G. Histone deacetylase inhibitors in clinical studies as templates for new anticancer agents. Molecules. 2015;20(3):3898-941. Epub 2015/03/05. doi: 10.3390/molecules20033898. PubMed PMID: 25738536; PMCID: PMC4372801.

37. Wagner J, Hackanson B, Lübbert M, Jung M. Histone deacetylase (HDAC) inhibitors in recent clinical trials for cancer therapy. Clin Epigenet. 2010;1(3-4):117-36. doi: 10.1007/s13148-010-0012-4.

38. O'Connor OA, Horwitz S, Masszi T, Van Hoof A, Brown P, Doorduijn J, Hess G, Jurczak W, Knoblauch P, Chawla S, Bhat G, Choi MR, Walewski J, Savage K, Foss F, Allen LF, Shustov A. Belinostat in Patients With Relapsed or Refractory Peripheral T-Cell Lymphoma: Results of the Pivotal Phase II BELIEF (CLN-19) Study. Journal of Clinical Oncology. 2015. doi: 10.1200/jco.2014.59.2782.

39. Poole RM. Belinostat: first global approval. Drugs. 2014;74(13):1543-54. Epub 2014/08/20. doi: 10.1007/s40265-014-0275-8. PubMed PMID: 25134672.

40. Fenichel MP. FDA Approves New Agent for Multiple Myeloma. Journal of the National Cancer Institute. 2015;107(6). doi: 10.1093/jnci/djv165.

41. Lee HZ, Kwitkowski VE, Del Valle PL, Ricci MS, Saber H, Habtemariam BA, Bullock J, Bloomquist E, Li Shen Y, Chen XH, Brown J, Mehrotra N, Dorff S, Charlab R, Kane RC, Kaminskas E, Justice R, Farrell AT, Pazdur R. FDA Approval: Belinostat for the Treatment of Patients with Relapsed or Refractory Peripheral T-cell Lymphoma. Clinical cancer research : an official journal of the American Association for Cancer Research. 2015;21(12):2666-70. Epub 2015/03/25. doi: 10.1158/1078-0432.ccr-14-3119. PubMed PMID: 25802282.

42. Tan S, Liu Z-P. Natural Products as Zinc-Dependent Histone Deacetylase Inhibitors. ChemMedChem. 2015;10(3):441-50. doi: 10.1002/cmdc.201402460.

43. Andrews KT, Haque A, Jones MK. HDAC inhibitors in parasitic diseases. Immunology and cell biology. 2012;90(1):66-77. Epub 2011/11/30. doi: 10.1038/icb.2011.97. PubMed PMID: 22124373.

44. Decroos C, Clausen DJ, Haines BE, Wiest O, Williams RM, Christianson DW. Variable Active Site Loop Conformations Accommodate the Binding of Macrocyclic Largazole Analogues to HDAC8. Biochemistry. 2015;54(12):2126-35. Epub 2015/03/21. doi: 10.1021/acs.biochem.5b00010. PubMed PMID: 25793284; PMCID: PMC4382410.

45. Durst KL, Lutterbach B, Kummalue T, Friedman AD, Hiebert SW. The inv(16) Fusion Protein Associates with Corepressors via a Smooth Muscle Myosin Heavy-Chain Domain. Molecular and Cellular Biology. 2003;23(2):607-19. doi: 10.1128/mcb.23.2.607-619.2003.

46. Wilson BJ, Tremblay AM, Deblois G, Sylvain-Drolet G, Giguere V. An acetylation switch modulates the transcriptional activity of estrogen-related receptor alpha. Molecular endocrinology. 2010;24(7):1349-58. Epub 2010/05/21. doi: 10.1210/me.2009-0441. PubMed PMID: 20484414.

47. Deardorff MA, Bando M, Nakato R, Watrin E, Itoh T, Minamino M, Saitoh K, Komata M, Katou Y, Clark D, Cole KE, De Baere E, Decroos C, Di Donato N, Ernst S, Francey LJ, Gyftodimou Y, Hirashima K, Hullings M, Ishikawa Y, Jaulin C, Kaur M, Kiyono T, Lombardi PM, Magnaghi-Jaulin L, Mortier GR, Nozaki N, Petersen MB, Seimiya H, Siu VM, Suzuki Y, Takagaki K, Wilde JJ, Willems PJ, Prigent C, Gillessen-Kaesbach G, Christianson DW, Kaiser FJ, Jackson LG, Hirota T, Krantz ID, Shirahige K. HDAC8 mutations in Cornelia de Lange syndrome affect the cohesin acetylation cycle. Nature. 2012;489(7415):313-7. Epub 2012/08/14. doi: 10.1038/nature11316. PubMed PMID: 22885700; PMCID: PMC3443318.

48. Niegisch G, Knievel J, Koch A, Hader C, Fischer U, Albers P, Schulz WA. Changes in histone deacetylase (HDAC) expression patterns and activity of HDAC inhibitors in urothelial cancers. Urologic Oncology: Seminars and Original Investigations. 2013;31(8):1770-9. doi: http://dx.doi.org/10.1016/j.urolonc.2012.06.015.

49. Oehme I, Deubzer HE, Wegener D, Pickert D, Linke J-P, Hero B, Kopp-Schneider A, Westermann F, Ulrich SM, von Deimling A, Fischer M, Witt O. Histone Deacetylase 8 in Neuroblastoma Tumorigenesis. Clinical Cancer Research. 2009;15(1):91-9. doi: 10.1158/1078-0432.ccr-08-0684.

50. Rettig I, Koeneke E, Trippel F, Mueller WC, Burhenne J, Kopp-Schneider A, Fabian J, Schober A, Fernekorn U, von Deimling A, Deubzer HE, Milde T, Witt O, Oehme I. Selective inhibition of HDAC8 decreases neuroblastoma growth in vitro and in vivo and enhances retinoic acid-mediated differentiation. Cell Death Dis. 2015;6:e1657. Epub 2015/02/20. doi: 10.1038/cddis.2015.24. PubMed PMID: 25695609.

51. Kaiser FJ, Ansari M, Braunholz D, Concepcion Gil-Rodriguez M, Decroos C, Wilde JJ, Fincher CT, Kaur M, Bando M, Amor DJ, Atwal PS, Bahlo M, Bowman CM, Bradley JJ, Brunner HG, Clark D, Del Campo M, Di Donato N, Diakumis P, Dubbs H, Dyment DA, Eckhold J, Ernst S, Ferreira JC, Francey LJ, Gehlken U, Guillen-Navarro E, Gyftodimou Y, Hall BD, Hennekam R, Hudgins L, Hullings M, Hunter JM, Yntema H, Innes AM, Kline AD, Krumina Z, Lee H, Leppig K, Lynch SA, Mallozzi MB, Mannini L, McKee S, Mehta SG, Micule I, Mohammed S, Moran E, Mortier GR, Moser JA, Noon SE, Nozaki N, Nunes L, Pappas JG, Penney LS, Perez-Aytes A, Petersen MB, Puisac B, Revencu N, Roeder E, Saitta S, Scheuerle AE, Schindeler KL, Siu VM, Stark Z, Strom SP, Thiese H, Vater I, Willems P, Williamson K, Wilson LC, Hakonarson H, Quintero-Rivera F, Wierzba J, Musio A, Gillessen-Kaesbach G, Ramos FJ, Jackson LG, Shirahige K, Pie J, Christianson DW, Krantz ID, Fitzpatrick DR, Deardorff MA. Loss-of-function HDAC8 mutations cause a phenotypic spectrum of Cornelia de Lange syndrome-like features, ocular hypertelorism, large fontanelle and X-linked inheritance. Hum Mol Genet. 2014;23(11):2888-900. Epub 2014/01/10. doi: 10.1093/hmg/ddu002. PubMed PMID: 24403048; PMCID: PMC4014191.

52. Stolfa DA, Marek M, Lancelot J, Hauser AT, Walter A, Leproult E, Melesina J, Rumpf T, Wurtz JM, Cavarelli J, Sippl W, Pierce RJ, Romier C, Jung M. Molecular basis for the antiparasitic activity of a mercaptoacetamide derivative that inhibits histone deacetylase 8 (HDAC8) from the human pathogen schistosoma mansoni. J Mol Biol. 2014;426(20):3442-53. Epub 2014/03/25. doi: 10.1016/j.jmb.2014.03.007. PubMed PMID: 24657767.

53. Haberland M, Mokalled MH, Montgomery RL, Olson EN. Epigenetic control of skull morphogenesis by histone deacetylase 8. Genes & development. 2009;23(14):1625-30. Epub 2009/07/17. doi: 23/14/1625 [pii] 10.1101/gad.1809209. PubMed PMID: 19605684; PMCID: 2714711.

54. Garber K. HDAC inhibitors overcome first hurdle. Nature biotechnology. 2007;25(1):17-9. Epub 2007/01/11. doi: nbt0107-17 [pii] 10.1038/nbt0107-17. PubMed PMID: 17211382.

55. Montgomery RL, Potthoff MJ, Haberland M, Qi X, Matsuzaki S, Humphries KM, Richardson JA, Bassel-Duby R, Olson EN. Maintenance of cardiac energy metabolism by histone deacetylase 3 in mice. J Clin Invest. 2008;118(11):3588-97. Epub 2008/10/03. doi: 10.1172/JCI35847. PubMed PMID: 18830415; PMCID: 2556240.

56. Hu E, Chen Z, Fredrickson T, Zhu Y, Kirkpatrick R, Zhang GF, Johanson K, Sung CM, Liu R, Winkler J. Cloning and characterization of a novel human class I histone deacetylase that functions as a transcription repressor. The Journal of biological chemistry. 2000;275(20):15254-64. Epub 2000/04/05. doi: 10.1074/jbc.M908988199. PubMed PMID: 10748112.

57. Buggy JJ, Sideris ML, Mak P, Lorimer DD, McIntosh B, Clark JM. Cloning and characterization of a novel human histone deacetylase, HDAC8. Biochem J. 2000;350 Pt 1:199-205. Epub 2000/08/06. PubMed PMID: 10926844; PMCID: PMC1221242.

58. Van den Wyngaert I, de Vries W, Kremer A, Neefs J, Verhasselt P, Luyten WH, Kass SU. Cloning and characterization of human histone deacetylase 8. FEBS Lett. 2000;478(1-2):77-83. Epub 2000/08/03. doi: S0014579300018135 [pii]. PubMed PMID: 10922473.

59. Riester D, Hildmann C, Grunewald S, Beckers T, Schwienhorst A. Factors affecting the substrate specificity of histone deacetylases. Biochemical and biophysical research communications. 2007;357(2):439-45. Epub 2007/04/13. doi: S0006-291X(07)00652-3 [pii] 10.1016/j.bbrc.2007.03.158. PubMed PMID: 17428445.

60. Gurard-Levin ZA, Kilian KA, Kim J, Bahr K, Mrksich M. Peptide arrays identify isoform-selective substrates for profiling endogenous lysine deacetylase activity. ACS chemical biology. 2010;5(9):863-73. Epub 2010/09/21. doi: 10.1021/cb100088g. PubMed PMID: 20849068; PMCID: 2941244.

61. Gurard-Levin ZA, Mrksich M. The Activity of HDAC8 Depends on Local and Distal Sequences of Its Peptide Substrates. Biochemistry. 2008;47:6242-50. Epub 05/10/2008.

62. Dose A, Liokatis S, Theillet FX, Selenko P, Schwarzer D. NMR profiling of histone deacetylase and acetyl-transferase activities in real time. ACS chemical biology. 2011;6(5):419-24. Epub 2011/02/10. doi: 10.1021/cb1003866. PubMed PMID: 21302972.

63. Juan LJ, Shia WJ, Chen MH, Yang WM, Seto E, Lin YS, Wu CW. Histone deacetylases specifically down-regulate p53-dependent gene activation. The Journal of biological chemistry. 2000;275(27):20436-43. Epub 2000/04/25. doi: 10.1074/jbc.M000202200M000202200 [pii]. PubMed PMID: 10777477.

64. Luo J, Su F, Chen D, Shiloh A, Gu W. Deacetylation of p53 modulates its effect on cell growth and apoptosis. Nature. 2000;408(6810):377-81. Epub 2000/12/01. doi: 10.1038/35042612. PubMed PMID: 11099047.

65. Waltregny D, de Leval L, Glénisson W, Ly Tran S, North BJ, Bellahcène A, Weidle U, Verdin E, Castronovo V. Expression of Histone Deacetylase 8, a Class I Histone Deacetylase, Is Restricted to Cells Showing Smooth Muscle Differentiation in Normal Human Tissues. The American Journal of Pathology. 2004;165(2):553-64. doi: 10.1016/s0002-9440(10)63320-2.

66. Waltregny D, Glénisson W, Tran SL, North BJ, Verdin E, Colige A, Castronovo V. Histone deacetylase HDAC8 associates with smooth muscle alpha-actin and is essential for smooth muscle cell contractility. The FASEB Journal. 2005. Epub March 16, 2005.

67. Gantt SL, Gattis SG, Fierke CA. Catalytic activity and inhibition of human histone deacetylase 8 is dependent on the identity of the active site metal ion. Biochemistry. 2006;45(19):6170-8. Epub 2006/05/10. doi: 10.1021/bi060212u. PubMed PMID: 16681389.

68. Gantt SL. Human histone deacetylase 8: Metal dependence and catalytic mechanism [Dissertation]: University of Michigan; 2006.

69. Fersht A. Structure and mechanism in protein science : a guide to enzyme catalysis and protein folding. New York: W.H. Freeman; 1999. xxi, 631 p. p.

70. Wegener D, Wirsching F, Riester D, Schwienhorst A. A fluorogenic histone deacetylase assay well suited for high-throughput activity screening. Chem Biol. 2003;10(1):61-8.

71. Gurard-Levin ZA, Kim J, Mrksich M. Combining mass spectrometry and peptide arrays to profile the specificities of histone deacetylases. Chembiochem : a European journal of chemical biology. 2009;10(13):2159-61. Epub 2009/08/19. doi: 10.1002/cbic.200900417. PubMed PMID: 19688789; PMCID: 2813191.

72. Wolfson NA, Pitcairn CA, Sullivan ED, Joseph CG, Fierke CA. An enzyme-coupled assay measuring acetate production for profiling histone deacetylase specificity. Analytical Biochemistry. 2014;456(0):61-9. doi: http://dx.doi.org/10.1016/j.ab.2014.03.012.

73. Wolfson NA, Pitcairn CA, Fierke CA. HDAC8 substrates: Histones and beyond. Biopolymers. 2013;99(2):112-26. doi: 10.1002/bip.22135.

74. Schultz BE, Misialek S, Wu J, Tang J, Conn MT, Tahilramani R, Wong L. Kinetics and comparative reactivity of human class I and class IIb histone deacetylases. Biochemistry. 2004;43(34):11083-91. Epub 2004/08/25. doi: 10.1021/bi0494471. PubMed PMID: 15323567.

75. Riester D, Wegener D, Hildmann C, Schwienhorst A. Members of the histone deacetylase superfamily differ in substrate specificity towards small synthetic substrates. Biochemical and biophysical research communications. 2004;324(3):1116-23. Epub 2004/10/16. doi: S0006-291X(04)02209-0 [pii] 10.1016/j.bbrc.2004.09.155. PubMed PMID: 15485670.

76. Smith BC, Denu JM. Acetyl-lysine analog peptides as mechanistic probes of protein deacetylases. The Journal of biological chemistry. 2007;282(51):37256-65. Epub 2007/10/24. doi: 10.1074/jbc.M707878200. PubMed PMID: 17951578.

77. Bar-Even A, Noor E, Savir Y, Liebermeister W, Davidi D, Tawfik DS, Milo R. The moderately efficient enzyme: evolutionary and physicochemical trends shaping enzyme parameters. Biochemistry. 2011;50(21):4402-10. Epub 2011/04/22. doi: 10.1021/bi2002289. PubMed PMID: 21506553.

78. Alarcon R, Orellana MS, Neira B, Uribe E, Garcia JR, Carvajal N. Mutational analysis of substrate recognition by human arginase type I--agmatinase activity of the N130D variant. FEBS J. 2006;273(24):5625-31. Epub 2007/01/11. doi: EJB5551 [pii] 10.1111/j.1742-4658.2006.05551.x. PubMed PMID: 17212779.

79. Singh RK, Cho K, Padi SK, Yu J, Haldar M, Mandal T, Yan C, Cook G, Guo B, Mallik S, Srivastava DK. Mechanism of N-Acylthiourea-mediated activation of human histone deacetylase 8 (HDAC8) at molecular and cellular levels. The Journal of biological chemistry. 2015;290(10):6607-19. Epub 2015/01/22. doi: 10.1074/jbc.M114.600627. PubMed PMID: 25605725; PMCID: PMC4358293.

80. Olson DE, Udeshi ND, Wolfson NA, Pitcairn CA, Sullivan ED, Jaffe JD, Svinkina T, Natoli T, Lu X, Paulk J, McCarren P, Wagner FF, Barker D, Howe E, Lazzaro F, Gale JP, Zhang Y-L, Subramanian A, Fierke CA, Carr SA, Holson EB. An unbiased approach to identify endogenous substrates of "histone" deacetylase 8. ACS chemical biology. 2014;9(10):2210-6. doi: 10.1021/cb500492r. PubMed PMID: 25089360; PMCID: 4201337.

81. Joshi P, Greco TM, Guise AJ, Luo Y, Yu F, Nesvizhskii AI, Cristea IM. The functional interactome landscape of the human histone deacetylase family. Mol Syst Biol. 2013;9:672. Epub 2013/06/12. doi: 10.1038/msb.2013.26. PubMed PMID: 23752268; PMCID: PMC3964310.

82. Wu J, Du C, Lv Z, Ding C, Cheng J, Xie H, Zhou L, Zheng S. The Up-Regulation of Histone Deacetylase 8 Promotes Proliferation and Inhibits Apoptosis in Hepatocellular Carcinoma. Dig Dis Sci. 2013;58(12):3545-53. doi: 10.1007/s10620-013-2867-7.

83. Karolczak-Bayatti M, Sweeney M, Cheng J, Edey L, Robson SC, Ulrich SM, Treumann A, Taggart MJ, Europe-Finner GN. Acetylation of Heat Shock Protein 20 (Hsp20) Regulates Human Myometrial Activity. Journal of Biological Chemistry. 2011;286(39):34346-55. doi: 10.1074/jbc.M111.278549.

84. Beckouët F, Hu B, Roig MB, Sutani T, Komata M, Uluocak P, Katis VL, Shirahige K, Nasmyth K. An Smc3 Acetylation Cycle Is Essential for Establishment of Sister Chromatid Cohesion. Molecular Cell. 2010;39(5):689-99. doi: http://dx.doi.org/10.1016/j.molcel.2010.08.008.

85. Zhang J, Shi X, Li Y, Kim B-J, Jia J, Huang Z, Yang T, Fu X, Jung SY, Wang Y, Zhang P, Kim S-T, Pan X, Qin J. Acetylation of Smc3 by Eco1 Is Required for S Phase Sister Chromatid Cohesion in Both Human and Yeast. Molecular Cell. 2008;31(1):143-51. doi: http://dx.doi.org/10.1016/j.molcel.2008.06.006.

86. Decroos C, Bowman CM, Moser JA, Christianson KE, Deardorff MA, Christianson DW. Compromised structure and function of HDAC8 mutants identified in Cornelia de Lange Syndrome spectrum disorders. ACS chemical biology. 2014;9(9):2157-64. doi: 10.1021/cb5003762. PubMed PMID: 25075551; PMCID: 4168803.

87. Horsfield J, Print CG, Mönnich M. Diverse developmental disorders from The One Ring: distinct molecular pathways underlie the cohesinopathies. Frontiers in Genetics. 2012;3. doi: 10.3389/fgene.2012.00171.

88. Villena JA, Kralli A. ERRalpha: a metabolic function for the oldest orphan. Trends Endocrinol Metab. 2008;19(8):269-76. Epub 2008/09/10. doi: S1043-2760(08)00117-3 [pii] 10.1016/j.tem.2008.07.005. PubMed PMID: 18778951; PMCID: 2786240.

89. Gantt SL, Joseph CG, Fierke CA. Activation and inhibition of histone deacetylase 8 by monovalent cations. The Journal of biological chemistry. 2010;285(9):6036-43. Epub 2009/12/24. doi: 10.1074/jbc.M109.033399. PubMed PMID: 20029090; PMCID: 2825397.

90. Mitelman F, Heim S. Quantitative acute leukemia cytogenetics. Genes Chromosomes Cancer. 1992;5(1):57-66. Epub 1992/07/01. PubMed PMID: 1384663.

91. Liu P, Tarle SA, Hajra A, Claxton DF, Marlton P, Freedman M, Siciliano MJ, Collins FS. Fusion between transcription factor CBF beta/PEBP2 beta and a myosin heavy chain in acute myeloid leukemia. Science. 1993;261(5124):1041-4. Epub 1993/08/20. PubMed PMID: 8351518.

92. Smith KT, Martin-Brown SA, Florens L, Washburn MP, Workman JL. Deacetylase inhibitors dissociate the histone-targeting ING2 subunit from the Sin3 complex. Chem Biol. 2010;17(1):65-74. Epub 2010/02/10. doi: S1074-5521(09)00443-8 [pii] 10.1016/j.chembiol.2009.12.010. PubMed PMID: 20142042; PMCID: 2819981.

93. Balkhi MY, Trivedi AK, Geletu M, Christopeit M, Bohlander SK, Behre HM, Behre G. Proteomics of acute myeloid leukaemia: Cytogenetic risk groups differ specifically in their proteome, interactome and post-translational protein modifications. Oncogene. 2006;25(53):7041-58. Epub 2006/05/30. doi: 1209689 [pii] 10.1038/sj.onc.1209689. PubMed PMID: 16732326.

94. Lu Q, Hutchins AE, Doyle CM, Lundblad JR, Kwok RP. Acetylation of cAMP-responsive element-binding protein (CREB) by CREB-binding protein enhances CREB-dependent transcription. The Journal of biological chemistry. 2003;278(18):15727-34. Epub 2003/02/22. doi: 10.1074/jbc.M300546200M300546200 [pii]. PubMed PMID: 12595525.

95. Gao J, Siddoway B, Huang Q, Xia H. Inactivation of CREB mediated gene transcription by HDAC8 bound protein phosphatase. Biochemical and biophysical research communications. 2009;379(1):1-5. Epub 2008/12/17. doi: 10.1016/j.bbrc.2008.11.135. PubMed PMID: 19070599.

96. Michael LF, Asahara H, Shulman AI, Kraus WL, Montminy M. The phosphorylation status of a cyclic AMP-responsive activator is modulated via a chromatin-dependent mechanism. Mol Cell Biol. 2000;20(5):1596-603. Epub 2000/02/12. PubMed PMID: 10669737; PMCID: 85343.

97. Yang Y-C, Chen C-N, Wu C-I, Huang W-J, Kuo T-Y, Kuan M-C, Tsai T-H, Huang J-S, Huang C-Y. NBM-T-L-BMX-OS01, Semisynthesized from Osthole, Is a Novel Inhibitor of Histone Deacetylase and Enhances Learning and Memory in Rats. Evidence-Based Complementary and Alternative Medicine. 2013;2013:18. doi: 10.1155/2013/514908.

98. Henikoff S, Henikoff JG. Amino acid substitution matrices from protein blocks. Proceedings of the National Academy of Sciences of the United States of America. 1992;89(22):10915-9. Epub 1992/11/15. PubMed PMID: 1438297; PMCID: 50453.

99. Bollen M. Combinatorial control of protein phosphatase-1. Trends Biochem Sci. 2001;26(7):426-31. Epub 2001/07/07. doi: S0968-0004(01)01836-9 [pii]. PubMed PMID: 11440854.

100. Leone V, Mansueto G, Pierantoni GM, Tornincasa M, Merolla F, Cerrato A, Santoro M, Grieco M, Scaloni A, Celetti A, Fusco A. CCDC6 represses CREB1 activity by recruiting histone deacetylase 1 and protein phosphatase 1. Oncogene. 2010;29(30):4341-51. Epub 2010/05/26. doi: onc2010179 [pii] 10.1038/onc.2010.179. PubMed PMID: 20498639.

101. Canettieri G, Morantte I, Guzman E, Asahara H, Herzig S, Anderson SD, Yates JR, 3rd, Montminy M. Attenuation of a phosphorylation-dependent activator by an HDAC-PP1 complex. Nature structural biology. 2003;10(3):175-81. Epub 2003/02/05. doi: 10.1038/nsb895nsb895 [pii]. PubMed PMID: 12567184.

102. Sengupta N, Seto E. Regulation of histone deacetylase activities. Journal of cellular biochemistry. 2004;93(1):57-67. Epub 2004/09/08. doi: 10.1002/jcb.20179. PubMed PMID: 15352162.

103. Hayakawa T, Nakayama J. Physiological roles of class I HDAC complex and histone demethylase. Journal of biomedicine & biotechnology. 2011;2011:129383. Epub 2010/11/05. doi: 10.1155/2011/129383. PubMed PMID: 21049000; PMCID: 2964911.

104. Haider S, Joseph CG, Neidle S, Fierke CA, Fuchter MJ. On the function of the internal cavity of histone deacetylase protein 8: R37 is a crucial residue for catalysis. Bioorganic & medicinal chemistry letters. 2011;21(7):2129-32. Epub 2011/02/16. doi: 10.1016/j.bmcl.2011.01.128. PubMed PMID: 21320778; PMCID: 3286521.

105. Dowling DP, Gantt SL, Gattis SG, Fierke CA, Christianson DW. Structural studies of human histone deacetylase 8 and its site-specific variants complexed with substrate and inhibitors. Biochemistry. 2008;47(51):13554-63. Epub 2008/12/05. doi: 10.1021/bi801610c. PubMed PMID: 19053282; PMCID: 2635894.

106. Dreiza CM, Brophy CM, Komalavilas P, Furnish EJ, Joshi L, Pallero MA, Murphy-Ullrich JE, von Rechenberg M, Ho YS, Richardson B, Xu N, Zhen Y, Peltier JM, Panitch A. Transducible heat shock protein 20 (HSP20) phosphopeptide alters cytoskeletal dynamics. Faseb J. 2005;19(2):261-3. Epub 2004/12/16. doi: 04-2911fje [pii] 10.1096/fj.04-2911fje. PubMed PMID: 15598710.

107. Vicente-Manzanares M, Ma X, Adelstein RS, Horwitz AR. Non-muscle myosin II takes centre stage in cell adhesion and migration. Nat Rev Mol Cell Biol. 2009;10(11):778-90. Epub 2009/10/24. doi: nrm2786 [pii] 10.1038/nrm2786. PubMed PMID: 19851336; PMCID: 2834236.

108. Lee H, Sengupta N, Villagra A, Rezai-Zadeh N, Seto E. Histone deacetylase 8 safeguards the human ever-shorter telomeres 1B (hEST1B) protein from ubiquitin-mediated degradation. Mol Cell Biol. 2006;26(14):5259-69. Epub 2006/07/01. doi: 10.1128/MCB.01971-05. PubMed PMID: 16809764; PMCID: 1592721.

109. Koyasu S, Nishida E, Kadowaki T, Matsuzaki F, Iida K, Harada F, Kasuga M, Sakai H, Yahara I. Two mammalian heat shock proteins, HSP90 and HSP100, are actin-binding proteins. Proceedings of the National Academy of Sciences of the United States of America. 1986;83(21):8054-8. Epub 1986/11/01. PubMed PMID: 3534880; PMCID: 386865.

110. Taiyab A, Rao Ch M. HSP90 modulates actin dynamics: inhibition of HSP90 leads to decreased cell motility and impairs invasion. Biochim Biophys Acta. 2011;1813(1):213-21. Epub 2010/10/05. doi: S0167-4889(10)00253-3 [pii] 10.1016/j.bbamcr.2010.09.012. PubMed PMID: 20883729.

111. Vannini A, Volpari C, Gallinari P, Jones P, Mattu M, Carfi A, De Francesco R, Steinkuhler C, Di Marco S. Substrate binding to histone deacetylases as shown by the crystal structure of the HDAC8-substrate complex. EMBO Rep. 2007;8(9):879-84. doi: http://www.nature.com/embor/journal/v8/n9/suppinfo/7401047_S1.html.

112. Somoza JR, Skene RJ, Katz BA, Mol C, Ho JD, Jennings AJ, Luong C, Arvai A, Buggy JJ, Chi E, Tang J, Sang BC, Verner E, Wynands R, Leahy EM, Dougan DR, Snell G, Navre M, Knuth MW, Swanson RV, McRee DE, Tari LW. Structural snapshots of human HDAC8 provide insights into the class I histone deacetylases. Structure. 2004;12(7):1325-34. Epub 2004/07/10. doi: 10.1016/j.str.2004.04.012. PubMed PMID: 15242608.

113. Whitehead L, Dobler MR, Radetich B, Zhu Y, Atadja PW, Claiborne T, Grob JE, McRiner A, Pancost MR, Patnaik A, Shao W, Shultz M, Tichkule R, Tommasi RA, Vash B, Wang P, Stams T. Human HDAC isoform selectivity achieved via exploitation of the acetate release channel with structurally unique small molecule inhibitors. Bioorg Med Chem. 2011;19(15):4626-34. doi: 10.1016/j.bmc.2011.06.030. PubMed PMID: 21723733.

114. Cole KE, Dowling DP, Boone MA, Phillips AJ, Christianson DW. Structural basis of the antiproliferative activity of largazole, a depsipeptide inhibitor of the histone deacetylases. Journal of the American Chemical Society. 2011;133(32):12474-7. Epub 2011/07/28. doi: 10.1021/ja205972n. PubMed PMID: 21790156; PMCID: PMC3162211.

115. Vannini A, Volpari C, Filocamo G, Casavola EC, Brunetti M, Renzoni D, Chakravarty P, Paolini C, De Francesco R, Gallinari P, Steinkuhler C, Di Marco S. Crystal structure of a eukaryotic zinc-dependent histone deacetylase, human HDAC8, complexed with a hydroxamic acid inhibitor. Proceedings of the National Academy of Sciences of the United States of America. 2004;101(42):15064-9. doi: 10.1073/pnas.0404603101. PubMed PMID: 15477595; PMCID: 524051.

116. Kunze MBA, Wright DW, Werbeck ND, Kirkpatrick J, Coveney PV, Hansen DF. Loop Interactions and Dynamics Tune the Enzymatic Activity of the Human Histone Deacetylase 8. Journal of the American Chemical Society. 2013;135(47):17862-8. doi: 10.1021/ja408184x.

117. Nobeli I, Favia AD, Thornton JM. Protein promiscuity and its implications for biotechnology. Nature biotechnology. 2009;27(2):157-67. Epub 2009/02/11. doi: 10.1038/nbt1519. PubMed PMID: 19204698.

118. Hedstrom L. Serine protease mechanism and specificity. Chem Rev. 2002;102(12):4501-24. Epub 2002/12/12. doi: cr000033x [pii]. PubMed PMID: 12475199.

119. Ollis DL, Cheah E, Cygler M, Dijkstra B, Frolow F, Franken SM, Harel M, Remington SJ, Silman I, Schrag J, et al. The alpha/beta hydrolase fold. Protein Eng. 1992;5(3):197-211. Epub 1992/04/01. PubMed PMID: 1409539.

120. Weikl TR, von Deuster C. Selected-fit versus induced-fit protein binding: kinetic differences and mutational analysis. Proteins. 2009;75(1):104-10. Epub 2008/09/19. doi: 10.1002/prot.22223. PubMed PMID: 18798570.

121. Tsuzuki S, Honda K, Uchimaru T, Mikami M, Tanabe K. Origin of attraction and directionality of the pi/pi interaction: model chemistry calculations of benzene dimer interaction. Journal of the American Chemical Society. 2002;124(1):104-12. Epub 2002/01/05. doi: ja0105212 [pii]. PubMed PMID: 11772067.

122. Sinnokrot MO, Valeev EF, Sherrill CD. Estimates of the ab initio limit for pi-pi interactions: the benzene dimer. Journal of the American Chemical Society. 2002;124(36):10887-93. Epub 2002/09/05. doi: ja025896h [pii]. PubMed PMID: 12207544.

123. Horovitz A, Serrano L, Avron B, Bycroft M, Fersht AR. Strength and co-operativity of contributions of surface salt bridges to protein stability. J Mol Biol. 1990;216(4):1031-44. Epub 1990/12/20. doi: S0022-2836(99)80018-7 [pii] 10.1016/S0022-2836(99)80018-7. PubMed PMID: 2266554.

124. Lombardi PM, Angell HD, Whittington DA, Flynn EF, Rajashankar KR, Christianson DW. Structure of prokaryotic polyamine deacetylase reveals evolutionary functional relationships with eukaryotic histone deacetylases. Biochemistry. 2011;50(11):1808-17. Epub 2011/01/28. doi: 10.1021/bi101859k. PubMed PMID: 21268586; PMCID: 3074186.

125. Bressi JC, Jennings AJ, Skene R, Wu Y, Melkus R, De Jong R, O'Connell S, Grimshaw CE, Navre M, Gangloff AR. Exploration of the HDAC2 foot pocket: Synthesis and SAR of substituted N-(2-aminophenyl)benzamides. Bioorganic & medicinal chemistry letters. 2010;20(10):3142-5. Epub 2010/04/16. doi: S0960-894X(10)00432-4 [pii] 10.1016/j.bmcl.2010.03.091. PubMed PMID: 20392638.

126. Bottomley MJ, Lo Surdo P, Di Giovine P, Cirillo A, Scarpelli R, Ferrigno F, Jones P, Neddermann P, De Francesco R, Steinkuhler C, Gallinari P, Carfi A. Structural and functional analysis of the human HDAC4 catalytic domain reveals a regulatory structural zinc-binding domain. The Journal of biological chemistry. 2008;283(39):26694-704. Epub 2008/07/11. doi: M803514200 [pii] 10.1074/jbc.M803514200. PubMed PMID: 18614528; PMCID: 3258910.

127. Schuetz A, Min J, Allali-Hassani A, Schapira M, Shuen M, Loppnau P, Mazitschek R, Kwiatkowski NP, Lewis TA, Maglathin RL, McLean TH, Bochkarev A, Plotnikov AN, Vedadi M, Arrowsmith CH. Human HDAC7 harbors a class IIa histone deacetylase-specific zinc binding motif and cryptic deacetylase activity. The Journal of biological chemistry. 2008;283(17):11355-63. Epub 2008/02/21. doi: M707362200 [pii] 10.1074/jbc.M707362200. PubMed PMID: 18285338; PMCID: 2431080.

128. Watson PJ, Fairall L, Santos GM, Schwabe JW. Structure of HDAC3 bound to co-repressor and inositol tetraphosphate. Nature. 2012;481(7381):335-40. doi: 10.1038/nature10728. PubMed PMID: 22230954; PMCID: 3272448.

129. Clausen DJ, Smith WB, Haines BE, Wiest O, Bradner JE, Williams RM. Modular synthesis and biological activity of pyridyl-based analogs of the potent Class I Histone Deacetylase Inhibitor Largazole. Bioorg Med Chem. 2015. doi: 10.1016/j.bmc.2015.03.063. PubMed PMID: 26054247.

130. Papadopoulos JS, Agarwala R. COBALT: constraint-based alignment tool for multiple protein sequences. Bioinformatics. 2007;23(9):1073-9. Epub 2007/03/03. doi: 10.1093/bioinformatics/btm076. PubMed PMID: 17332019.

131. Neumann H, Hancock SM, Buning R, Routh A, Chapman L, Somers J, Owen-Hughes T, van Noort J, Rhodes D, Chin JW. A method for genetically installing site-specific acetylation in recombinant histones defines the effects of H3 K56 acetylation. Mol Cell. 2009;36(1):153-63. doi: 10.1016/j.molcel.2009.07.027. PubMed PMID: 19818718; PMCID: 2856916.

132. Finnin MS, Donigian JR, Cohen A, Richon VM, Rifkind RA, Marks PA, Breslow R, Pavletich NP. Structures of a histone deacetylase homologue bound to the TSA and SAHA inhibitors. Nature. 1999;401(6749):188-93.

133. Wu R, Wang S, Zhou N, Cao Z, Zhang Y. A proton-shuttle reaction mechanism for histone deacetylase 8 and the catalytic role of metal ions. Journal of the American Chemical Society. 2010;132(27):9471-9. Epub 2010/06/24. doi: 10.1021/ja103932d. PubMed PMID: 20568751; PMCID: 2908479.

134. Kasner SE, Ganz MB. Regulation of intracellular potassium in mesangial cells: a fluorescence analysis using the dye, PBFI. Am J Physiol. 1992;262(3 Pt 2):F462-7. Epub 1992/03/01. PubMed PMID: 1558163.

135. Chang CJ, Jaworski J, Nolan EM, Sheng M, Lippard SJ. A tautomeric zinc sensor for ratiometric fluorescence imaging: application to nitric oxide-induced release of intracellular zinc. Proceedings of the National Academy of Sciences of the United States of America. 2004;101(5):1129-34. Epub 2004/01/22. doi: 10.1073/pnas.0308079100 0308079100 [pii]. PubMed PMID: 14734801; PMCID: 337018.

136. Bozym RA, Thompson RB, Stoddard AK, Fierke CA. Measuring Picomolar Intracellular Exchangeable Zinc in PC-12 Cells Using a Ratiometric Fluorescence Biosensor. ACS chemical biology. 2006;1(2):103-11. doi: 10.1021/cb500043a.

137. Wang D, Hosteen O, Fierke CA. ZntR-mediated transcription of zntA responds to nanomolar intracellular free zinc. J Inorg Biochem. 2012. Epub 2012/03/31. doi: S0162-0134(12)00052-9 [pii] 10.1016/j.jinorgbio.2012.02.008. PubMed PMID: 22459916.

138. Douglas BE, McDaniel DH, Alexander JJ. Concepts and models of inorganic chemistry. 3rd ed. New York: Wiley; 1994. xviii, 928, 65 p. p.

139. de Ruijter AJ, van Gennip AH, Caron HN, Kemp S, van Kuilenburg AB. Histone deacetylases (HDACs): characterization of the classical HDAC family. Biochem J. 2003;370(Pt 3):737-49. Epub 2002/11/14. doi: 10.1042/bj20021321. PubMed PMID: 12429021; PMCID: PMC1223209.

140. Yang XJ, Gregoire S. Class II histone deacetylases: from sequence to function, regulation, and clinical implication. Mol Cell Biol. 2005;25(8):2873-84. Epub 2005/03/31. doi: 25/8/2873 [pii] 10.1128/MCB.25.8.2873-2884.2005. PubMed PMID: 15798178; PMCID: 1069616.

141. Nakagawa M, Oda Y, Eguchi T, Aishima S, Yao T, Hosoi F, Basaki Y, Ono M, Kuwano M, Tanaka M, Tsuneyoshi M. Expression profile of class I histone deacetylases in human cancer tissues. Oncol Rep. 2007;18(4):769-74. Epub 2007/09/06. PubMed PMID: 17786334.

142. Tsai SC, Seto E. Regulation of histone deacetylase 2 by protein kinase CK2. The Journal of biological chemistry. 2002;277(35):31826-33. Epub 2002/06/26. doi: 10.1074/jbc.M204149200. PubMed PMID: 12082111.

143. Lee H, Rezai-Zadeh N, Seto E. Negative Regulation of Histone Deacetylase 8 Activity by Cyclic AMP-Dependent Protein Kinase A. Molecular and Cellular Biology. 2004;24(2):765-73. doi: 10.1128/mcb.24.2.765-773.2004.

144. Pflum MK, Tong JK, Lane WS, Schreiber SL. Histone deacetylase 1 phosphorylation promotes enzymatic activity and complex formation. The Journal of biological chemistry. 2001;276(50):47733-41. Epub 2001/10/17. doi: 10.1074/jbc.M105590200. PubMed PMID: 11602581.

145. Galasinski SC, Resing KA, Goodrich JA, Ahn NG. Phosphatase inhibition leads to histone deacetylases 1 and 2 phosphorylation and disruption of corepressor interactions. The Journal of biological chemistry. 2002;277(22):19618-26. Epub 2002/03/29. doi: 10.1074/jbc.M201174200. PubMed PMID: 11919195.

146. Ha CH, Kim JY, Zhao J, Wang W, Jhun BS, Wong C, Jin ZG. PKA phosphorylates histone deacetylase 5 and prevents its nuclear export, leading to the inhibition of gene transcription and cardiomyocyte hypertrophy. Proceedings of the National Academy of Sciences of the United States of America. 2010;107(35):15467-72. Epub 2010/08/19. doi: 10.1073/pnas.1000462107. PubMed PMID: 20716686; PMCID: PMC2932618.

147. Chang C-WJ, Lee L, Yu D, Dao K, Bossuyt J, Bers DM. Acute β-Adrenergic Activation Triggers Nuclear Import of Histone Deacetylase 5 and Delays Gq-induced Transcriptional Activation. Journal of Biological Chemistry. 2013;288(1):192-204. doi: 10.1074/jbc.M112.382358.

148. Greco TM, Yu F, Guise AJ, Cristea IM. Nuclear import of histone deacetylase 5 by requisite nuclear localization signal phosphorylation. Molecular & cellular proteomics : MCP. 2011;10(2):M110 004317. Epub 2010/11/18. doi: 10.1074/mcp.M110.004317. PubMed PMID: 21081666; PMCID: 3033682.

149. Seto E, Yang X-J. Regulation of Histone Deacetylase Activities and Functions by Phosphorylation and Dephosphorylation. In: Bradshaw R, Dennis E, editors. Handbook of Cell Signaling. 2 ed. San Diego: Academic Press; 2010. p. 2379-88.

150. Cai R, Kwon P, Yan-Neale Y, Sambuccetti L, Fischer D, Cohen D. Mammalian histone deacetylase 1 protein is posttranslationally modified by phosphorylation. Biochemical and biophysical research communications. 2001;283(2):445-53. Epub 2001/05/01. doi: 10.1006/bbrc.2001.4786. PubMed PMID: 11327722.

151. Eom GH, Cho YK, Ko J-H, Shin S, Choe N, Kim Y, Joung H, Kim H-S, Nam K-I, Kee HJ, Kook H. Casein Kinase-2α1 Induces Hypertrophic Response by Phosphorylation of Histone Deacetylase 2 S394 and its Activation in the Heart. Circulation. 2011;123(21):2392-403. doi: 10.1161/circulationaha.110.003665.

152. Gupta R, Jung E, Brunak S. Prediction of N-glycosylation sites in human proteins. In preparation. 2004.

153. Feng JH, Jing FB, Fang H, Gu LC, Xu WF. Expression, purification, and S-nitrosylation of recombinant histone deacetylase 8 in Escherichia coli. Biosci Trends. 2011;5(1):17-22. Epub 2011/03/23. PubMed PMID: 21422596.

154. Eom GH, Nam YS, Oh JG, Choe N, Min HK, Yoo EK, Kang G, Nguyen VH, Min JJ, Kim JK, Lee IK, Bassel-Duby R, Olson EN, Park WJ, Kook H. Regulation of acetylation of histone deacetylase 2 by p300/CBP-associated factor/histone deacetylase 5 in the development of cardiac hypertrophy. Circ Res. 2014;114(7):1133-43. Epub 2014/02/15. doi: 10.1161/circresaha.114.303429. PubMed PMID: 24526703.

155. Qiu Y ZY, Becker M, John S, Parekh BS, Huang S, Hendarwanto A, Martinez ED, Chen Y, Lu H, Adkins NL, Stavreva DA, Wiench M, Georgel PT, Schiltz RL, Hager GL. HDAC1 acetylation is linked to progressive modulation of steroid receptor-induced gene transcription. Mol Cell. 2006;22(5):669-79.

156. Khochbin S, Verdel A, Lemercier C, Seigneurin-Berny D. Functional significance of histone deacetylase diversity. Current opinion in genetics & development. 2001;11(2):162-6. PubMed PMID: 11250139.

157. Li G, Jiang H, Chang M, Xie H, Hu L. HDAC6 alpha-tubulin deacetylase: a potential therapeutic target in neurodegenerative diseases. Journal of the neurological sciences. 2011;304(1-2):1-8. doi: 10.1016/j.jns.2011.02.017. PubMed PMID: 21377170.

158. D'Mello SR. Histone deacetylases as targets for the treatment of human neurodegenerative diseases. Drug News Perspect. 2009;22(9):513-24. doi: 10.1358/dnp.2009.9.1428871. PubMed PMID: 20072728; PMCID: 3934413.

159. Marks P, Rifkind RA, Richon VM, Breslow R, Miller T, Kelly WK. Histone deacetylases and cancer: causes and therapies. Nature reviews Cancer. 2001;1(3):194-202. doi: 10.1038/35106079. PubMed PMID: 11902574.

160. Verdin E. Histone deacetylases : transcriptional regulation and other cellular functions. Totowa, N.J.: Humana Press; 2006. xi, 340 p. p.

161. Marek M, Kannan S, Hauser AT, Moraes Mourao M, Caby S, Cura V, Stolfa DA, Schmidtkunz K, Lancelot J, Andrade L, Renaud JP, Oliveira G, Sippl W, Jung M, Cavarelli J, Pierce RJ, Romier C. Structural basis for the inhibition of histone deacetylase 8 (HDAC8), a key epigenetic player in the blood fluke Schistosoma mansoni. PLoS Pathog. 2013;9(9):e1003645. doi: 10.1371/journal.ppat.1003645. PubMed PMID: 24086136; PMCID: 3784479.

162. Saha A, Pandian GN, Sato S, Taniguchi J, Hashiya K, Bando T, Sugiyama H. Synthesis and biological evaluation of a targeted DNA-binding transcriptional activator with HDAC8 inhibitory activity. Bioorganic & Medicinal Chemistry. 2013;21(14):4201-9. doi: http://dx.doi.org/10.1016/j.bmc.2013.05.002.

163. Kuo Y-M, Andrews AJ. Quantitating the Specificity and Selectivity of Gcn5-Mediated Acetylation of Histone H3. PLoS One. 2013;8(2). Epub Feb 21, 2013. doi: 10.1371/journal.pone.0054896; PMCID: PMC3578832.

164. Neumann H, Peak-Chew SY, Chin JW. Genetically encoding N(epsilon)-acetyllysine in recombinant proteins. Nat Chem Biol. 2008;4(4):232-4. doi: 10.1038/nchembio.73. PubMed PMID: 18278036.

165. Wegener D, Hildmann C, Riester D, Schwienhorst A. Improved fluorogenic histone deacetylase assay for high-throughput-screening applications. Anal Biochem. 2003;321(2):202-8. Epub 2003/09/27. PubMed PMID: 14511685.

166. Huang X, Hernick M. A fluorescence-based assay for measuring N-acetyl-1-D-myo-inosityl-2-amino-2-deoxy-alpha-D-glucopyranoside deacetylase activity. Anal Biochem. 2011;414(2):278-81. Epub 2011/04/12. doi: S0003-2697(11)00224-7 [pii] 10.1016/j.ab.2011.04.001. PubMed PMID: 21477577.

167. Luger K, Mader AW, Richmond RK, Sargent DF, Richmond TJ. Crystal structure of the nucleosome core particle at 2.8 A resolution. Nature. 1997;389(6648):251-60. Epub 1997/09/26. doi: 10.1038/38444. PubMed PMID: 9305837.

168. Luger K, Rechsteiner TJ, Richmond TJ. Preparation of nucleosome core particle from recombinant histones. Methods in enzymology. 1999;304:3-19. Epub 1999/06/18. PubMed PMID: 10372352.

169. Kuo YM, Andrews AJ. Quantitating the specificity and selectivity of Gcn5-mediated acetylation of histone H3. PLoS One. 2013;8(2):e54896. doi: 10.1371/journal.pone. 0054896. PubMed PMID: 23437046; PMCID: 3578832.

170. Eisenthal R, Danson MJ, Hough DW. Catalytic efficiency and kcat/KM: a useful comparator? Trends in Biotechnology. 2007;25(6):247-9. doi: http://dx.doi.org/10.1016/ j.tibtech.2007.03.010.

171. Northrop DB. On the Meaning of Km and V/K in Enzyme Kinetics. Journal of Chemical Education. 1998;75(9):1153. doi: 10.1021/ed075p1153.

172. Hedstrom L. Enzyme Specificity and Selectivity. eLS: John Wiley & Sons, Ltd; 2001.

173. Norris KL, Lee J-Y, Yao TP. Acetylation Goes Global: The Emergence of Acetylation Biology. Science Signaling. 2009;2(97):76. doi: 10.1126/scisignal.297pe76.

174. Smith KT, Workman JL. Introducing the acetylome. Nature biotechnology. 2009;27(10):917-9. Epub 2009/10/10. doi: 10.1038/nbt1009-917. PubMed PMID: 19816449.

175. Deardorff MA, Kaur M, Yaeger D, Rampuria A, Korolev S, Pie J, Gil-Rodríguez C, Arnedo M, Loeys B, Kline AD, Wilson M, Lillquist K, Siu V, Ramos FJ, Musio A, Jackson LS, Dorsett D, Krantz ID. Mutations in Cohesin Complex Members SMC3 and SMC1A Cause a Mild Variant of Cornelia de Lange Syndrome with Predominant Mental Retardation. The American Journal of Human Genetics. 2007;80(3):485-94. doi: http://dx.doi.org/10.1086/511888.

176. Vinkenborg JL, Nicolson TJ, Bellomo EA, Koay MS, Rutter GA, Merkx M. Genetically encoded FRET sensors to monitor intracellular Zn2+ homeostasis. Nat Meth. 2009;6(10):737-40. doi: http://www.nature.com/nmeth/journal/v6/n10/suppinfo/nmeth.1368_S1.html.

177. Epsztejn S, Kakhlon O, Glickstein H, Breuer W, Cabantchik ZI. Fluorescence Analysis of the Labile Iron Pool of Mammalian Cells. Analytical Biochemistry. 1997;248(1):31-40. doi: http://dx.doi.org/10.1006/abio.1997.2126.

178. Petrat F, de Groot H, Rauen U. Subcellular distribution of chelatable iron: a laser scanning microscopic study in isolated hepatocytes and liver endothelial cells. Biochemical Journal. 2001;356(Pt 1):61-9. PubMed PMID: PMC1221812.

179. Haase H, Hebel S, Engelhardt G, Rink L. Flow cytometric measurement of labile zinc in peripheral blood mononuclear cells. Anal Biochem. 2006;352(2):222-30. Epub 2006/03/21. doi: 10.1016/j.ab.2006.02.009. PubMed PMID: 16545333.

180. Krezel A, Maret W. Zinc-buffering capacity of a eukaryotic cell at physiological pZn. J Biol Inorg Chem. 2006;11(8):1049-62. Epub 2006/08/23. doi: 10.1007/s00775-006-0150-5. PubMed PMID: 16924557.

181. Chabosseau P, Tuncay E, Meur G, Bellomo EA, Hessels A, Hughes S, Johnson PR, Bugliani M, Marchetti P, Turan B, Lyon AR, Merkx M, Rutter GA. Mitochondrial and ER-targeted eCALWY probes reveal high levels of free Zn2+. ACS chemical biology. 2014;9(9):2111-20. Epub 2014/07/11. doi: 10.1021/cb5004064. PubMed PMID: 25011072.

182. Kim B, Pithadia AS, Fierke CA. Kinetics and Thermodynamics of Metal-binding to Histone Deacetylase 8. Protein Science. 2015;24(3):11. doi: 10.1002/pro.2623.

183. Gattis SG. Mechanism and metal specificity of zinc-depdendent deacetylases [Dissertation]: University of Michigan; 2010.

184. Kim AM, Vogt S, O'Halloran TV, Woodruff TK. Zinc availability regulates exit from meiosis in maturing mammalian oocytes. Nat Chem Biol. 2010;6(9):674-81. doi: 10.1038/nchembio.419. PubMed PMID: 20693991; PMCID: 2924620.

185. Huang X, Kocabas E, Hernick M. The activity and cofactor preferences of N-acetyl-1-D-myo-inosityl-2-amino-2-deoxy-alpha-D-glucopyranoside deacetylase (MshB) change depending on environmental conditions. The Journal of biological chemistry. 2011;286(23):20275-82. doi: 10.1074/jbc.M111.234229. PubMed PMID: 21507949; PMCID: 3121509.

186. Gattis SG, Hernick M, Fierke CA. Active site metal ion in UDP-3-O-((R)-3-hydroxymyristoyl)-N-acetylglucosamine deacetylase (LpxC) switches between Fe(II) and Zn(II) depending on cellular conditions. The Journal of biological chemistry. 2010;285(44):33788-96. doi: 10.1074/jbc.M110.147173. PubMed PMID: 20709752; PMCID: 2962478.

187. Huguet F, Melet A, Alves de Sousa R, Lieutaud A, Chevalier J, Maigre L, Deschamps P, Tomas A, Leulliot N, Pages JM, Artaud I. Hydroxamic acids as potent inhibitors of Fe(II) and Mn(II) E. coli methionine aminopeptidase: biological activities and X-ray structures of oxazole hydroxamate-EcMetAP-Mn complexes. ChemMedChem. 2012;7(6):1020-30. doi: 10.1002/cmdc.201200076. PubMed PMID: 22489069.

188. Li JY, Chen LL, Cui YM, Luo QL, Li J, Nan FJ, Ye QZ. Specificity for inhibitors of metal-substituted methionine aminopeptidase. Biochemical and biophysical research communications. 2003;307(1):172-9. PubMed PMID: 12849997.

189. Kröncke K-D. Cellular stress and intracellular zinc dyshomeostasis. Archives of Biochemistry and Biophysics. 2007;463(2):183-7. doi: 10.1016/j.abb.2007.03.008.

190. Mrksich M. Mass spectrometry of self-assembled monolayers: a new tool for molecular surface science. ACS nano. 2008;2(1):7-18. Epub 2009/02/12. doi: 10.1021/nn7004156. PubMed PMID: 19206542; PMCID: 2600870.

191. Wolfson NA. Determining HDAC8 Substrate Specificity [Dissertation]: University of Michigan; 2014.

192. Baumann M, Stürmer R, Bornscheuer UT. A High-Throughput-Screening Method for the Identification of Active and Enantioselective Hydrolases. Angewandte Chemie International Edition. 2001;40(22):4201-4. doi: 10.1002/1521-3773(20011119)40:22<4201::AID-ANIE4201>3.0.CO;2-V.

193. Kim B, Pitcairn CA, Lopez JE, Fierke CA. Second Shell Residues Modulate the Reactivity and Metal Selectivity of Histone Deacetylase 8. *In preparation*.

194. Kim AM, Bernhardt ML, Kong BY, Ahn RW, Vogt S, Woodruff TK, O'Halloran TV. Zinc sparks are triggered by fertilization and facilitate cell cycle resumption in mammalian eggs. ACS chemical biology. 2011;6(7):716-23. doi: 10.1021/cb200084y. PubMed PMID: 21526836; PMCID: 3171139.

195. Spahl DU, Berendji-Grun D, Suschek CV, Kolb-Bachofen V, Kroncke KD. Regulation of zinc homeostasis by inducible NO synthase-derived NO: nuclear metallothionein translocation and intranuclear Zn2+ release. Proceedings of the National Academy of Sciences of the United States of America. 2003;100(24):13952-7. doi: 10.1073/pnas.2335190100. PubMed PMID: 14617770; PMCID: 283527.

196. Berendji D, Kolb-Bachofen V, Meyer KL, Grapenthin O, Weber H, Wahn V, Kröncke K-D. Nitric oxide mediates intracytoplasmic and intranuclear zinc release. FEBS Letters. 1997;405(1):37-41. doi: http://dx.doi.org/10.1016/S0014-5793(97)00150-6.

197. Maret W, Krężel A. Cellular Zinc and Redox Buffering Capacity of Metallothionein/Thionein in Health and Disease. Molecular Medicine. 2007;13(7-8):371-5. doi: 10.2119/2007-00036.Maret. PubMed PMID: PMC1952669.

198. Kruszewski M. Labile iron pool: the main determinant of cellular response to oxidative stress. Mutation research. 2003;531(1-2):81-92. Epub 2003/11/26. PubMed PMID: 14637247.

199. Suzuki T, Ota Y, Ri M, Bando M, Gotoh A, Itoh Y, Tsumoto H, Tatum PR, Mizukami T, Nakagawa H, Iida S, Ueda R, Shirahige K, Miyata N. Rapid Discovery of Highly Potent and Selective Inhibitors of Histone Deacetylase 8 Using Click Chemistry to Generate Candidate Libraries. Journal of Medicinal Chemistry. 2012;55(22):9562-75. doi: 10.1021/jm300837y.

200. Suzuki T, Muto N, Bando M, Itoh Y, Masaki A, Ri M, Ota Y, Nakagawa H, Iida S, Shirahige K, Miyata N. Design, Synthesis, and Biological Activity of NCC149 Derivatives as Histone Deacetylase 8-Selective Inhibitors. ChemMedChem. 2014;9(3):657-64. doi: 10.1002/cmdc.201300414.

201. Basu A, Rose KL, Zhang J, Beavis RC, Ueberheide B, Garcia BA, Chait B, Zhao Y, Hunt DF, Segal E, Allis CD, Hake SB. Proteome-wide prediction of acetylation substrates. Proceedings of the National Academy of Sciences. 2009;106(33):13785-90. doi: 10.1073/pnas.0906801106.

202. Johnson DG, Dent SY. Chromatin: receiver and quarterback for cellular signals. Cell. 2013;152(4):685-9. doi: 10.1016/j.cell.2013.01.017. PubMed PMID: 23375745; PMCID: 3644977.

203. Izzo A, Schneider R. Chatting histone modifications in mammals. Briefings in functional genomics. 2010;9(5-6):429-43. Epub 2011/01/27. doi: 10.1093/bfgp/elq024. PubMed PMID: 21266346; PMCID: 3080777.

204. Liu Z, Wang Y, Cheng H, Deng W, Pan Z, Ullah S, Ren J, Xue Y. GPS 3.0: web servers for the prediction of protein post-translational modification sites. *submitted*. 2015.

205. Khoury GA, Thompson JP, Smadbeck J, Kieslich CA, Floudas CA. Forcefield_PTM: Charge and AMBER Forcefield Parameters for Frequently Occurring Post-Translational Modifications. J Chem Theory Comput. 2013;9(12):5653-74. doi: 10.1021/ct400556v. PubMed PMID: 24489522; PMCID: 3904396.

206. Khoury GA, Smadbeck J, Tamamis P, Vandris AC, Kieslich CA, Floudas CA. Forcefield_NCAA: ab initio charge parameters to aid in the discovery and design of therapeutic proteins and peptides with unnatural amino acids and their application to complement inhibitors of the compstatin family. ACS Synth Biol. 2014;3(12):855-69. doi: 10.1021/sb400168u. PubMed PMID: 24932669; PMCID: 4277759.

207. Wang J, Wang W, Kollman PA, Case DA. Automatic atom type and bond type perception in molecular mechanical calculations. J Mol Graph Model. 2006;25(2):247-60. doi: 10.1016/j.jmgm.2005.12.005. PubMed PMID: 16458552.

208. Wang J, Wolf RM, Caldwell JW, Kollman PA, Case DA. Development and testing of a general amber force field. J Comput Chem. 2004;25(9):1157-74. doi: 10.1002/jcc.20035. PubMed PMID: 15116359.

209. Jakalian A, Jack DB, Bayly CI. Fast, efficient generation of high-quality atomic charges. AM1-BCC model: II. Parameterization and validation. J Comput Chem. 2002;23(16):1623-41. doi: 10.1002/jcc.10128. PubMed PMID: 12395429.

210. Case DA, Berryman JT, Betz RM, Cerutti DS, Cheatham TEI, Goetz AW, Homeyer N, Izadi P, Janowksi P, Kaus J, Kovalenko A, Lee TS, LeGrand S, Li P, Luchko T, Luo R, Madej B, Merz KM, Monard G, Needham P, Nguyen H, Nguyen HT, Omelyan I, Onufriev A, Roe DR, Roitberg A, Salomon-Ferrer R, Simmerling CL, Swails J, Walker RC, Wang J, Wolf RM, Wu X, York, Darden TA, Cheatham TE, Simmerling CL, Wang J, Duke RE, Luo R, Walker RC, Zhang W, Merz KM, Roberts B, Hayik S, Roitberg A, Seabra G, Swails J, Walker RC, Wang J, Wolf RM, Xu X, York DM, Kollman PA. AMBER 15. University of California, San Francisco; 2015.

211. Joung IS, Cheatham TE, 3rd. Determination of alkali and halide monovalent ion parameters for use in explicitly solvated biomolecular simulations. J Phys Chem B. 2008;112(30):9020-41. doi: 10.1021/jp8001614. PubMed PMID: 18593145; PMCID: 2652252.

212. Darden T, York D, Pedersen L. Particle mesh Ewald: An N·log(N) method for Ewald sums in large systems. J Chem Phys. 1993;98(12):10089-92. doi: doi:http://dx.doi.org/10.1063/1.464397.

213. Ryckaert J-P, Ciccotti G, Berendsen HJC. Numerical integration of the cartesian equations of motion of a system with constraints: molecular dynamics of n-alkanes. J Comput Phys. 1977;23(3):327-41. doi: http://dx.doi.org/10.1016/0021-9991(77)90098-5.

214. Berendsen HJC, Postma JPM, van Gunsteren WF, DiNola A, Haak JR. Molecular dynamics with coupling to an external bath. J Chem Phys. 1984;81(8):3684-90. doi: doi:http://dx.doi.org/10.1063/1.448118.

215. Ohnmacht SA, Marchetti C, Gunaratnam M, Besser RJ, Haider SM, Di Vita G, Lowe HL, Mellinas-Gomez M, Diocou S, Robson M, Šponer J, Islam B, Barbara Pedley R, Hartley JA, Neidle S. A G-quadruplex-binding compound showing anti-tumour activity in an in vivo model for pancreatic cancer. Sci Rep. 2015;5. doi: 10.1038/srep11385 http://www.nature.com/srep/2015/150616/srep11385/abs/srep11385.html#supplementary-information.

216. Harvey MJ, Giupponi G, Fabritiis GD. ACEMD: Accelerating Biomolecular Dynamics in the Microsecond Time Scale. Journal of Chemical Theory and Computation. 2009;5(6):1632-9. doi: 10.1021/ct9000685.

217. Lindahl E, Hess B, van der Spoel D. GROMACS 3.0: a package for molecular simulation and trajectory analysis. J Mol Model. 2001;7(8):306-17. doi: 10.1007/s008940100045.

218. Pronk S, Páll S, Schulz R, Larsson P, Bjelkmar P, Apostolov R, Shirts MR, Smith JC, Kasson PM, van der Spoel D, Hess B, Lindahl E. GROMACS 4.5: a high-throughput and highly parallel open source molecular simulation toolkit. Bioinformatics. 2013;29(7):845-54. doi: 10.1093/bioinformatics/btt055.

219. Humphrey W, Dalke A, Schulten K. VMD: Visual molecular dynamics. J Mol Graphics. 1996;14(1):33-8. doi: citeulike-article-id:2088499 doi: 10.1016/0263-7855(96)00018-5.

220. DeLano WL. The PyMOL Molecular Graphics System. The PyMOL Molecular Graphics System Version 174. Schrodinger, LLC.2008.

221. Fernandez-Recio J, Totrov M, Abagyan R. ICM-DISCO docking by global energy optimization with fully flexible side-chains. Proteins. 2003;52(1):113-7. doi: 10.1002/prot.10383. PubMed PMID: 12784376.

222. Otwinowski Z, Minor W. Processing of X-ray diffraction data collected in oscillation mode. Methods Enzymol. 1997;276:307-26.

223. Adams PD, Afonine PV, Bunkoczi G, Chen VB, Davis IW, Echols N, Headd JJ, Hung LW, Kapral GJ, Grosse-Kunstleve RW, McCoy AJ, Moriarty NW, Oeffner R, Read RJ, Richardson DC, Richardson JS, Terwilliger TC, Zwart PH. PHENIX: a comprehensive Python-based system for macromolecular structure solution. Acta Crystallogr D Biol Crystallogr. 2010;66(Pt 2):213-21. doi: 10.1107/S0907444909052925. PubMed PMID: 20124702; PMCID: 2815670.

224. Emsley P, Lohkamp B, Scott WG, Cowtan K. Features and development of Coot. Acta Crystallogr D Biol Crystallogr. 2010;66(Pt 4):486-501. doi: 10.1107/S0907444910007493. PubMed PMID: 20383002; PMCID: 2852313.

225. Wood TE, Dalili S, Simpson CD, Sukhai MA, Hurren R, Anyiwe K, Mao X, Suarez Saiz F, Gronda M, Eberhard Y, MacLean N, Ketela T, Reed JC, Moffat J, Minden MD, Batey RA, Schimmer AD. Selective inhibition of histone deacetylases sensitizes malignant cells to death receptor ligands. Mol Cancer Ther. 2010;9(1):246-56. doi: 10.1158/1535-7163.MCT-09-0495. PubMed PMID: 20053768.

226. Tran PV, Kennedy BC, Lien Y-C, Simmons RA, Georgieff MK. Fetal iron deficiency induces chromatin remodeling at the Bdnf locus in adult rat hippocampus2015 2015-02-15 00:00:00. R276-R82 p.

227. Rhoads TW, Lopez NI, Zollinger DR, Morre JT, Arbogast BL, Maier CS, DeNoyer L, Beckman JS. Measuring copper and zinc superoxide dismutase from spinal cord tissue using electrospray mass spectrometry. Anal Biochem. 2011;415(1):52-8. Epub 2011/04/02. doi: 10.1016/j.ab.2011.03.029. PubMed PMID: 21453670; PMCID: 3118564.

228. Nandal A, Ruiz JC, Subramanian P, Ghimire-Rijal S, Sinnamon RA, Stemmler TL, Bruick RK, Philpott CC. Activation of the HIF prolyl hydroxylase by the iron chaperones PCBP1 and PCBP2. Cell metabolism. 2011;14(5):647-57. Epub 2011/11/08. doi: 10.1016/j.cmet.2011.08.015. PubMed PMID: 22055506; PMCID: 3361910.

229. Philpott CC. Coming into view: eukaryotic iron chaperones and intracellular iron delivery. The Journal of biological chemistry. 2012;287(17):13518-23. doi: 10.1074/jbc.R111.326876. PubMed PMID: 22389494; PMCID: 3340153.